RCA VICTOR RESEARCH REPORT
NO. 7-801-39

ELECTROCHEMICAL PROPERTIES OF SEEDED PLASMA FLOW FIELDS II

A.I. Carswell
C. Richard
A.K. Ghosh

FINAL TECHNICAL SUMMARY REPORT
June 1965

Sponsored by

ADVANCED RESEARCH PROJECTS AGENCY

under

ARPA Order No. 665
Contract No. NON-4596(00)

RCA VICTOR COMPANY, LTD.
RESEARCH LABORATORIES
MONTREAL, CANADA

RCA Victor Company, Ltd.
Research Laboratories
Montreal, Canada

Electrochemical Properties of Seeded Plasma Flow Fields II.

A.I. Carswell
C. Richard
A.K. Ghosh

Final Technical Summary Report to ARPA

ARPA Order No. [redacted] 665
Project Code No. 4740
Contract No. NON-4596(00)

Prepared by A.I. Carswell

C. Richard

Asoke K Ghosh

Approved by F.R. Osborne
Director, Microwave &
Plasma Physics Laboratory

F.R. Ross Carron
for Director of Research

RCA Victor Research Report
7-801-39
June 1965

- ABSTRACT -

The report summarizes the work performed under ARPA contract No: ~~[illegible]~~ [NON-4596(00)] during the period December 1, 1964 to May 31, 1965.

The effectiveness of various electronegative gases (O_2, CO_2, NO, SF_6, H_2O), as a means of reducing the ionization in plasma flow fields (nitrogen plasma) are experimentally investigated and compared. In the thermal condition prevailing ($T_e \simeq 10^4$ °K), SF_6 and water vapour are found to be the most effective in quenching the plasma. Electrostatic probe, optical emission spectroscopy, thermocouple and NO titration techniques are employed to monitor the plasma properties. The complex nature of the short duration "pink" afterglow in nitrogen is studied in some detail both in flowing and non-flowing systems in order to ascertain more quantitatively the effectiveness of the different "quenching" gases. The effects of gas pressure, wall condition and gas purity on the afterglow behaviour are closely examined in view of the reproducibility of measurements. A theoretical study of the limitations and applicability of electrostatic probe methods to plasmas containing negative ions is made and computations of characteristics are presented. Results of measurements of the flow velocity by different techniques are compared and the importance of an accurate determination of plasma flow field velocity is discussed.

TABLE OF CONTENTS

APPENDICES

ACKNOWLEDGEMENTS

The authors wish to express their appreciation to Dr. T.W. Johnston for his assistance with the probe diagnostics and in particular for the computations in Appendix C. The contributions of Dr. E. Fjarlie to some of the spectroscopic studies and to Appendix D are gratefully acknowledged. We are also indebted to Mr. J. Sheppard and Mr. B. Challice for their technical assistance with the experiments and report preparation.

ELECTROCHEMICAL PROPERTIES OF SEEDED PLASMA FLOW-FIELDS II

I INTRODUCTION

The purpose of the present program is to investigate the effectiveness of the electron attachment process as a means of reducing the ionization in plasma flow fields. In earlier investigations (Carswell & Cloutier, 1964; Cloutier & Carswell,1963; Carswell & Richard, 1964) it was found that large reductions in the ionization of argon plasmas could be obtained with sulfur hexafluoride seeding. In this report a summary is given of the results obtained with seeding of nitrogen plasma flow systems with a variety of electronegative (electron attaching) gases. The seed gases used were: NO, CO_2, O_2, SF_6 and H_2O, and in all cases these were introduced into the afterglow of a pure nitrogen discharge flowing at a velocity in range from 2×10^3 cm/sec to 10^4 cm/sec and at pressures of the order of 3 Torr.

It has been found in these studies that the electrochemical properties of the flow systems are very sensitive to changes in: gas pressure, wall conditions, gas purity and excitation power level, and that reproducible quantitative measurements can only be made if these parameters are adequately controlled and measured. In order to do this it has been necessary to utilize a number of diagnostic techniques including probes, and optical emission spectroscopy. In many instances it has been necessary to examine the limitations of the techniques themselves to ascertain the limits of their usefulness for the study of the complicated plasma systems encountered in the seeded afterglows. The results of several such investigations are included as appendices to this report.

In view of its complexity, the afterglow in pure nitrogen has been studied in some detail and results are presented for both the steady state "flowing" afterglow systems and (non-flowing) pulsed afterglows having identical excitation conditions. These investigations have been centered on the so-called "short-duration" or "pink" afterglow in nitrogen which is of considerable interest and importance because of the presence of extremely high energy carriers (~ 22ev) and an enhanced degree of ionization compared to the normal long duration nitrogen afterglow.

The short duration afterglow is useful for seeding studies, since it can provide (in a region free of external fields) plasmas with electron densities two to three orders of magnitude lower than in the primary discharge and electron temperatures about one order of magnitude lower. Also, since the maximum afterglow ionization occurs 10-15 milliseconds after the discharge, supersonic velocities are not required to achieve adequate separation of the afterglow from the primary discharge in the flow systems.

A description of the experimental arrangement is presented in Section II. The results for the pure N_2 systems are given in Section III with some of the related topics also being covered in the appendices. In Section IV, the results of seeded N_2 systems are given for the various seed gases. In Section V the relative effectiveness of the seed gases for plasma quenching are discussed in terms of the various electron attachment processes occurring.

II APPARATUS

As discussed in the previous report, (Carswell & Richard, 1964), it has been found that the tube walls of the flow system can cause large, and in some cases unpredictable, changes in the afterglow characteristics. In order to minimize the wall effects two new flow systems have been constructed. One is a scaled up version of the former flow system using a uniform tube of 2.5 cm i.d. and for the purposes of the present report this will be called the "small" flow system. The second is a much larger flow system using a free-jet flow configuration in a pyrex tube 6 inches i.d. and this will be termed the "large" system.

2.1 Large Flow System

A schematic diagram of the large flow system is shown in Fig.1. The primary aim in the apparatus design was to obtain a subsonic free-jet type of flow so that the vacuum chamber walls were not in close proximity to the active afterglow flow region.

This was achieved by flowing the nitrogen through a tube of diameter 19 mm i.d. which served as the excitation section. (The 1 kw rf source described previously was used to produce the discharge.) From the 19 mm tube the afterglow products flowed out into the main analysis chamber which was composed of a 7 foot length of pyrex pipe having an inside diameter of 6 inches. The location of the discharge region with respect to the end of the 19 mm tube could be varied by sliding the electrodes as described in the previous report (Carswell & Richard, 1964).

All seeding and analyses of the stream were performed in the large glass pipe where sufficient space was available to allow seeding orifices and electrical probes to be moved to any desired location in the afterglow jet.

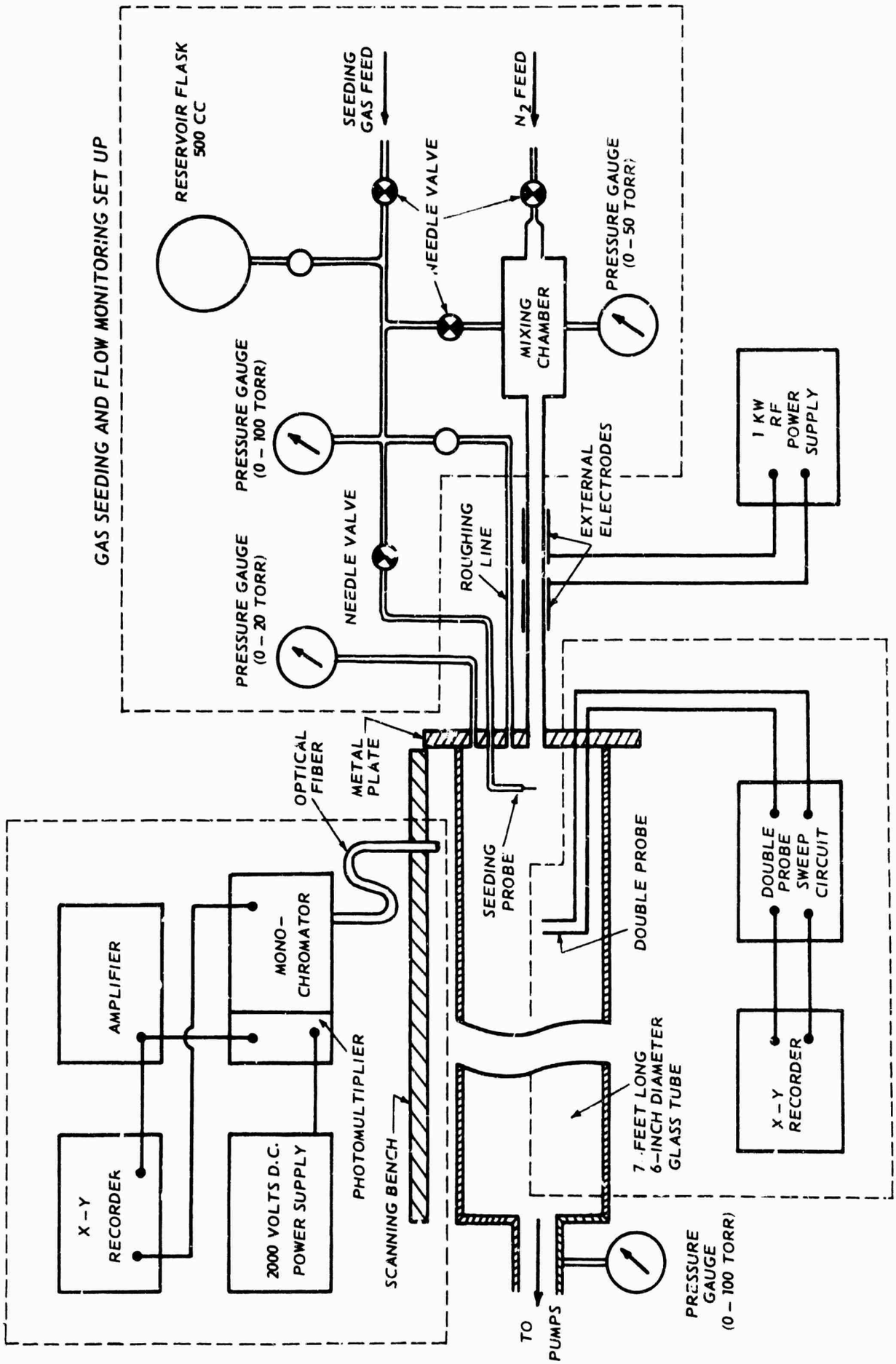

Figure 1 – Schematic diagram of the large flow system

With this system a much wider range of pressures and flow velocities are attainable than in the former systems since the pumping speed was not limited by the conductance of the glass tubing. Flow velocities between zero and 10^4 cm/sec have been attained with pressures ranging from about 0.1 to 20 Torr.

With the large system it is possible to obtain very reproducible conditions in the afterglow and no problem was encountered in reproducing the "pink" glow from day to day. In fact, pink glow regions up to 7 ft. in length have been produced. With the new system it is also possible to produce streams which are quite turbulent. The turbulence is readily observable because of the luminosity of the afterglow and this feature should provide very useful data on the effects of turbulence in seeded streams. No quantitative measurements have been performed on the turbulent flows as yet, but very definite visual effects are apparent. It has also been noted that significant heating of the apparatus is created in the region of turbulence so that the turbulence is causing a marked change in the energy release from the afterglow.

As shown in Fig.1, the new system includes an improved gas handling system for the seed gases. Precision gauges and needle valves are used throughout for maximum control of the gas flow. Seeding ratios as small as 10^{-5} can be measured with the present system. (Smaller values can be obtained by using mixtures of the seed gas with N_2 in the gas seeding system.)

The apparatus also includes facilities for measuring the spectral emission from the afterglow. A prism monochromator (reciprocal linear dispersion $\simeq$ 30 Å/mm) with a range extending from 0.4μ to 3μ and a grating spectrometer ($\simeq$ 12 Å/mm) are used to provide a detailed spectral analysis. The radiation from the afterglow can be directed into the spectrometers via a flexible optical fibre system so that by scanning the fibre along the discharge

any portion of the afterglow can be examined without moving the bulky spectrometer. The scanning bench for the fibre is fitted with an electrical position indicator so that plots of light output as a function of position can be plotted directly on an X-Y recorder.

2.2 Small Flow System

Although the large tube provides afterglow plasmas with very small interaction effects because of the free-jet configuration, this type of system suffers from the disadvantage that the directed velocity of the flow is not constant as it expands out into the large tube. In general, the shape of the visible afterglow in the large tube is determined by the relative magnitudes of the directed flow velocity down the tube and the radial diffusion velocity.

In order to provide a flow facility which did not have these defects, the "small" system shown in Fig.2 was constructed. This system consists of a pyrex tube 2.5 cm i.d. and about 1.8 meters long. The same 1 kw rf supply was used to excite the discharge in both flow systems. The pumping line to the vacuum systems was placed at right angles to the downstream end of the flow tube so that electrical probes could be introduced into the flow as shown in Fig.2. These probes were inserted through O-ring seals and their length was sufficient (~ 2m) to allow any point in the flow tube to be examined. The probes can be moved under vacuum while the gas is flowing so that probing of a complete steady-state flow is possible. This arrangement avoids the problems encountered previously using fixed probes and a movable rf source.

The seed gases could be introduced via needle valves either upstream or downstream from the main discharge as shown in Fig.2. The relative position of the downstream seeding probe in the afterglow could be varied by adjusting

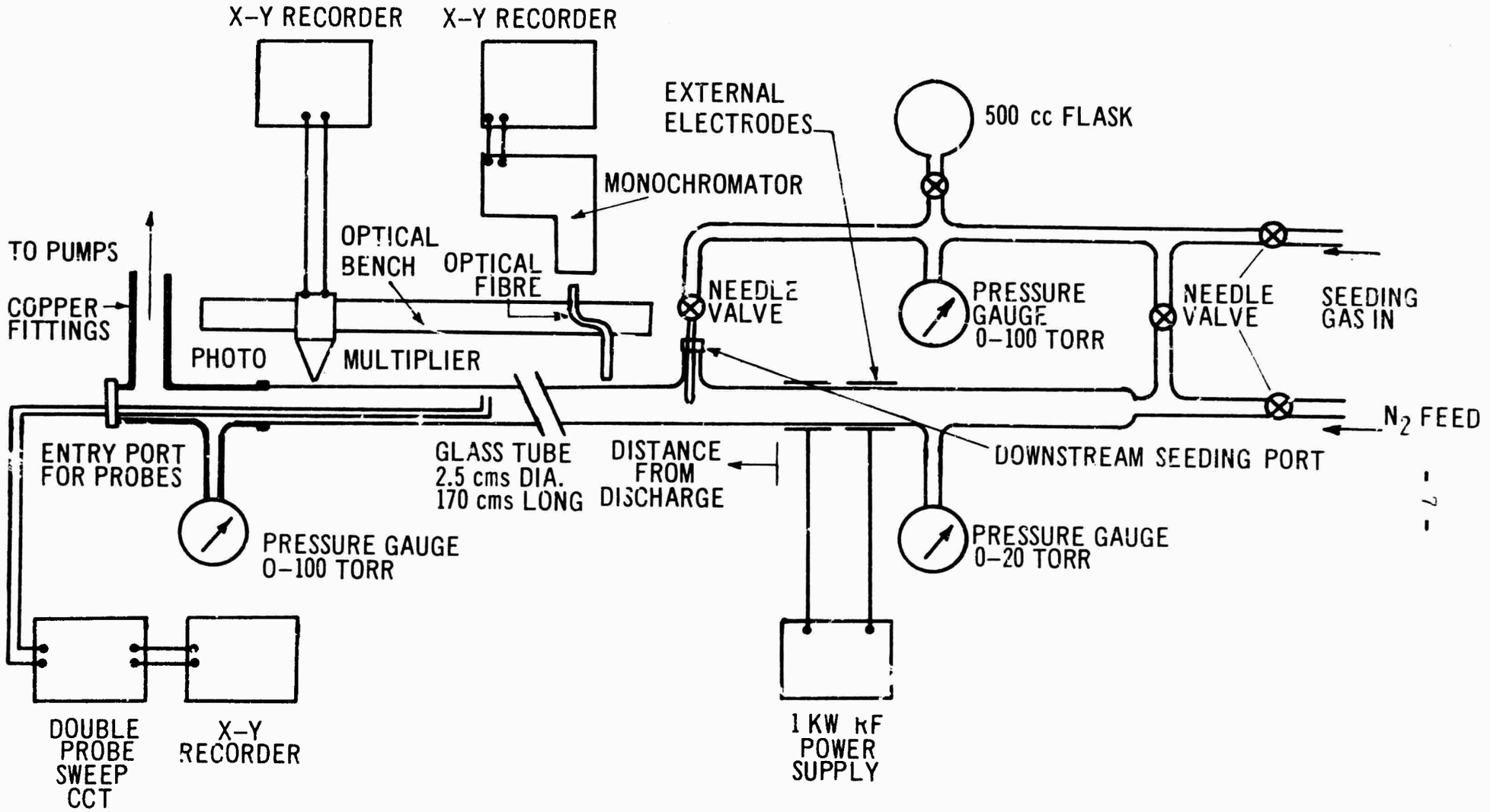

Fig. 2 Schematic diagram of the small flow system.

either the flow velocity or the rf excitation electrodes.

In addition to the two spectrometers mentioned above, optical emission studies of the afterglow in the small tube were made using photomultipliers and a series of interference filters to select the appropriate wavelength range. The light entering the photomultiplier-filter assembly passed through a 0.5 mm slit and diaphragms were arranged to pass a beam having an angle of about 4 degrees. The photomultiplier assembly was mounted on a two meter long optical bench with an electrical position indicator providing an output voltage proportional to the position on the bench.

The interference filters used, had a pass band of approximately 100 Å and centre frequencies were chosen to correspond with several of the most intense molecular nitrogen ion and neutral emission bands. (e.g. the first negative 0,0, 0,1 and 0,2 bands at 3914 Å, 4278 Å and 4709 Å respectively, and the first positive $\Delta v = 4$ series at approximately 5800 Å).

III PURE NITROGEN AFTERGLOW STUDIES

Although the primary aim of the present investigation was to examine the properties of seeded nitrogen flow systems it was necessary to spend considerable time in the early phases of the program investigating the properties of the afterglows of pure nitrogen. The studies were necessary since all measurements of the seeded systems had to be compared with the unseeded afterglows to provide meaningful comparisons of the "quenching" efficiencies of the particular seed gas. This meant that the "pure" N_2 afterglows had to be reproducible and quantitatively controlled during the measurements.

Because of the complicated (and as yet not fully understood) behaviour of the nitrogen afterglows the above requirements could only be satisfied when adequate knowledge of the short duration afterglow was obtained. Since only limited data on the short duration "pink" glow is available in the literature, measurements were made to determine the quantitative values in the present apparatus and the spatial variations of the various afterglow parameters such as: electron and ion densities, electron, ion and gas temperatures, nitrogen atom densities, etc. In addition, the studies of the pure nitrogen systems served as a means of assessing the several diagnostic techniques in plasmas uncomplicated by the presence of electronegative gases.

In this section, the measurements on the afterglows in pure N_2 flow systems are summarized. In appendix A, some results of afterglow studies in non-flowing pulsed N_2 discharges are also given. The pulsed discharge work was undertaken initially to provide a cross-check on the velocity measurements made in the flow systems. It was hoped that by relating the time history display of the pulsed afterglows with the spatial variation observed in the flowing systems under identical discharge conditions, more accurate measurements could

be made of the time scale in the flow systems. For studies of the seeded systems, this time scale must be established as accurately as possible if quantitative rates of attachment, recombination etc. are to be derived.

This work uncovered a series of phenomena not previously considered in the literature. The establishment of the flow velocity in the afterglow region with any degree of accuracy has been found to be very difficult primarily because of the relatively large and irregular temperature variations involved in the flow systems. In Appendix B a separate discussion is given of comparative measurements of the flow velocity using several techniques such as: total gas volume "throughput", spatially separated photomultipliers, velocity of sound measurements and pulsed techniques. The results presented illustrate the need for caution in quoting flow velocities and the large possible uncertainties in the afterglow time scale which can result from the velocity determinations.

Detailed double probe measurements of the pure N_2 afterglows were undertaken to provide information on the quantitative spatial variation of the charged particle densities and electron temperatures. The double probe used for these measurements was introduced as shown in Fig.2. The two parallel cylindrical electrodes exposed to the plasma were 0.25 mm in diameter and 11 mm in length and were separated by 8 mm. The rather large electrode separation (approx. 64 electrode radii) was required to prevent overlap of the two "sheaths" over the range of conditions encountered in the experiment. With smaller separations it was found that apparently spuriously high values of the electron temperature were recorded whenever the electron density decreased below about 10^8/cc.

Sample results for two different flow conditions in the small flow system are shown in Figures 3 and 4. The results shown were taken from series of probe voltage-current characteristics scanned in the afterglow every 2 centimeters. Fig.3a shows the actual "saturation" current collected by the probe as a function of position in an N_2 afterglow at 2Torr flowing at 3100 cm/sec.

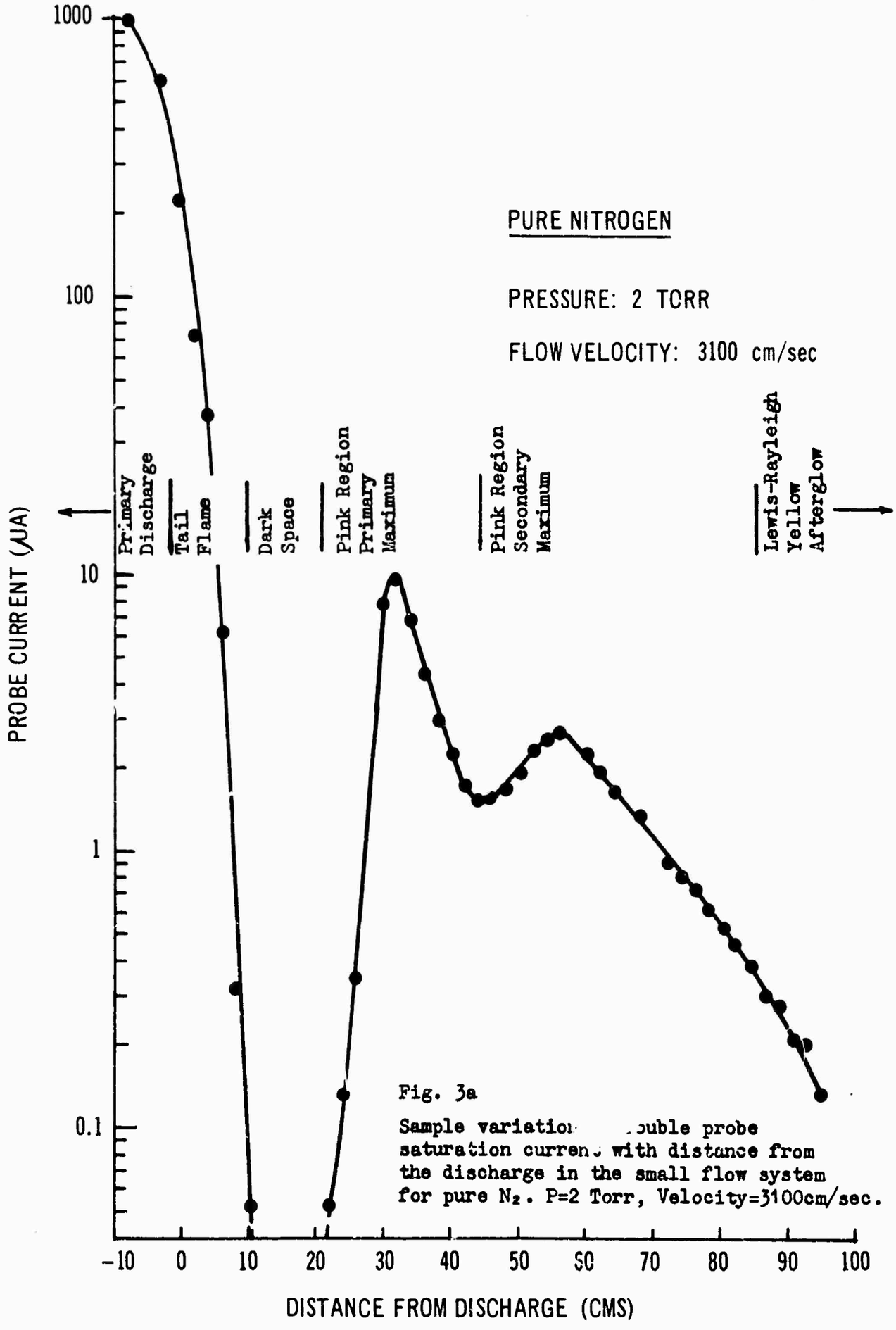

Fig. 3a

Sample variation of double probe saturation current with distance from the discharge in the small flow system for pure N_2. P=2 Torr, Velocity=3100cm/sec.

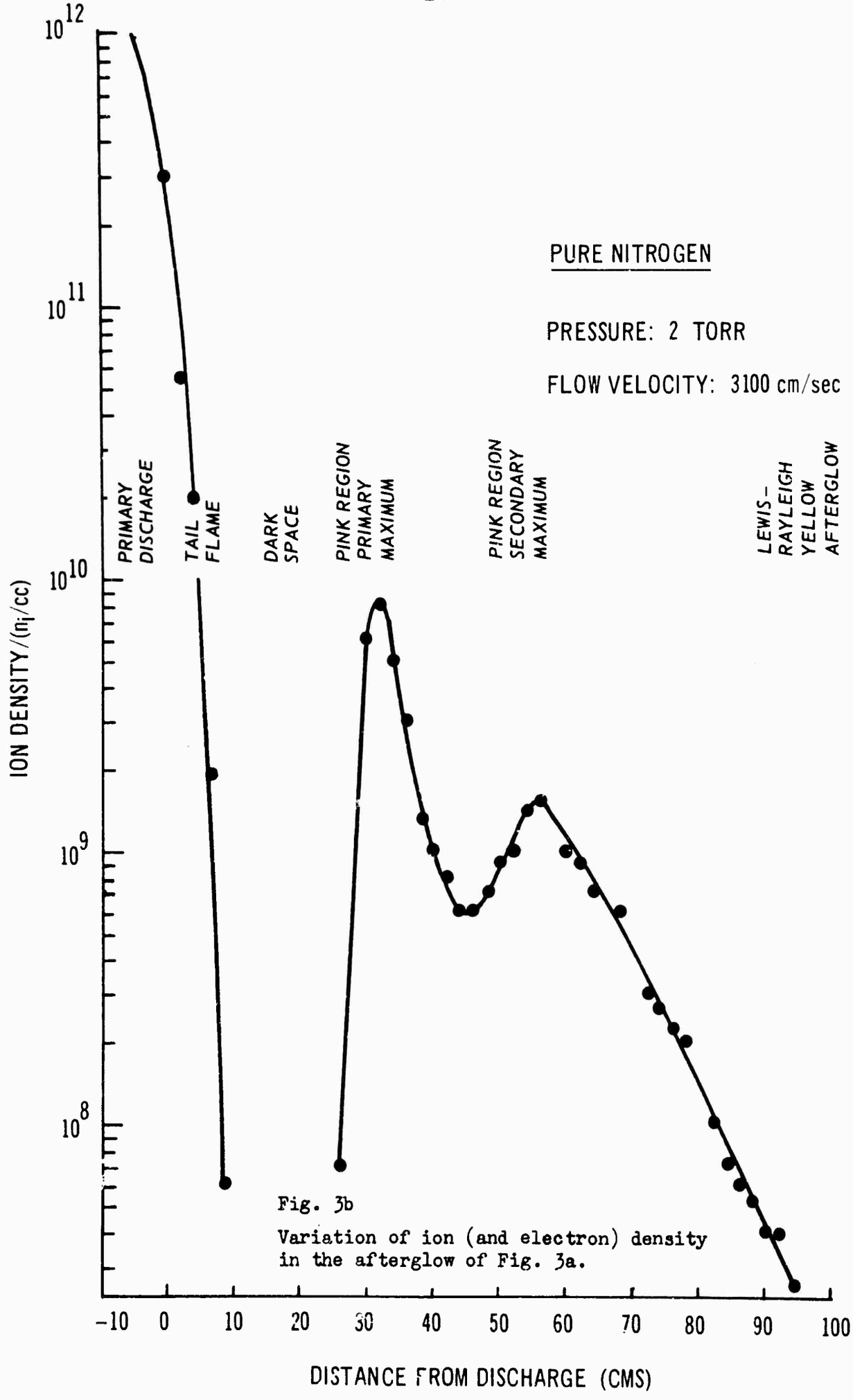

Fig. 3b

Variation of ion (and electron) density in the afterglow of Fig. 3a.

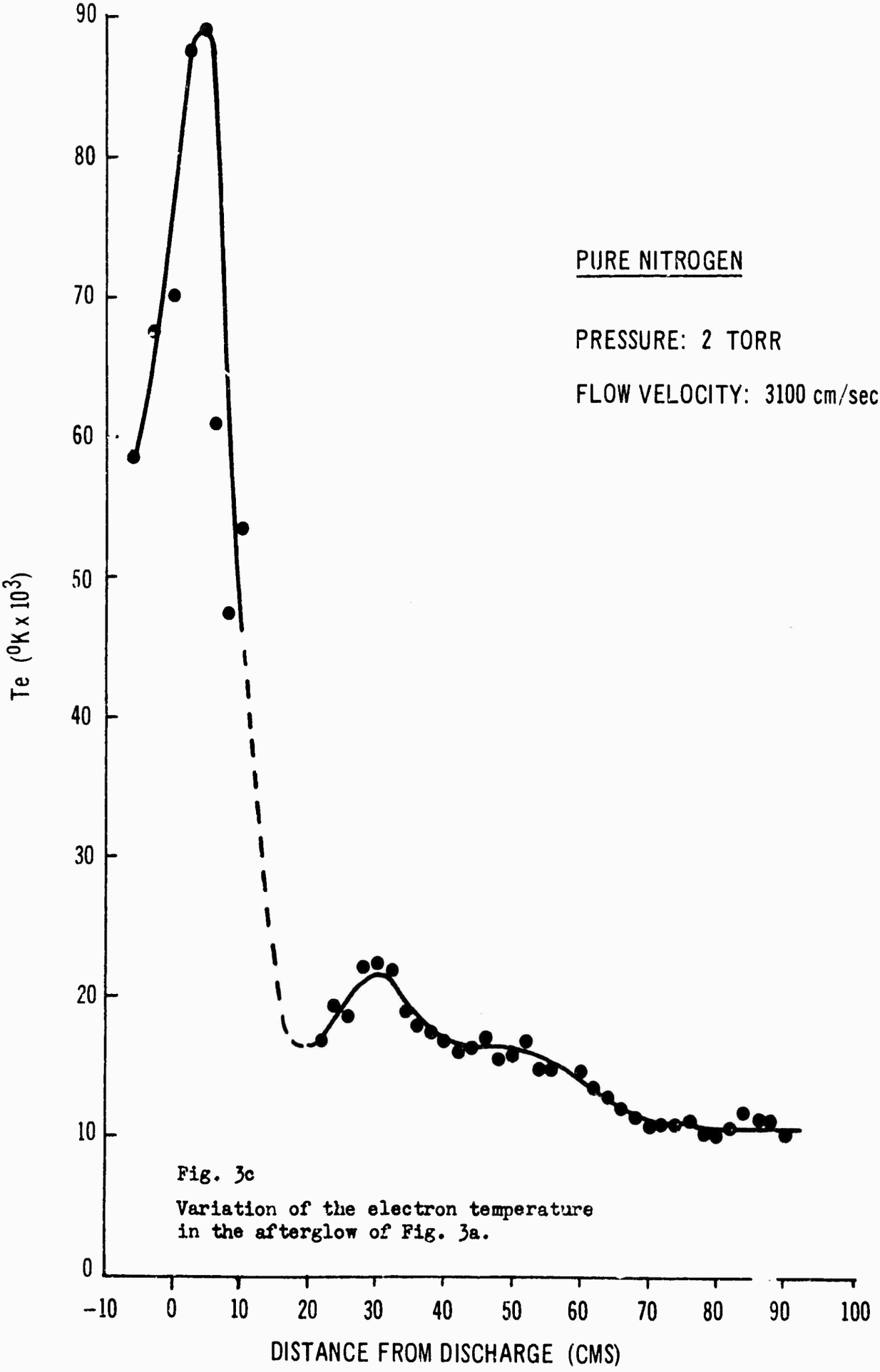

Fig. 3c

Variation of the electron temperature in the afterglow of Fig. 3a.

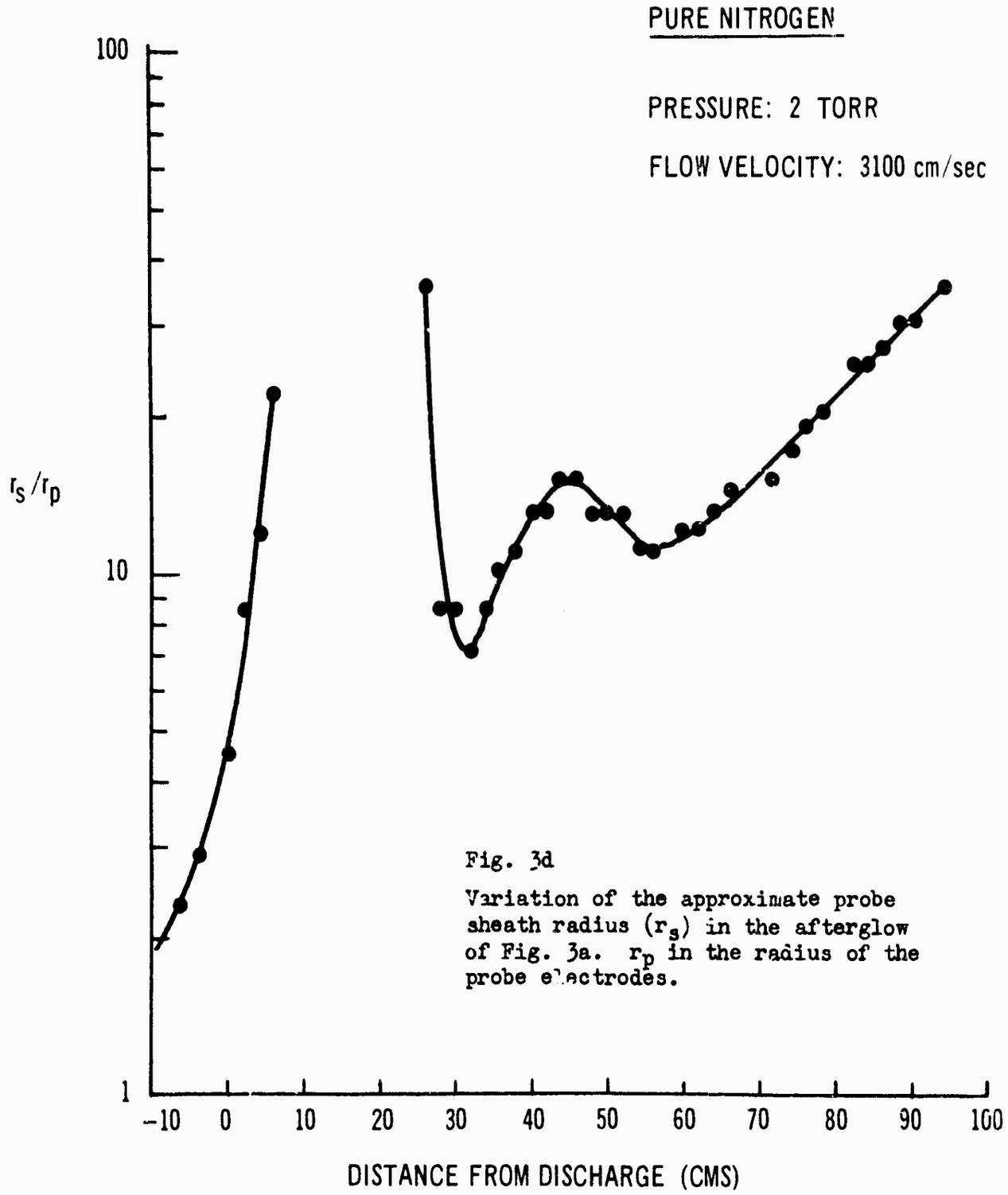

Fig. 3d

Variation of the approximate probe sheath radius (r_s) in the afterglow of Fig. 3a. r_p in the radius of the probe electrodes.

Fig.3b and 3c show respectively, the variation in ion (and electron) density and electron temperature T_e computed from the probe characteristics according to the simple theory of Johnson & Malter (1952). In the computation of the ion density in Fig. 3b, the electron temperature is used instead of the ion temperature erroneously used in the Johnson & Malter paper. As a rough indication of the probe interaction distance, the ratio r_s/r_p of the sheath radius r_s to the probe electrode radius r_p is plotted in Fig. 3d. From this plot it is apparent that in the "dark space" upstream from the pink glow the probe electrodes could be expected to interact because of overlapping of the sheaths (i.e. $r_s/r_p > 32$) even with the large electrode separation.

A similar set of results is shown in Fig. 4 for an N_2 afterglow at a pressure of 2 Torr and a velocity of 3700 cm/sec. The data shown in Figures 3 and 4 illustrate the good spatial resolution and reproducibility obtainable with the probe measurements over an ion density range of about five orders of magnitude. However, the absolute accuracy of the values obtained is difficult to establish because of the limitations of the theory used in the reduction of the characteristics (e.g. assumption of no collisions and of constant ion current collection etc.). An effort to improve the quantitative accuracy of the probe measurements by a more rigorous analysis has been made and this is described in detail in Appendix C. In both Figures 3 and 4, the probe measurements show the presence of two maxima in the afterglow ionization with the peaks being more clearly separated in Fig.3 than in Fig.4. In both cases, the first maximum occurs at a distance corresponding to a time of approximately 10 milliseconds in the afterglow (measuring from the downstream end of the discharge electrode as shown in Fig.2). The second maximum occurs about 18 msec after the discharge. The peak positions and their relative intensities with respect to each other and the main discharge have been found to be very

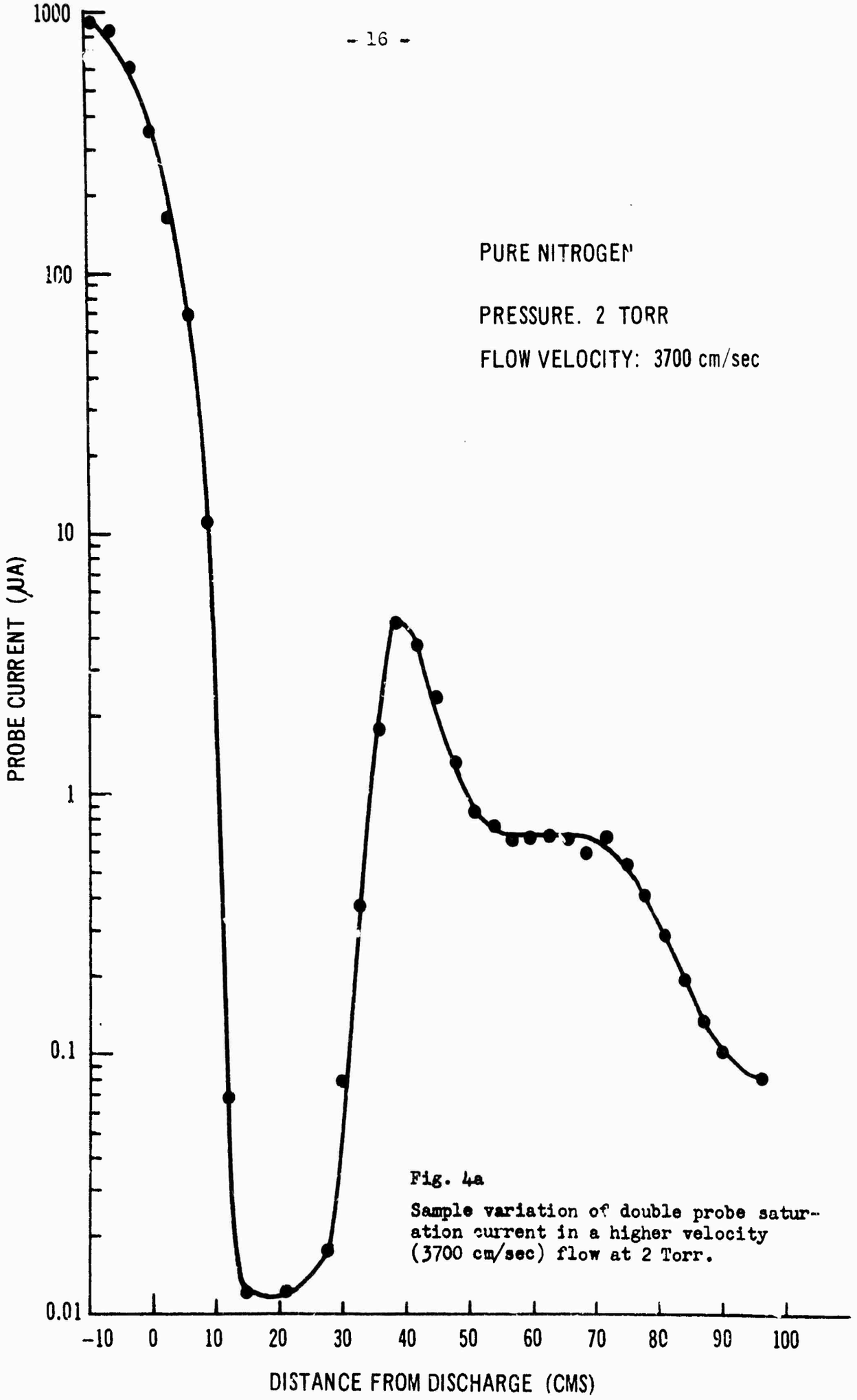

Fig. 4a

Sample variation of double probe saturation current in a higher velocity (3700 cm/sec) flow at 2 Torr.

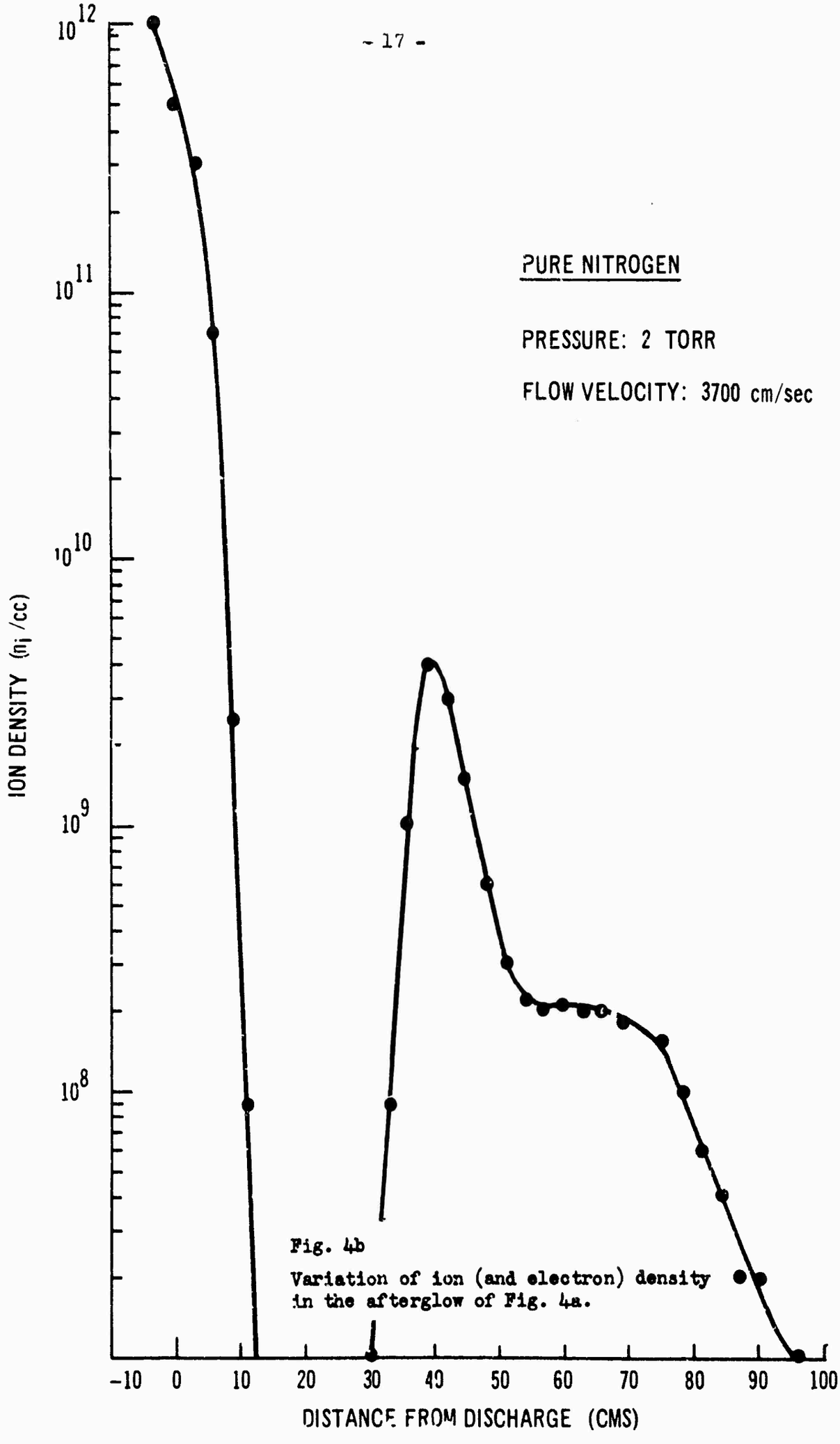

Fig. 4b

Variation of ion (and electron) density in the afterglow of Fig. 4a.

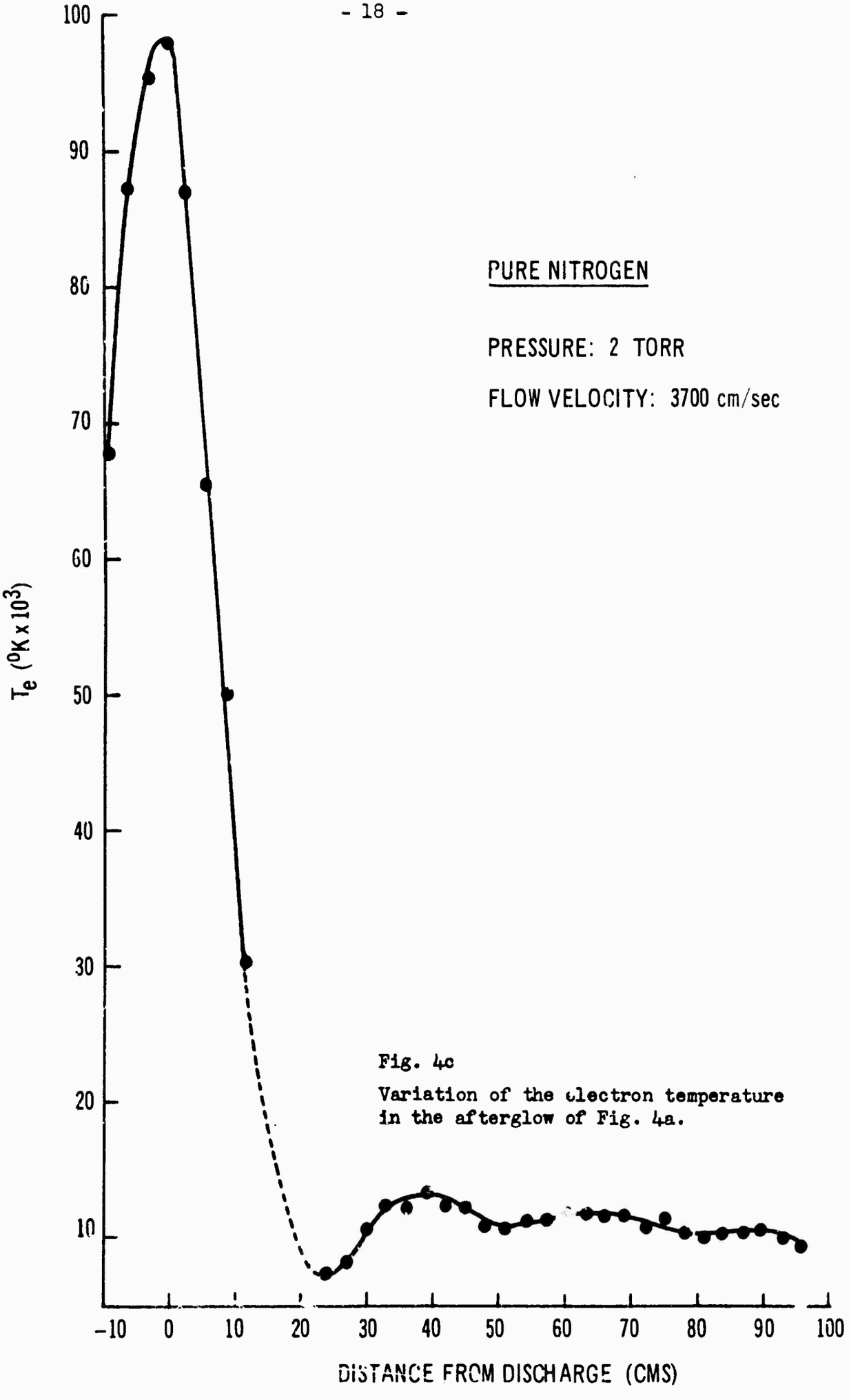

Fig. 4c

Variation of the electron temperature in the afterglow of Fig. 4a.

sensitive to the excitation power level, wall conditions and impurity level in the discharge. (See Appendix A also) The ion (and electron) density variations shown in Figures 3 and 4 are, however, typical of the runs made. The discharge electron density was in excess of 10^{11}/cc and the peak of the primary pink maximum had an electron density between 10^9 and 10^{10}/cc. The secondary peak was generally about one order of magnitude less than the primary. In the dark space upstream from the pink region, the electron density is usually less than 10^7/cc.

The electron temperature T_e, decays rapidly from a value of about 10^5 °K in the primary discharge to about 10^4 °K throughout the pink afterglow region. In most cases no pronounced secondary peaks in the T_e curves were observed although some small peaks appear to be present in Fig. 3c and 4c. In both Figs. 3c and 4c, the electron temperature is seen to be a maximum at the downstream end of the discharge with lower values being recorded within the discharge region. The visible "orange" tail flame (Figs. 3 and 4) extended about 10 cm from the electrodes and was still being excited by the discharge fields.

As a result of the probe measurements in the pure N_2 , it has been found that the pink afterglow displays all of the expected properties of a plasma with electron and ion densities such as those shown in Figures 3 and 4. Also, contrary to some reports, it has been found in the present study, that the pink glow is affected by a magnetic field of sufficient strength. Since the magnetic field effects could only be expected to be very pronounced if the cyclotron frequency exceeds the collision frequency, previous investigations in smaller tubes at higher pressures would make the magnetic field effect more difficult to observe.

In addition to the probe studies, measurements of the pure N_2 systems have been made using the optical emission from the afterglows. In Figures 5

and 6, sample results of the axial variations are shown for two different flow conditions. These measurements were made by scanning a photomultiplier, with appropriate filter, along the flow tube as described in Section 2.2. The variation in intensity as a function of position was plotted directly on the X-Y recorder. Fig.5 shows a sample of a flow exhibiting two peaks in the afterglow and Fig. 6 shows a sample of a flow exhibiting three peaks in the afterglow. The filters used were chosen to transmit the (0,0) band at 3914 Å of the first Negative nitrogen system, (i.e. excited N_2^+ ion emission) and the strong $\Delta v = 4$ band at about 5800 Å of the nitrogen first Positive system (excited neutral N_2 emission). Simultaneous probe measurements of the afterglow electron density are also shown in Fig.6.

From such results it was found that the "structure" of the afterglow as seen from the three measurables (1) N_2^+ ion emission, (2) neutral N_2 emission and (3) probe measurements of the electron and ion density, was virtually identical. It was found in general that the peak positions and relative heights corresponded in all three cases. Usually relative height of the secondary maxima as seen with the 5780 Å filter appeared a little lower than indicated by the 3914 Å and probe measurements indicating a slight difference in the ratio of ions to neutrals, but this difference was usually small ($\sim$ 10-25%) and may not be too significant in view of the fact that the secondary peaks in the pink afterglow are very sensitive to the flow conditions (more so than is the primary pink maximum). Also, as shown in Fig.6, it was generally found that the peaks appear more clearly resolved with the probe than with the optical measurements. This appears to indicate that the probes provide a somewhat better spatial resolution than the photomultipliers (which integrate along their line of sight). As also shown in Figs. 5 and 6, the tail flame of the discharge has a higher relative concentration of N_2 molecules with respect to N_2^+ ions than the pink region.

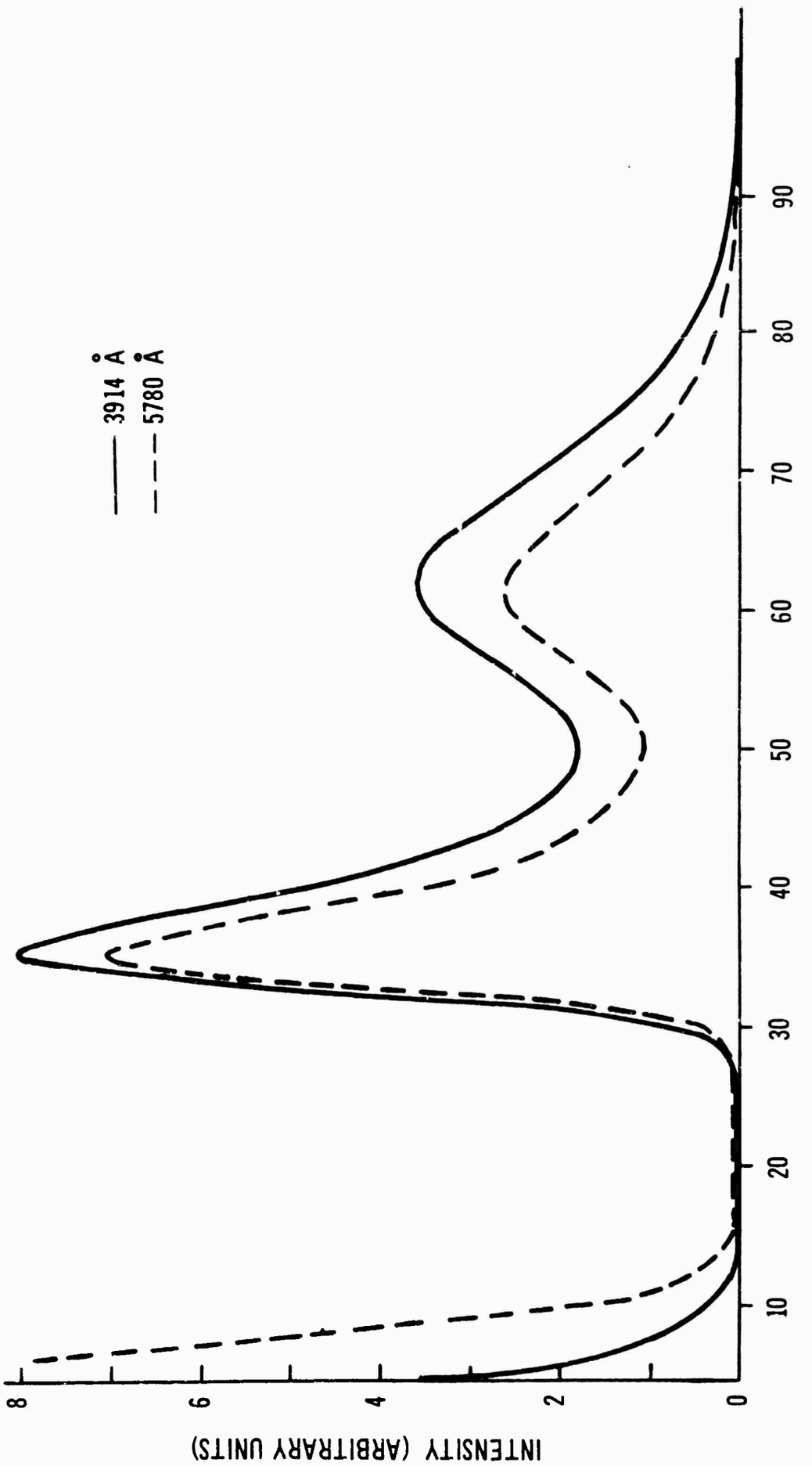

Fig. 5 Axial variation of the visible emission from a typical pure N_2 afterglow. Curves show the variation for the $(0_{+}0)$ first Negative (N_2^+ ion) and $\Delta v=4$ first Positive (excited N_2) bands at 3914 Å and 5780 Å (2 Torr, 2600 cm/sec).

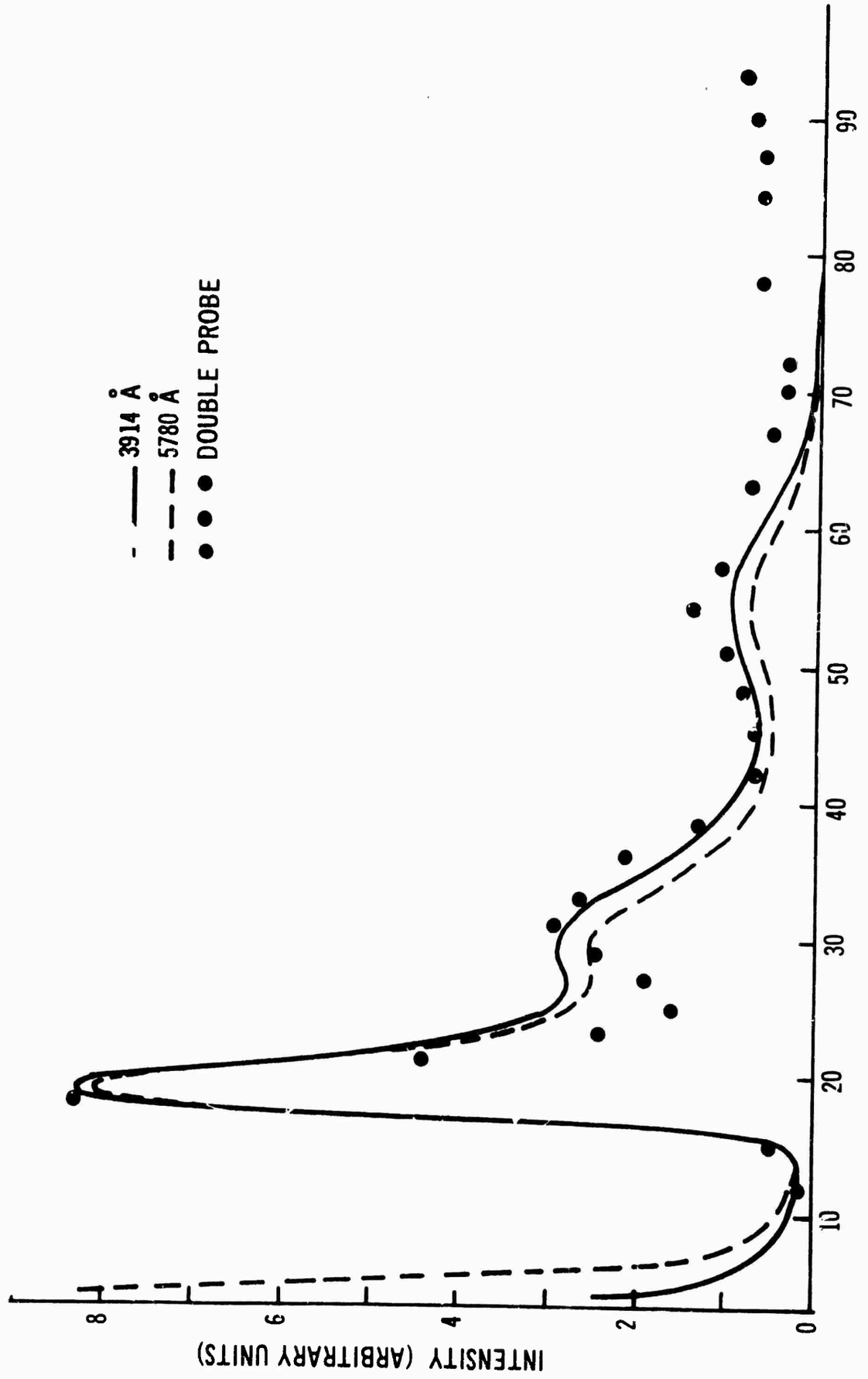

Fig. 6 Comparison of the axial variation of the afterglow properties of pure N_2 recorded by (1) optical emission at 3914 Å and 5780 Å and (2) by double probe measurements. The curves are normalized to have equal intensity in the primary peak (at 19cm). Note the three maxima in the afterglow (2 Torr; 1800cm/sec).

The simultaneous use of the probes and optical emission illustrated in Figs. 5 and 6 provides a rapid means for making detailed studies of the axial dependence of the afterglow and such displays will be discussed further in connection with the seeding investigations.

One immediately obvious property of the pure N_2 afterglow is the pronounced heating of the discharge tube walls in the region of the pink glow. In an effort to measure the temperature variation quantitatively, a thermocouple was introduced into the flow in place of the electrical probe shown in Fig.2. To reduce the thermal inertia of the system, the metal (iron-constantan) conductors at the hot junction were left uninsulated so that recombination of the active species could occur directly on the metal surfaces. In this way, the temperature measured should be higher (by the amount of the recombination energy) than the gas kinetic temperature within the discharge region. As a result, such thermocouple readings should provide a measure of the upper limit of the "temperature" in the flow system. Typical results are shown in Figures 7a and 7b for two different flow conditions in the small system. Although not shown in the Figures, the measurements were extended back to the primary discharge (d = 0) where temperatures of the order of 400°C were recorded.

In Fig.7, the variation of the 3914 Å emission is shown along with the thermocouple measurements and in both cases the thermocouple reading is seen to exhibit a peak in the region of the primary pink maximum. (Evidence of a small secondary peak is also seen in Fig.7a.) At this peak the temperature recorded was of the order of 150°C (425°K), with the value in the minimum upstream being 20-25 degrees lower. The relative positions of the peaks in the 3914 Å emission and the thermocouple readings were difficult to establish accurately but for pronounced single maxima such as shown in Fig.7b, the highest temperature was always recorded in the region of the

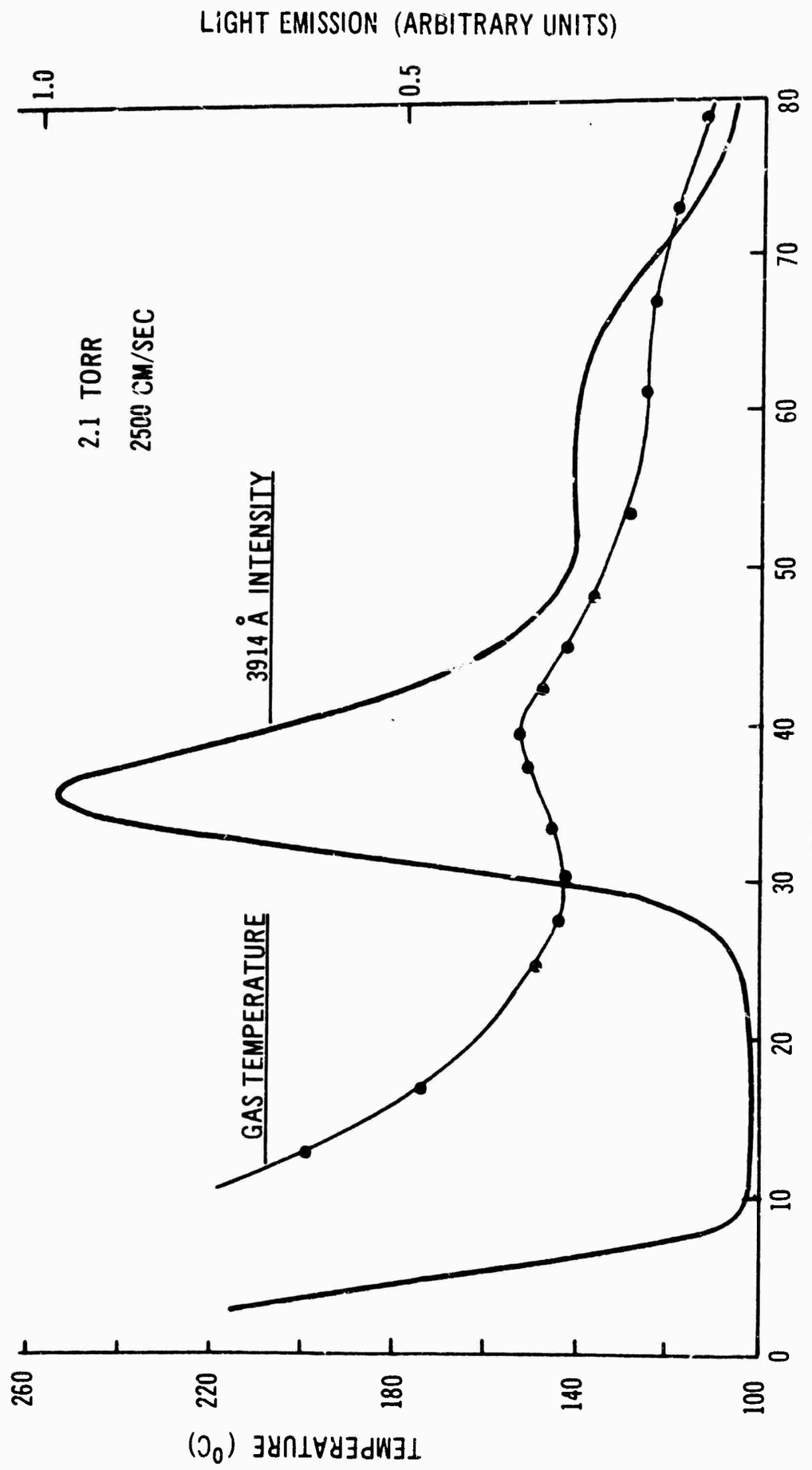

Fig. 7a Thermocouple measurements of the gas temperature in a typical N_2 afterglow (2.1 Torr; 2500cm/sec). The (0,0) band of N_2^+ emission for the same flow is shown for comparison.

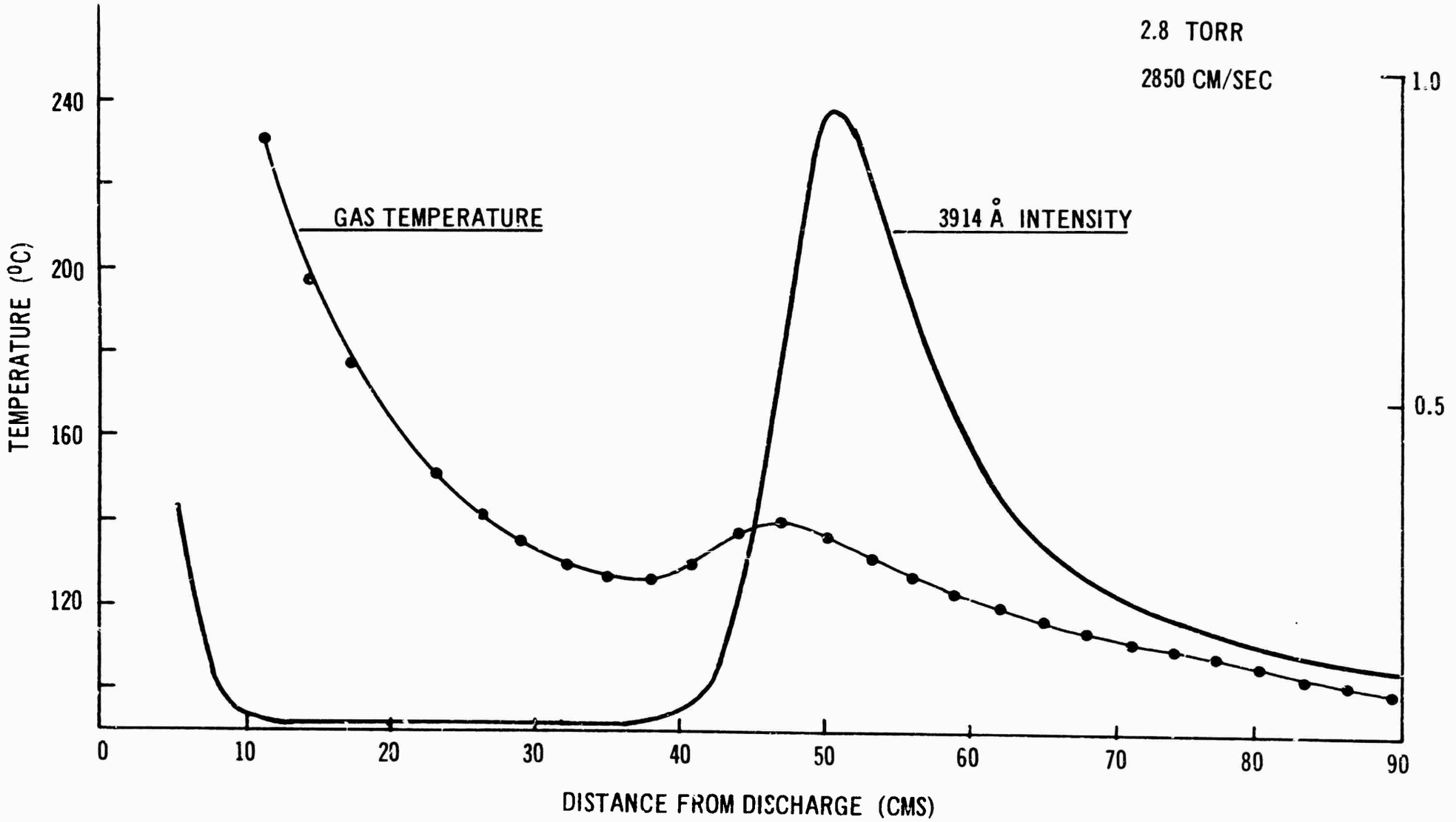

Fig. 7b Thermocouple measurements of the gas temperature in a typical N_2 afterglow (2.8 Torr; 2850 cm/sec) having a pronounced single maximum.

upstream edge of the pink maximum i.e. where the rate of the ion production was most rapid.

As shown in Fig.., the temperature varies quite rapidly in the flow system and as will be discussed in detail in Appendix B, this has a pronounced effect on the flow velocity in the afterglow region which must be taken into account. Since the gas is being locally heated and cooled as it flows down the tube, it is undergoing local expansions and contractions which will result in accelerations and decelerations of the mean flow velocity. Since the temperature varies by more than a factor of two (- 700/300) in traversing the primary discharge, such effects can be quite important in establishing the positions of the various afterglow maxima in the flow system. When calculating the flow velocities quoted in the figures, a temperature corresponding to the average recorded in the pink glow region was used (~ 400°K).

In addition to the optical emission studies carried out using the interference filters as described above, a more detailed spectroscopic examination of the optical emission was also undertaken. A quartz prism spectrometer was used for a quantitative examination of the spectral range from about 0.3μ to 3μ and a grating instrument was used for higher resolution studies in the visible.

Sample spectra taken with the grating spectrometer covering the wavelength region from 3500 Å to 6000 Å are shown in Fig.8. In Fig.8a and 8b spectra of the primary discharge in pure N_2 are shown and Fig. 8c shows a spectrum of the pink afterglow. In these figures a slit width equivalent to about 1.5 Å was used. Glass lenses were employed in the instrument and a photomultiplier was used as the detector. The relative line intensities shown have not been corrected to take this into account.

Because of the method of rf coupling the primary discharge was not uniform in intensity or spectral content. Between the electrodes, the

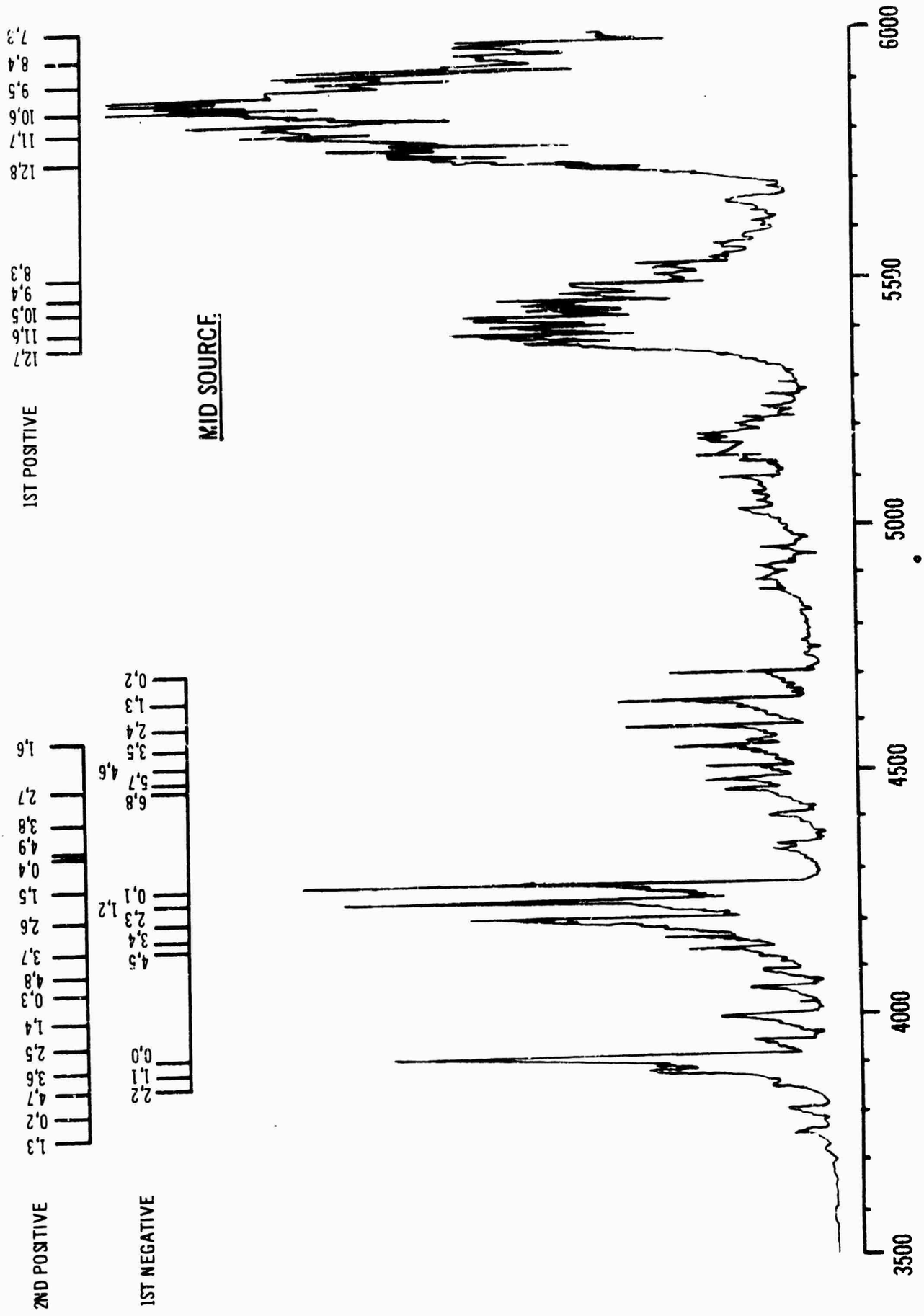

Fig. 8a Sample spectrum of the N_2 primary discharge (between the electrodes) recorded with the grating spectrometer. Slit width equivalent to ≈ 1.5 Å.

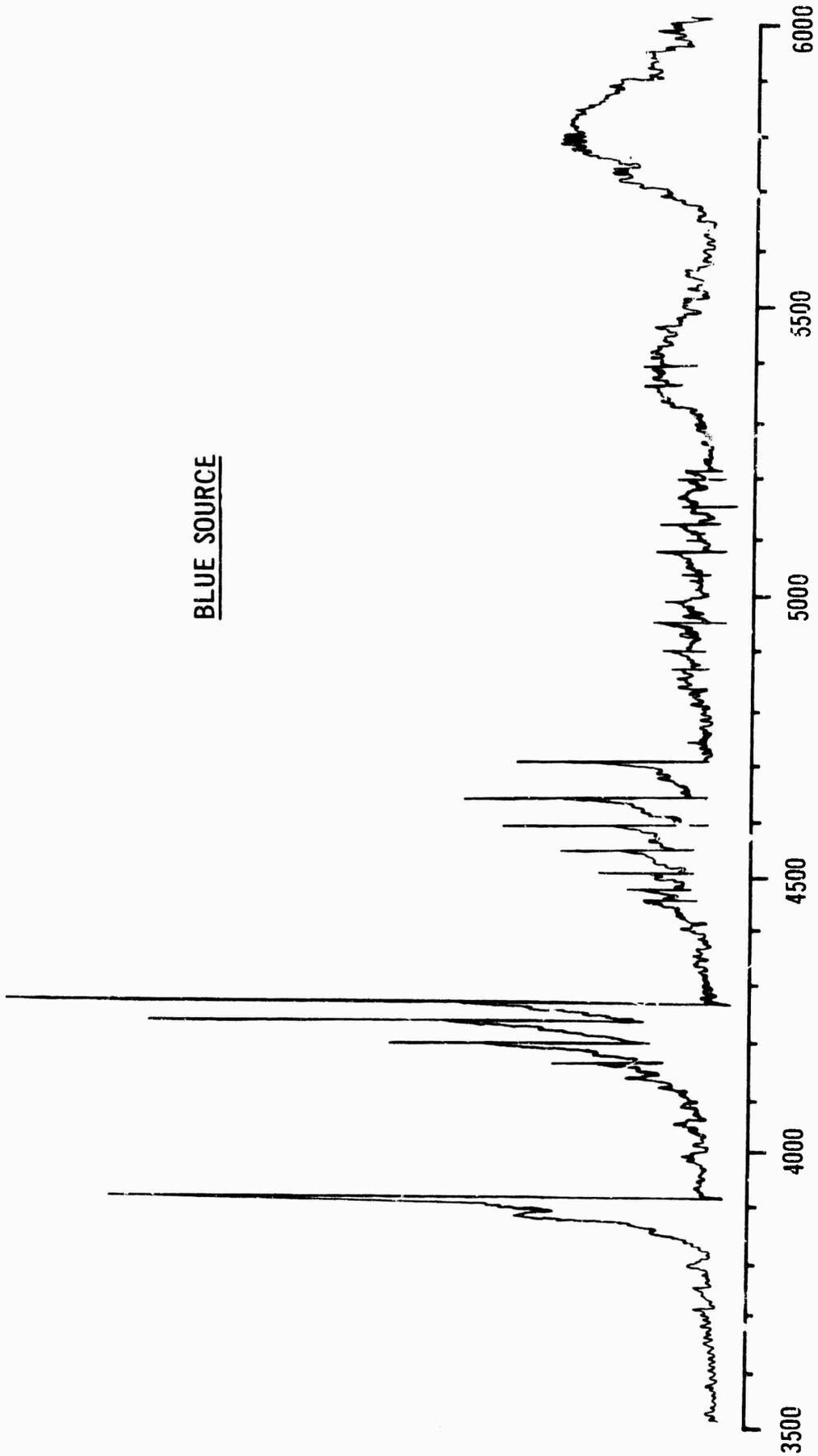

Fig. 8b Sample spectrum of the N_2 primary discharge under the electrodes (blue source) showing the enhancement of N_2^+ (1st Negative system) emission.

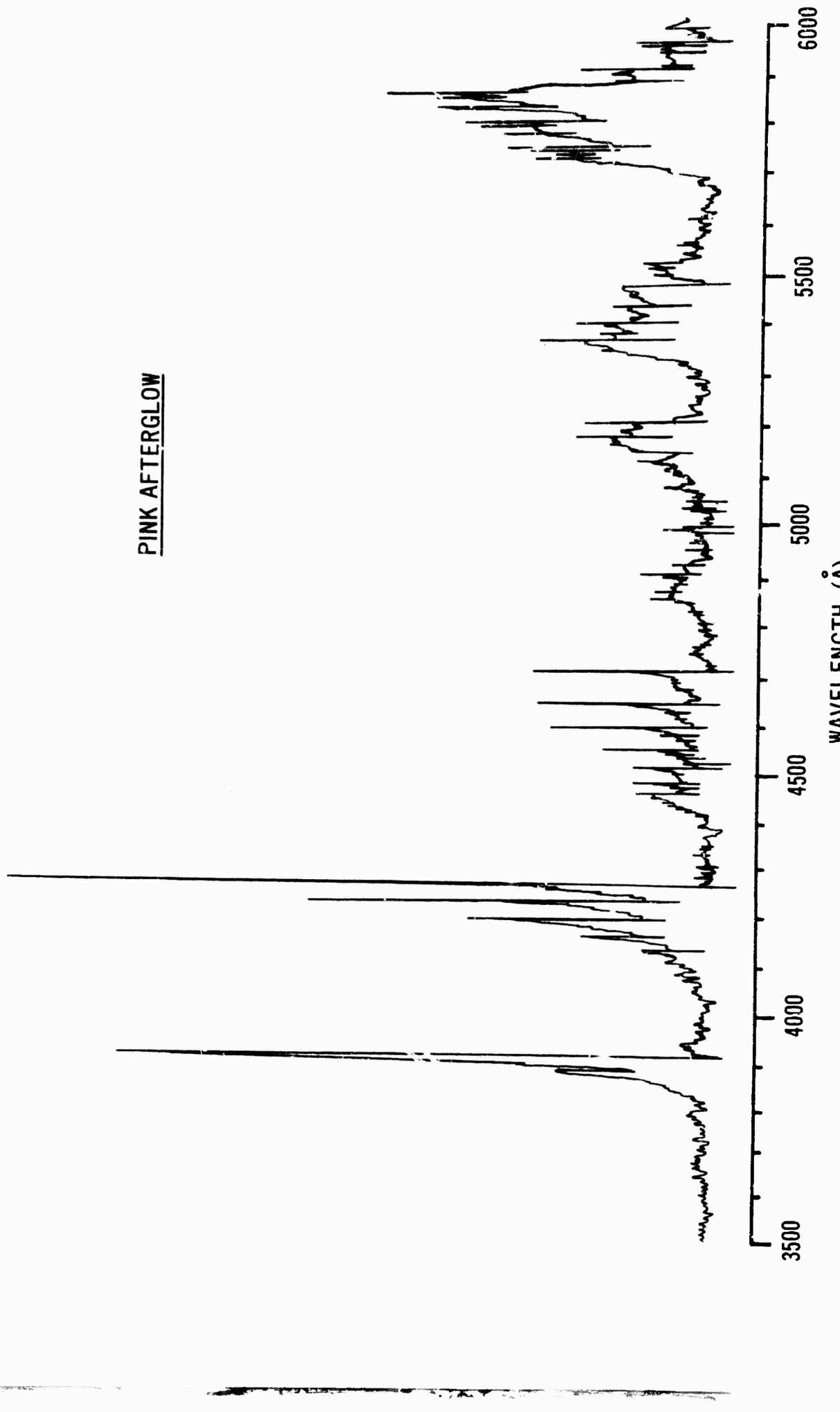

Fig. 8c Sample spectrum of the N_2 pink afterglow.

characteristic nitrogen "orange" colour was emitted and the spectrum for this is shown in Fig. 8a. Under the electrodes the discharge had a very definite blue colouration and the corresponding spectra of this "blue source" region is shown in Fig.8b. A comparison of 8a and b shows that the midsource region emits strongly the N_2 first and second positive systems as well as the first negative (N_2^+ ion) system. The blue source emission is, however, almost entirely composed of first negative system emission. The pink glow also exhibits strong N_2^+ ion emission in the first negative bands along with first positive system emission. Second positive emission in the pink glow is extremely weak. These results are in agreement with previous reports (Beale & Broida, 1959).

Comparison of the first negative bands in the source (Fig.8a) with those in the pink glow (Fig.8c) shows a pronounced difference in the intensity distribution of the vibrational bands. A summary of some of the intensity variations taken from Fig.8 (a and c) is given in Table I. The intensities have all been normalized with respect to the first negative (0,0) band equal to unity in both the source and afterglow spectra (i.e. the relative intensity of the source and pink glow is not apparent from the results quoted).

The final column of the table is most meaningful, showing the changes in the relative band intensities (with respect to 3914 Å intensity) between the source and the pink region. The ratio shown should not depend markedly on the detector response, glass absorption etc., since the same instrument was used in both cases. The 1st Negative transitions originating from $v' = 0$ show a ratio = 1 which is to be expected because of the normalization, but the transitions for $v' = 1,2$ and 3 show a value of about 0.6 indicating that the populations of the higher vibrational levels of the N_2^+ ions in the pink glow are considerably lower than in the main discharge. The variation of

Band	Mid-Source	Pink Afterglow	Afterglow/source
(0,0) (1st Neg)	1	1	1
(0,1)	1.4	1.2	.85
(0,2)	.34	.31	.91
(1,1)	.41	.28	.68
(1,2)	1.2	.69	.57
(1,3)	.47	.31	.65
(2,3)	.81	.41	.5
(2,4)	.43	.28	.65
(3,4)	.37	.23	.62
(3,5)	.33	.20	.6
(10,5) (1st Pos)	.76	.24	.31
(10,6)	1.55	.48	.31

Table I - Intensity Comparison between Source and Pink Glow

intensities in the various 1stneg band systems of the pink glow also show a more nearly "thermalized" distribution than in the discharge. The fact that vibrational equilibrium does not exist in the discharge is not too surprising however, since in the main discharge the N_2^+ ions are being generated by electron bombardment in the presence of intense rf fields.

Table I and Fig.8 also illustrate the relative decrease in emission of the 1st positive system in the pink glow since the corresponding ratio is only about 0.3.

Measurement of the intensity distribution in the rotational structure of the 1st negative bands allows a measurement of the rotational temperature of the ions. The techniques whereby this is achieved are outlined in Appendix D of this report. Results of such rotational temperature measurements are shown in Fig.9.

Fig.9a shows a spectrum of the $\Delta v = 1$ series of the N_2^+ ion with a spectrometer resolution such that the rotational structure is just "resolved". Using such spectra, rotational temperature measurements were made for both the primary discharge and the pink afterglow. The (0,0) and (0,1) bands at 3914 Å and 4278 Å were used so that at each location the temperature was determined twice. Sample results are shown in Fig.9b for the (0,0) band and in (9c) for the (0,1) band using the technique of plotting log (I/K') vs K'(K'+1) as described in Appendix D.

In all cases a rather good straight-line plot was obtained so that the temperature determination was not difficult. Measurements at the two bands generally produced temperatures in agreement to within 5-10%. Under typical operating conditions (pressure = 2Torr) the rotational ion temperature of the source was found to be 1050 ± 75 °K and at the pink glow maximum 550 ± 25 °K. No attempt at a comprehensive study of the rotational temperatures as a function of the discharge properties was undertaken because of the limited spectrometer resolution (~ 1 Å) available. The spectrometer is, however, being modified to increase the resolution by a factor of three so that more accurate measurements can be made.

In general, however, it was found that for a given set of flow conditions, the rotational temperatures recorded both in the discharge and the pink glow were higher (by about 100°K in the pink glow and about 250°K in the discharge) than those recorded with the thermocouple.

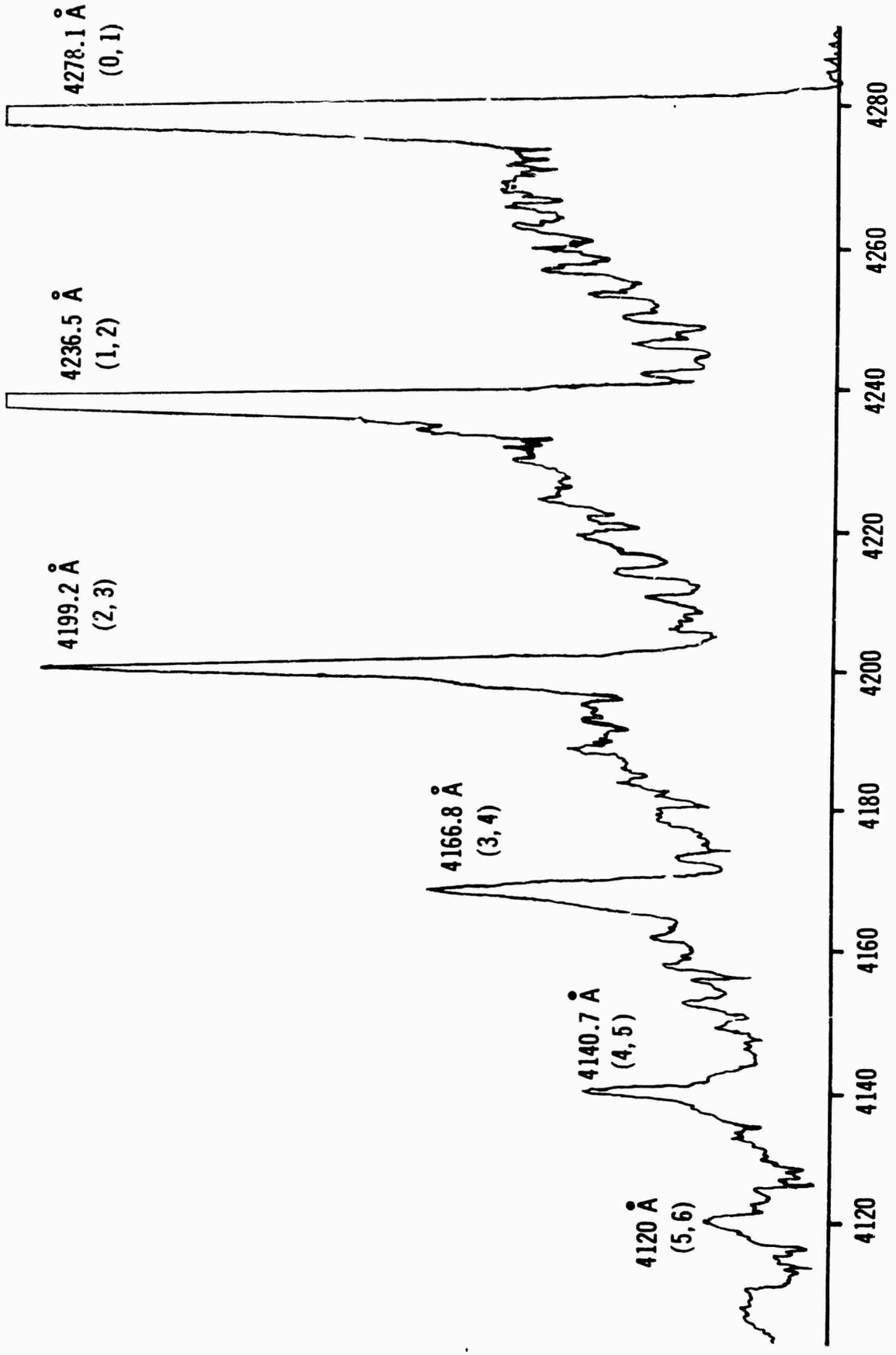

Fig. 9a Sample spectrum of the 1st Neg. $\Delta v=1$ band from which rotational temperatures of the ions are determined.

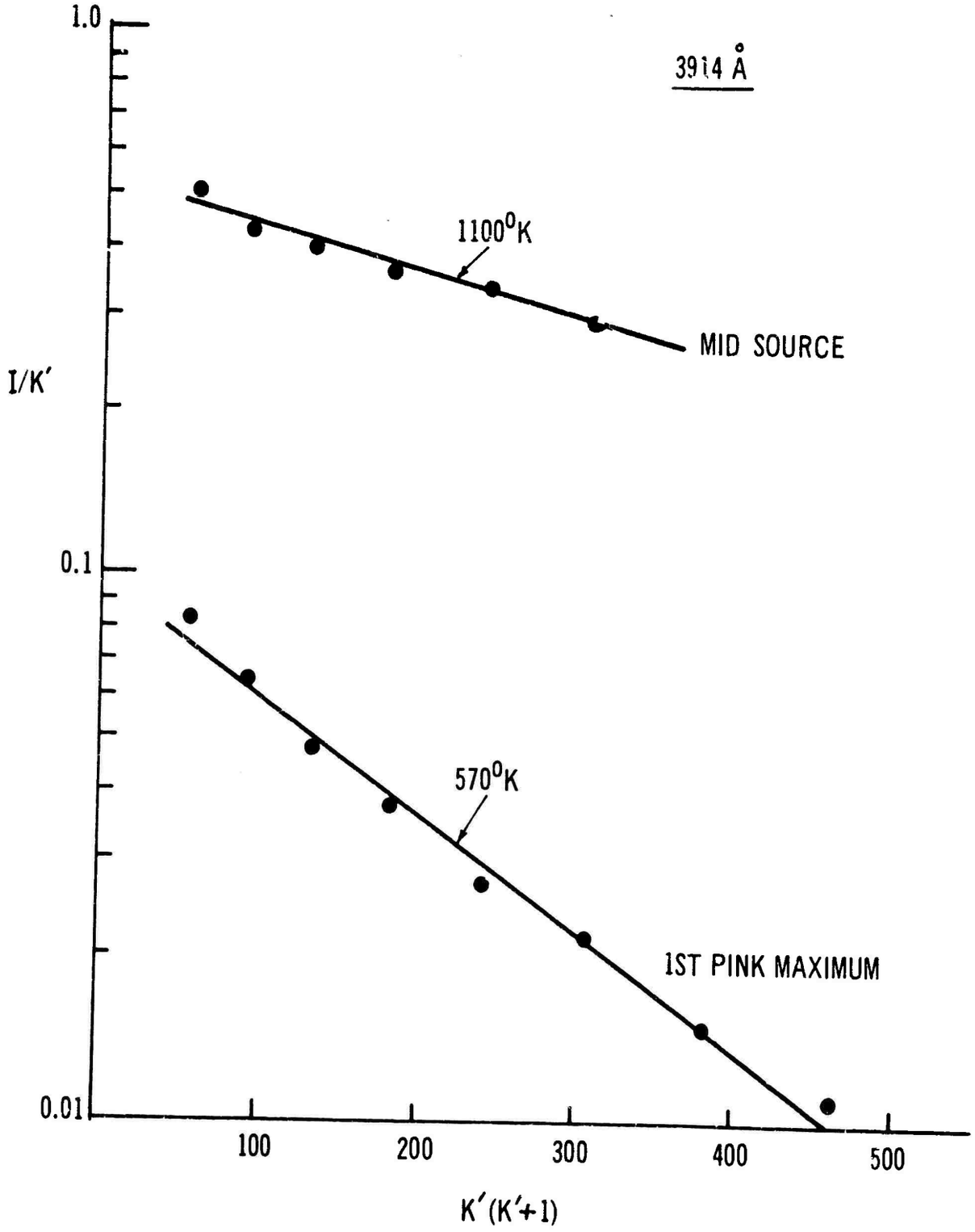

Fig. 9b Sample rotational temperature determinations for the N_2 discharge and the pink glow using the (0,0) band at 3914 Å.

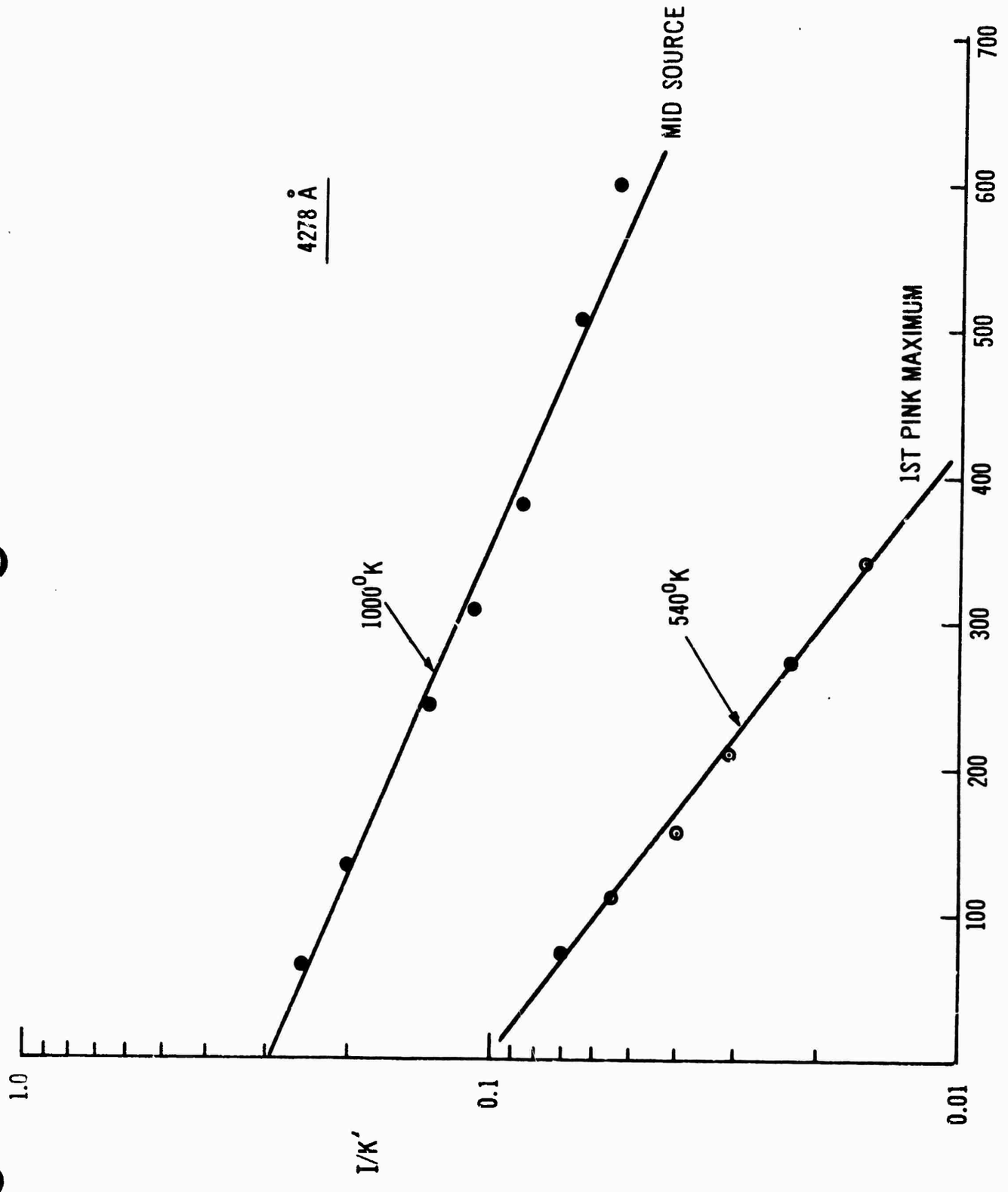

Fig. 9c Sample rotational temperature determinations for the N_2 discharge and the pink glow using the (0,1) band at 4278 Å.

IV SEEDED NITROGEN AFTERGLOW STUDIES

4.1 Introduction

In the present study, the attaching properties of several electronegative gases have been investigated in order to evaluate their suitability as a seed gas for plasma quenching.

Electronegative gases have high probability of forming negative ions by electron capture. There are several mechanisms by which the negative ions are formed .(McDaniel, 1964)

1. Radiative attachment of a free electron by a neutral atom; $e + A \rightarrow A^- + h\nu$.
2. Capture of a free electron by an atom with a third body taking up the excess energy; $e + A + B \rightarrow A^- + B + K.E.$
3. Dissociative attachment by a molecule, the excess of energy going into dissociation of the molecule; $e + XY \rightarrow [XY]^{-*} \rightarrow X+Y^-$
4. Capture of a free electron by a molecule, with vibrational excitation of the molecular ion and its subsequent stabilisation in collision with another molecule (non-dissociative attachment);

$$e + XY \rightarrow [XY]^{-*} ;$$

$$[XY]^{-*} + A \rightarrow [XY]^- + A + K.E. + P.E.$$

The effect of the formation of negative ions on plasma is to replace the highly mobile electrons with less mobile negative ions and thereby altering the electromagnetic properties of the plasma. Most probably the reaction proceeds one step further, leading to a charge exchange process (Carswell et al 1964) between positive ions and negative ions and thus quenching the plasma due to mutual neutralization .

The seeding technique depends on the choice of a gas with large electron capture cross section corresponding to the capture process at the appropriate thermal conditions. Common electro-negative gases with their maximum capture cross sections for attachment are listed below. (Bachynski 1965).

Gas	Maximum cross sections	ev.for maximum attachment
O_2	1.3×10^{-18}	6.2
CO	2.27×10^{-18}	10.1
CO_2	5.1×10^{-19}	7.8
H_2O	4.8×10^{-18}	6.4
HBr	5.9×10^{-17}	.5
I_2	3×10^{-15}	0
SF_6	1.2×10^{-15}	0
	5.7×10^{-16}	.01
CCl_4	1.3×10^{-16}	.02

It must be emphasized that, depending on the thermal conditions, dissociative attachment may not be efficient enough for a good quenching of the plasma. But other processes such as three body attachment may be important at that thermal condition giving rise to high attachment efficiency. As will be discussed below one should also consider the attachment coefficient (η) which takes into account the overall attachment probability irrespective of the process involved. This attachment coefficient η is defined as the number of attachments per electron, per unit length, which is dimensionally equivalent to α, the ionization coefficient (i.e. number of ion pairs produced per electron per cm). Thus, η is the probability that an electron in passing unit length will attach to a gas molecule either by a dissociative process or non-dissociative process.

In the present experiments the following gases have been examined NO, C_2, CO_2, SF_6, H_2O.

4.2 NO Seeding of N_2

The seeding of NO into the nitrogen flow was originally undertaken to use the well-known titration technique for determination of the ground state nitrogen atom concentration in the afterglow. While doing so, however, it became evident that NO had an appreciable quenching effect on the excited species of the afterglow.

In the present section, a brief summary of the titration measurements is given and the experimental results of NO quenching of the N_2 afterglow are reported and discussed.

4.2.1 NO Titration

The NO titration method has been widely used (Kaufman & Kelso, 1957; Harteck & Reeves 1958) in assessing the ground state nitrogen atom concentration of a flowing nitrogen afterglow. It is based on the fast reaction taking place between the nitrogen atom and the NO molecule in which the latter is decomposed. The sequence of events is as follows. Firstly, we get

$$N + NO \rightarrow N_2 + O \qquad (1)$$

If there is an excess of nitrogen atoms on NO molecules, some of the former will react with the oxygen atoms to form NO molecules and eventually produce a typical bluish glow; $N + O + M \rightarrow NO^* + M \rightarrow NO + M + h\nu(\beta\text{-bands})$ (2)

On the other hand, if there is an excess of NO molecules they will combine with the oxygen atoms and produce NO_2 molecules accompanied by a green emission.

$$NO + O \rightarrow NO_2 + h\nu \qquad (3)$$

The end point of the titration is defined by the transition dark period which is easily observed when neither of the blue nor the green emission corresponding respectively to excesses of N and NO are present. The N atom concentration is then calculated from the calibrated NO flow.

The method was used to estimate the N atom concentration for several

different nitrogen flows employed in these studies. In all cases, the nitrogen atom concentration was found to be in the range from 0.5×10^{15} to 1×10^{15}/cc.

The experimental arrangement shown in Fig.2 was used to carry out the titration and the NO was seeded into the region of the dark space preceding the pink glow while the colour transition region used in the titration procedure was located somewhat (about 40 cm) downstream (i.e. in the L-R glow following the pink). For the titration method to be valid, all of the NO molecules must react only with ground state nitrogen atoms. According to Clark and Fairchild (1963), who have carried out photoelectric absorption measurements of the atomic nitrogen concentrations in a similar flowing nitrogen afterglow, it appears that this is the case. Indeed, they obtained corroborative results from the absorption and the NO titration methods assuming, in the latter case, complete disappearance of NO in reaction with ground state nitrogen atoms.

However, there is some question as to the accuracy of the NO titration method as it is normally used even under the assumption of exclusive N-NO reaction. The difficulties stem from the following considerations.

Let us suppose that an NO flow equal to the N-atoms concentration is being admitted to the afterglow in such a way that the titration end point manifestation should be observed. Because the NO stream leaving the seeding probe cannot mix instantaneously with the main flow, there will be an initial transition region or boundary (the nature of which will depend on the specific flow conditions) between the NO and the afterglow. Across this boundary, the NO concentration will vary from pure NO in the "core" of the NO flow down to the equilibrium value in the afterglow. While this transition is occurring, NO molecules will react with N-atoms in the common layer and NO, being in

great excess on the core side of this region, will combine with most of the O-atoms just formed (eq.3). In fact, these two successive reactions are so strong and sudden that at seeding rates around the titration rate, the NO jet is easily observable as an all green stream (NO_2) in the present system.

This mechanism will deplete the NO molecule concentration with the result that on achievement of uniform mixing, the N-atoms will be in excess. These will serve to sustain, to a certain degree, the L-R afterglow or combine with the free O-atoms to generate excited NO of violet emission by the reaction of equation (2). The end point titration will not be observed until the NO flow rate is augmented.

Consequently, the values of the ground state N atom concentration measured, will be an upper limit to the true concentration. It is difficult to assess the possible magnitude of this error since it will depend on the conditions of the flow mixing for each choice of NO injection and flow system. By proper design. it should be possible to keep the error small.

4.2.2 NO Quenching of N_2 afterglow

As mentioned above, nitric oxide was not initially selected because of its electron removal capabilities, but in the course of the NO titration experiments, its efficiency in destroying the intensity of the nitrogen afterglow was evident and it was decided to carry out measurements of its quenching ability.

A complete assessment of the quenching properties of a seed gas with a view to an explanatory account should include the possibility of examining the effect produced on each of the species. The available instrumentation allowed the observation of three of the significant variables of the afterglow namely: the first positive system (excited N_2) and the first negative system (excited N_2^+) by optical technique, and the total ion density through the

double floating probe method. In the following seeding experiments, the afterglow is examined with the 5780Å filter looking at the $\Delta v=4$ transitions of N_2^*. The 3914 Å filter monitors the N_2^+ first negative system while the total ion concentration variation is detected by the change in the saturation current flowing between the (20 volt) biased double probe.

Figure 10a, b and c shows the longitudinal variation of each of the above parameters downstream from the discharge for different NO/N_2 seeding ratios and main flow conditions of 3.7 Torr pressure and 2480 cm/sec velocity. Fig. 11a and b illustrate the same variation for the first negative (3914 Å) and the first positive (5780 Å) systems respectively for a wider range of NO/N_2 seeding ratios in the case of main flow conditions of 2.9 Torr pressure and 2190 cm/sec velocity. All curves are normalized to the pure nitrogen afterglow case.

A first look at the family of curves (Fig.11) reveals a downstream shift of the intensity maximum for increasing seeding ratios up to the titration ratio. There is only one exception to this trend, that is for the seeding ratio of the first positive system (Fig.11b) where an upstream shift was recorded. No particular meaning is attached to this since it is obvious that the whole curve was displaced either spuriously or inadvertantly along the x-axis of the recorder. The downstream shift of the maximum could be a consequence of the pressure increase created by the seed gas or could be caused by a true reduction of the ion concentration at the upstream edge of the pink glow.

At the titration point, the pink glow maxima disappear completely and the emission intensities down the tube are reduced to the "background" level. For seeding ratios increasing above the titration point, a maximum develops near the seed probe which gets smaller and closer to the probe as

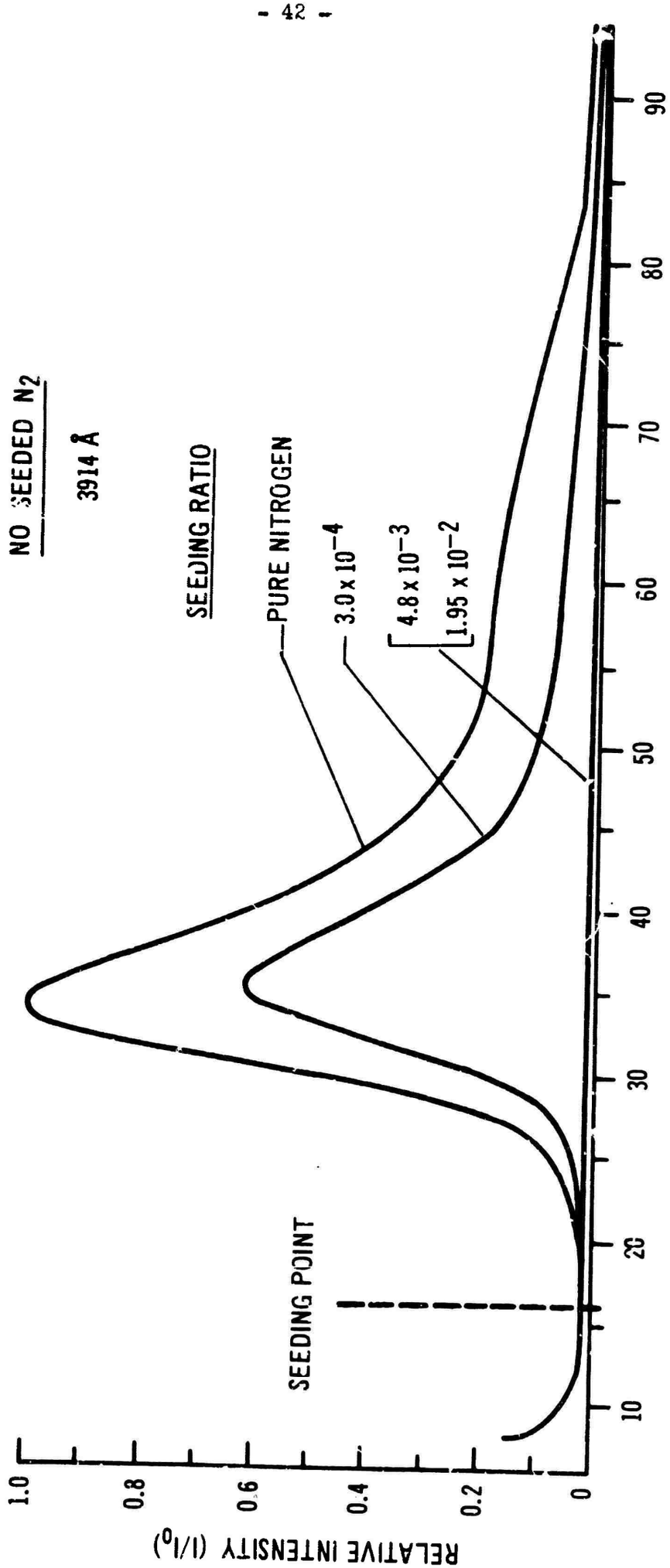

Fig. 10a Relative variation of the emission intensity of the first negative system (3914 Å) downstream along the afterglow for different NO/N_2 seeding ratios. Curves are normalized to the maximum intensity obtained in the pink region of the pure nitrogen afterglow. ($p = 3.7$ Torr, flow velocity = 2480 cm/sec).

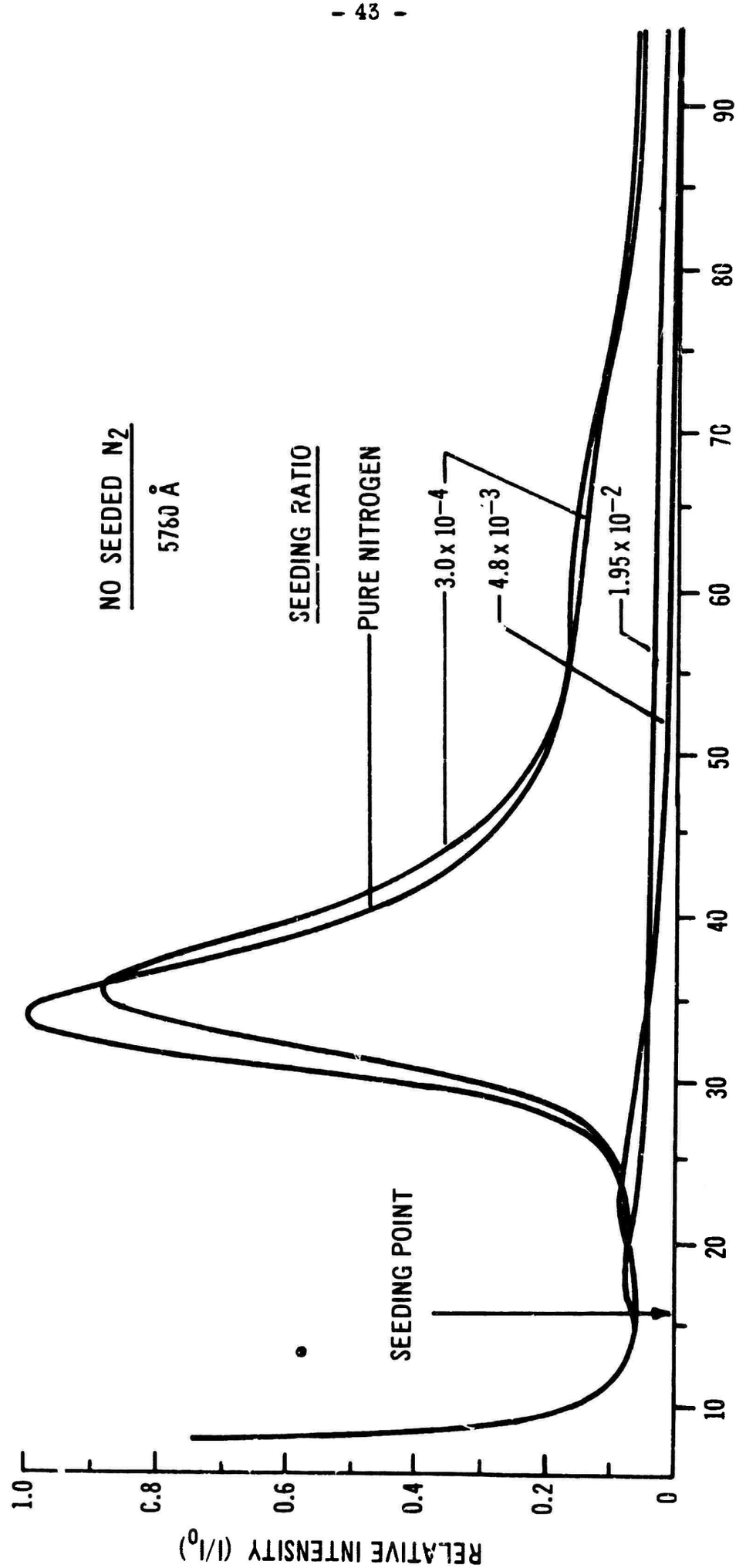

Fig. 10b Relative variation of the emission intensity of the first positive system (5780 Å) downstream along the afterglow for different NO/N_2 seeding ratios. Curves are normalized to the maximum intensity obtained in the pink region of the pure nitrogen afterglow. ($p = 3.7$ Torr, flow velocity = 2480 cm sec).

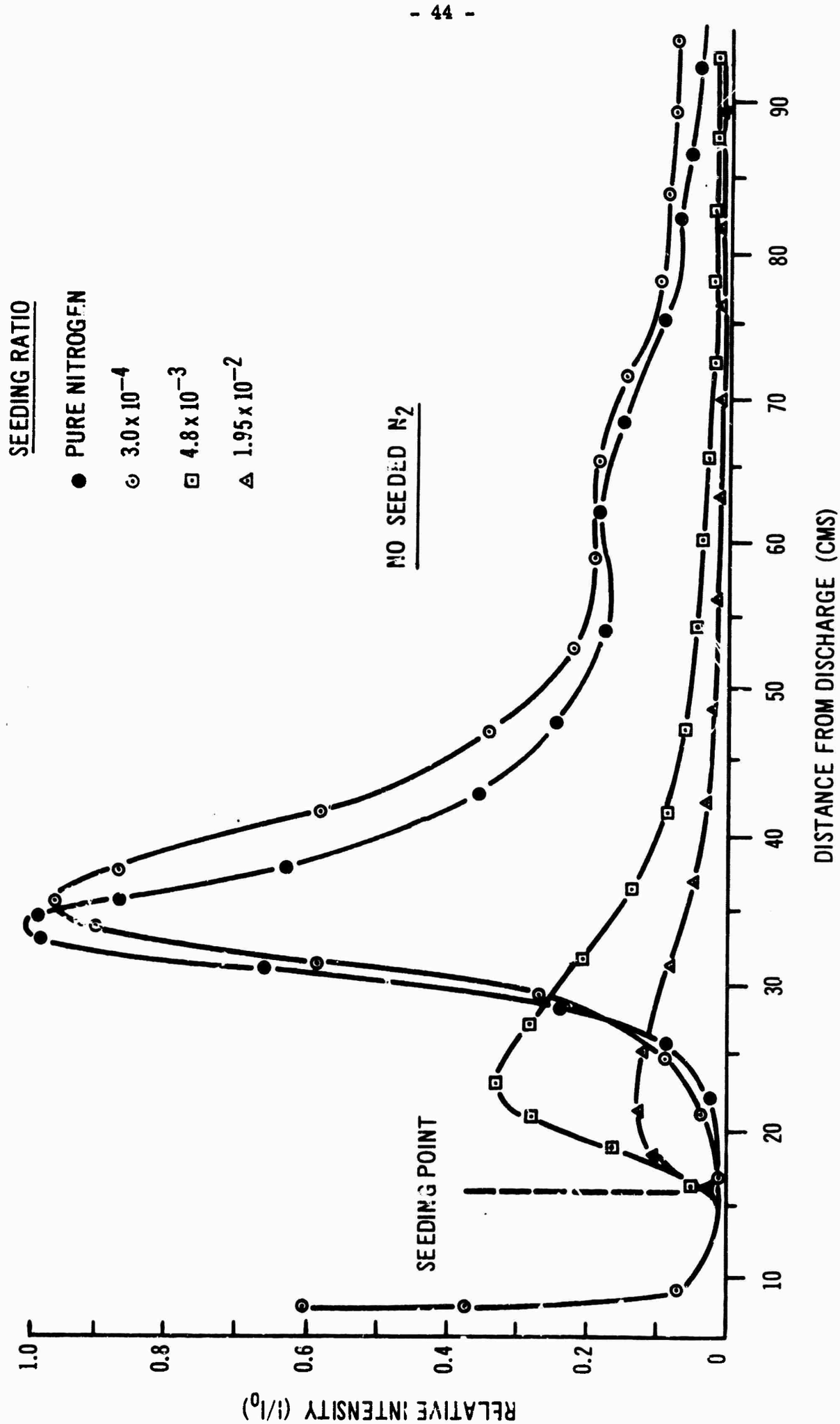

Fig. 10c Relative variation of the total ion concentration (double probe saturation current) downstream along the afterglow for different NO/N_2 seeding ratios. Curves are normalized to the maximum obtained in the pink region of the pure nitrogen afterglow. ($p = 3.7$ Torr, flow velocity = 2480 cm/sec).

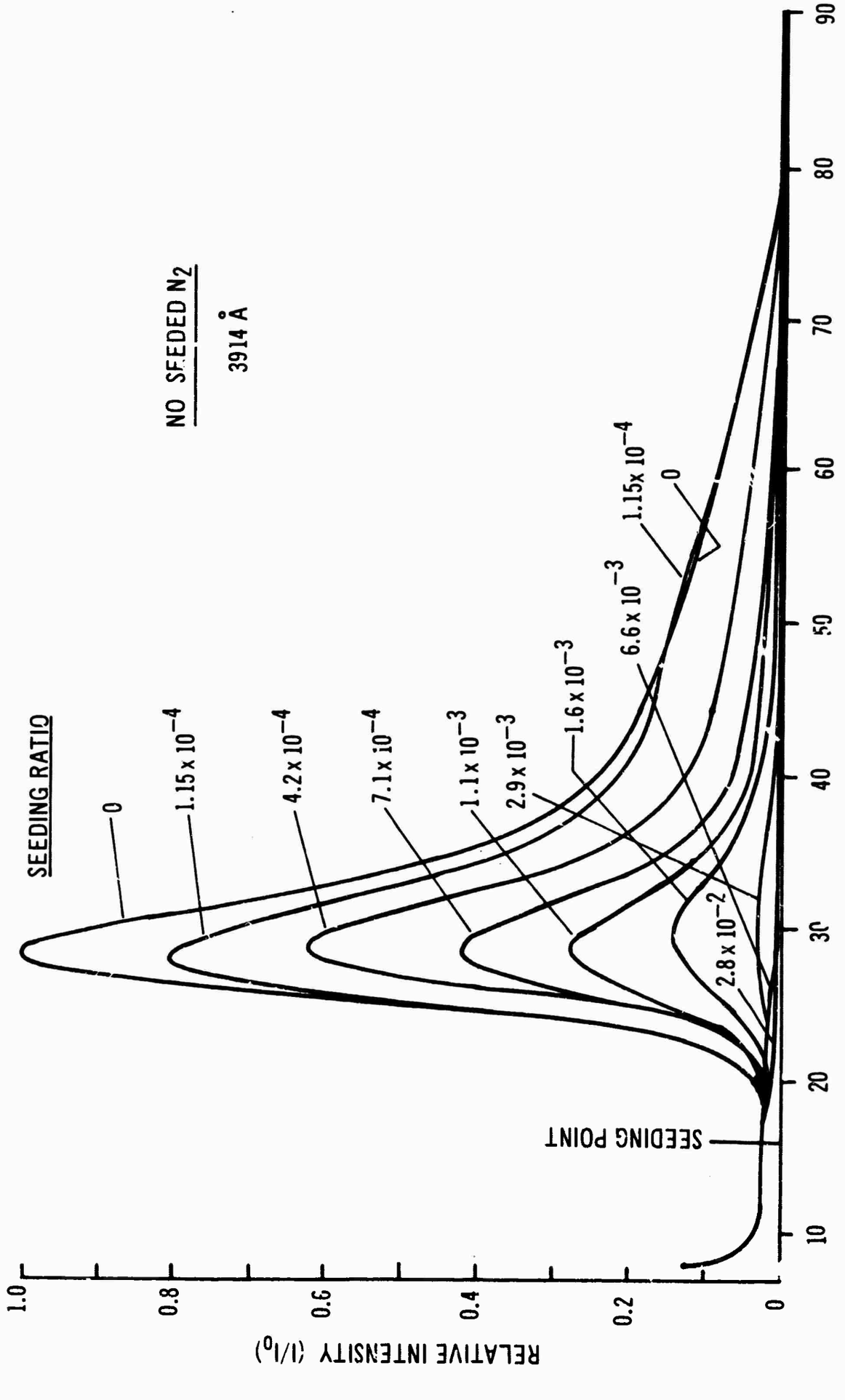

Fig. 11a Relative variation of the emission intensity of the first negative system (3914 Å) downstream along the afterglow for various NO/N_2 seeding ratios. Curves are normalized to the maximum intensity obtained in the pink region of pure nitrogen afterglow. ($p = 2.9$ Torr, flow velocity = 2190 cm/sec)

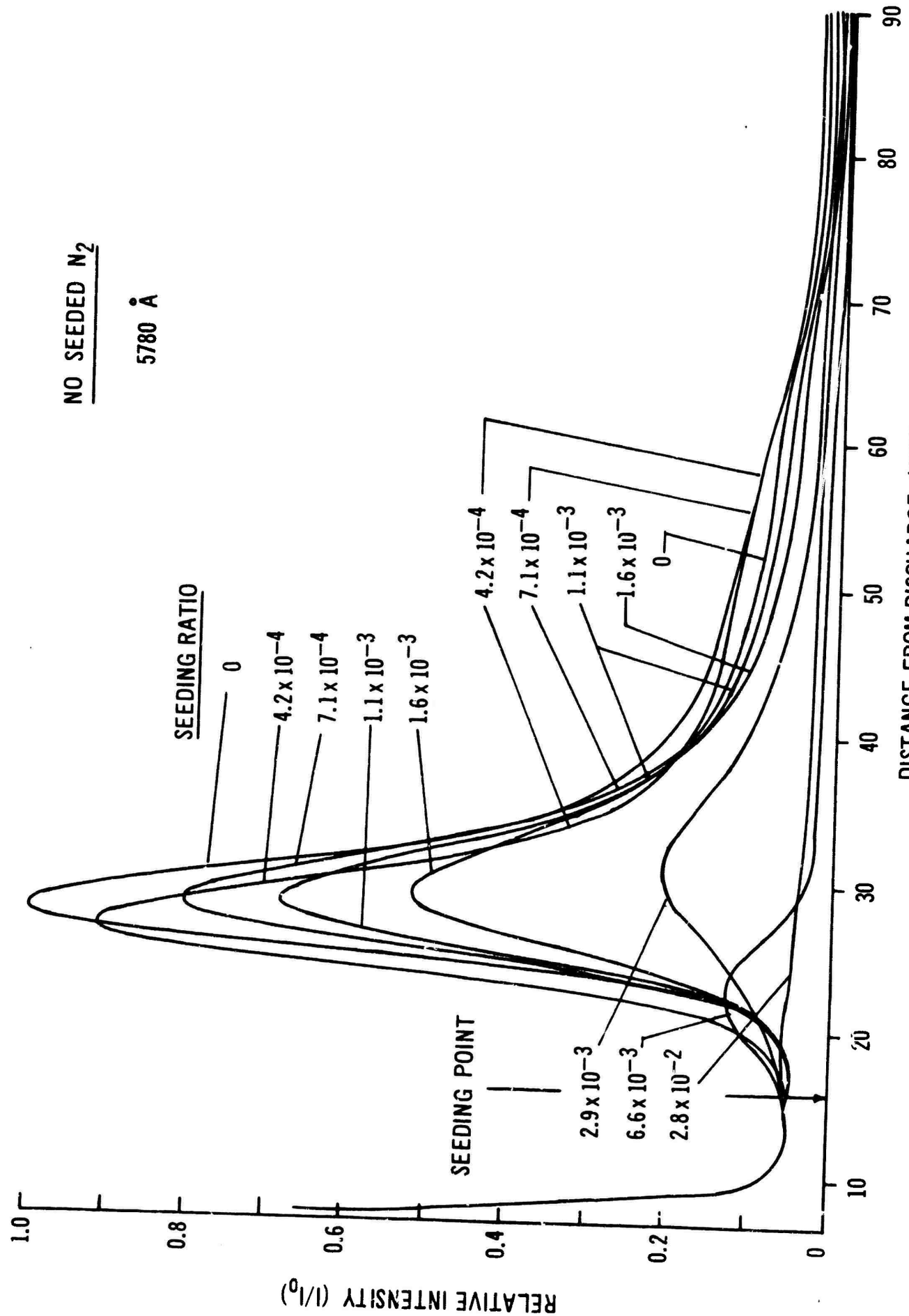

Fig. 11b Relative variation of the emission intensity of the first positive system (5780 Å) downstream along the afterglow for various NO/N_2 seeding ratios. Curves are normalized to the maximum intensity obtained in the pink region of the pure nitrogen afterglow. (p = 2.9 Torr, flow velocity = 2190 cm/sec).

the seeding ratio is increased. (Fig.10b,c and Fig.11b). This maximum is not seen, however, in the case of the optical emission (Fig.10a and Fig.11a) while it reaches considerable height with the double probe. The upstream end of the plots also presents some interesting features. Firstly, the superimposition of the traces obtained upstream from the seed probe shows that no appreciable back diffusion takes place. Secondly, the dark space is not only poorly populated in excited neutral $[N_2(B^3)]$ and ionized $[N_2^+(B^2)]$ nitrogen molecules, but the total ion concentration is less than 1% of that existing at the maximum of the pure nitrogen pink afterglow. Finally, at the far left of the figures, the steep increase of the intensities points out the high concentration in the discharge tail flame (active discharge fields blown down the tube by the gas flow) of the three systems investigated, mainly of the first positive and the total ion density.

Fig.12 presents a plot of comparative quenching produced on both emitting systems (3914 Å and 5780 Å) and the total ion concentration as a function of the seeding ratio. The measuring probes were located at the maximum of the pure nitrogen pink afterglow. As already evident in Fig.10 and 11, the negative system $[N_2^+(B^2)]$ is more easily affected by NO seeding while the first positive $[N_2(B^3)]$ roughly follows the behaviour of the total ion concentration measured by the probe. All three curves exhibit a minimum at the titration point followed by a maximum which is well developed in the case of the double probe. These successive minimum and maximum were to be expected from the axial scans (Fig.10 and 11) where it is seen that the upstream maximum which builds up at titration seeding ratios extends its tail end past the probing positions (Fig.10c).

It is also interesting to compare, for a given seeding ratio, the relative longitudinal variation of the three systems investigated. This can be found in Fig.13 where the curves are shown for NO/N_2 ratios of 0, 3.0×10^{-4}

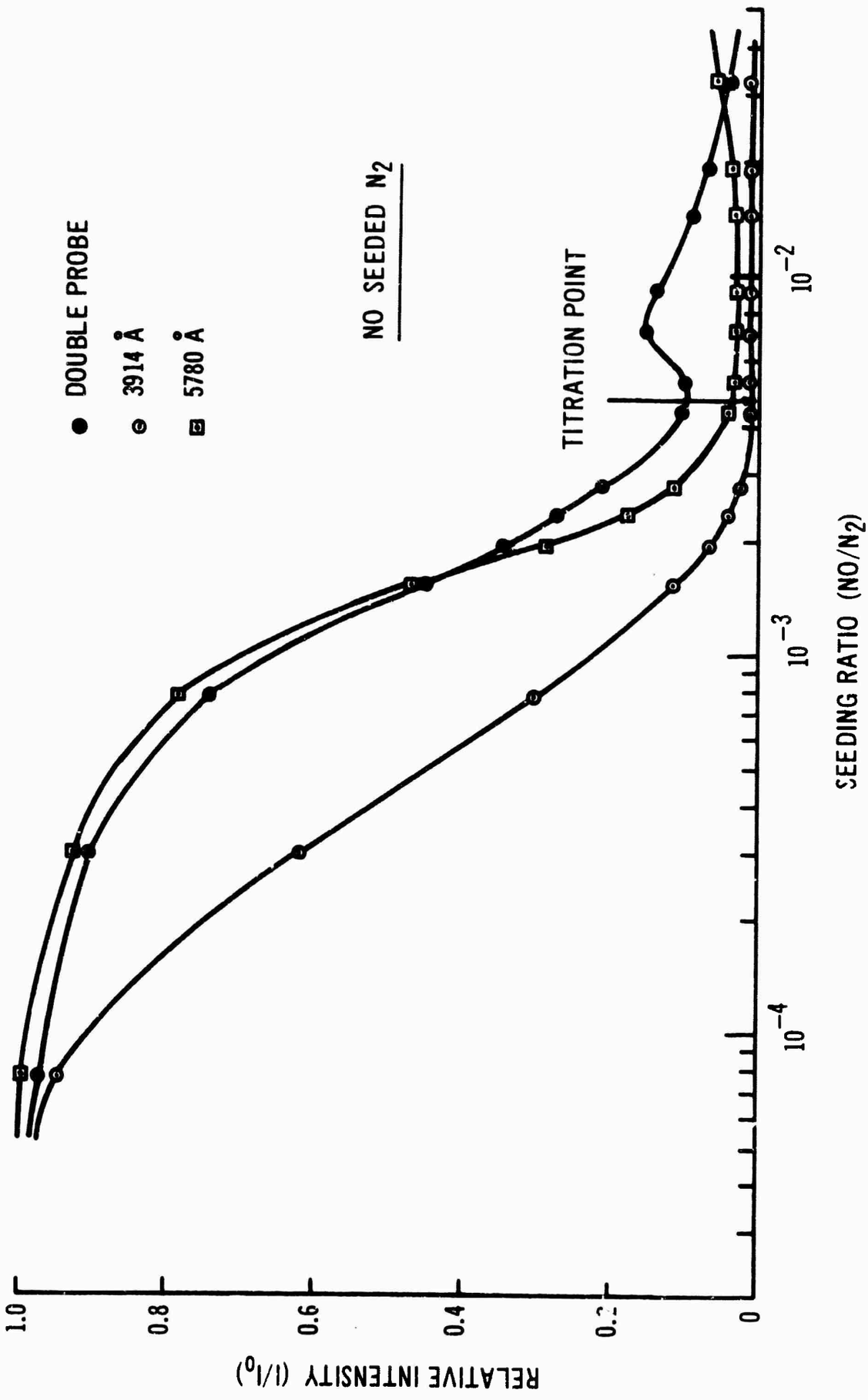

Fig. 12 Comparative plot of the quenching produced in the three investigated systems by nitric oxide as function of NO/N_2 seeding ratio. Curves are normalized at their maximum. (p = 3.7 Torr, flow velocity = 2480 cm/sec.)

and 4.8×10^{-4} (titration) respectively in a,b and e. In order to make such a plot, the curves were normalized to the same value at the maximum. Except for the case (e), the curves in general do not diverge by more than 15% of the value at the maximum.

The total ion current follows a pattern which resembles very much that of the neutral system [N_2 (B^3)]. Relating this last observation to similar ones made in connection with Fig.10, 11 and 12, it would appear that NO seeding has very similar quantitative effects on both the total ion and the excited neutral nitrogen molecule [$N_2(B^3)$] concentrations.

Spectra of the NO seeded N_2 afterglow running from 3500 Å up to about 6000 Å have been recorded, but no additional strong lines other than those belonging to the pink nitrogen afterglow were detected (cf. Fig.8).

4.2.3 Discussion

A theory of the excitation mechanisms of the nitrogen afterglow recently put forward by Prag & Clark (1963) seems to account for the observed features of the short lived pink glow. It postulates the formation in the discharge of a metastable sextet S, nitrogen atom N($3s\ ^6S^0$), 17.2 ev. (not yet directly observed) which participates in the formation of a loosely bound N_4 molecule sufficiently energetic (25.5 ev) to produce all of the known delayed excitations. The reaction would be as follows:

$$N(3s\ ^6S^0) + N + N_2(x) \rightarrow N_4 \qquad (1)$$

The dark space prior to the pink region would primarily contain ground-state N_2 molecules, ground-state and low-lying metastable nitrogen atoms, excited nitrogen molecules ($N_2[A^3]$) and N_4 molecules.

From the interactions of ground-state N atoms and $N_2[A]$ molecules with N_4 molecules, all the observed excited species can be generated.

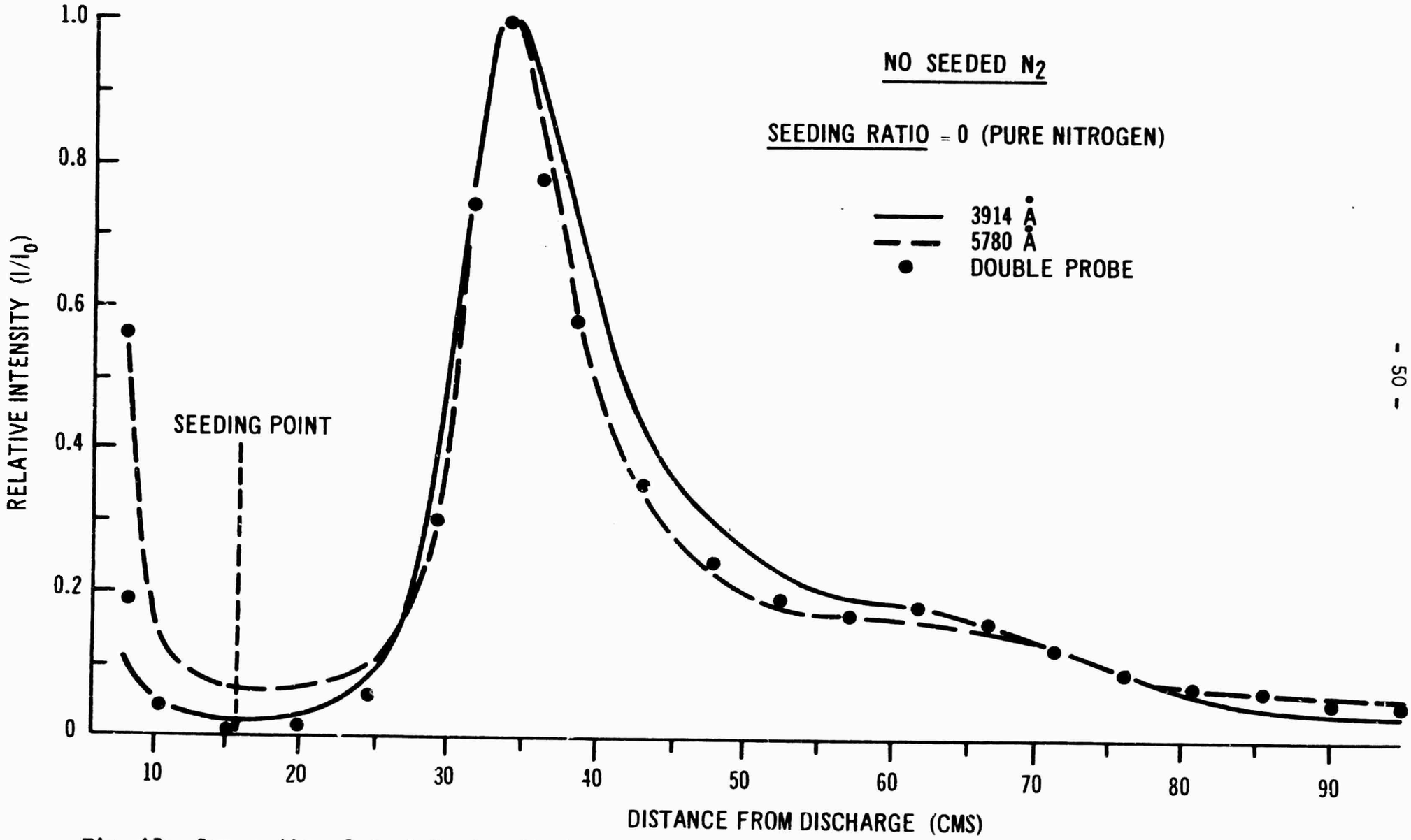

Fig. 13a Comparative plot of the longitudinal distribution of the three investigated systems in the case of an NO/N_2 seeding ratio of zero (pure nitrogen). Curves are normalized at their maximum. (p = 3.7 Torr, flow velocity = 2480 cm/sec)

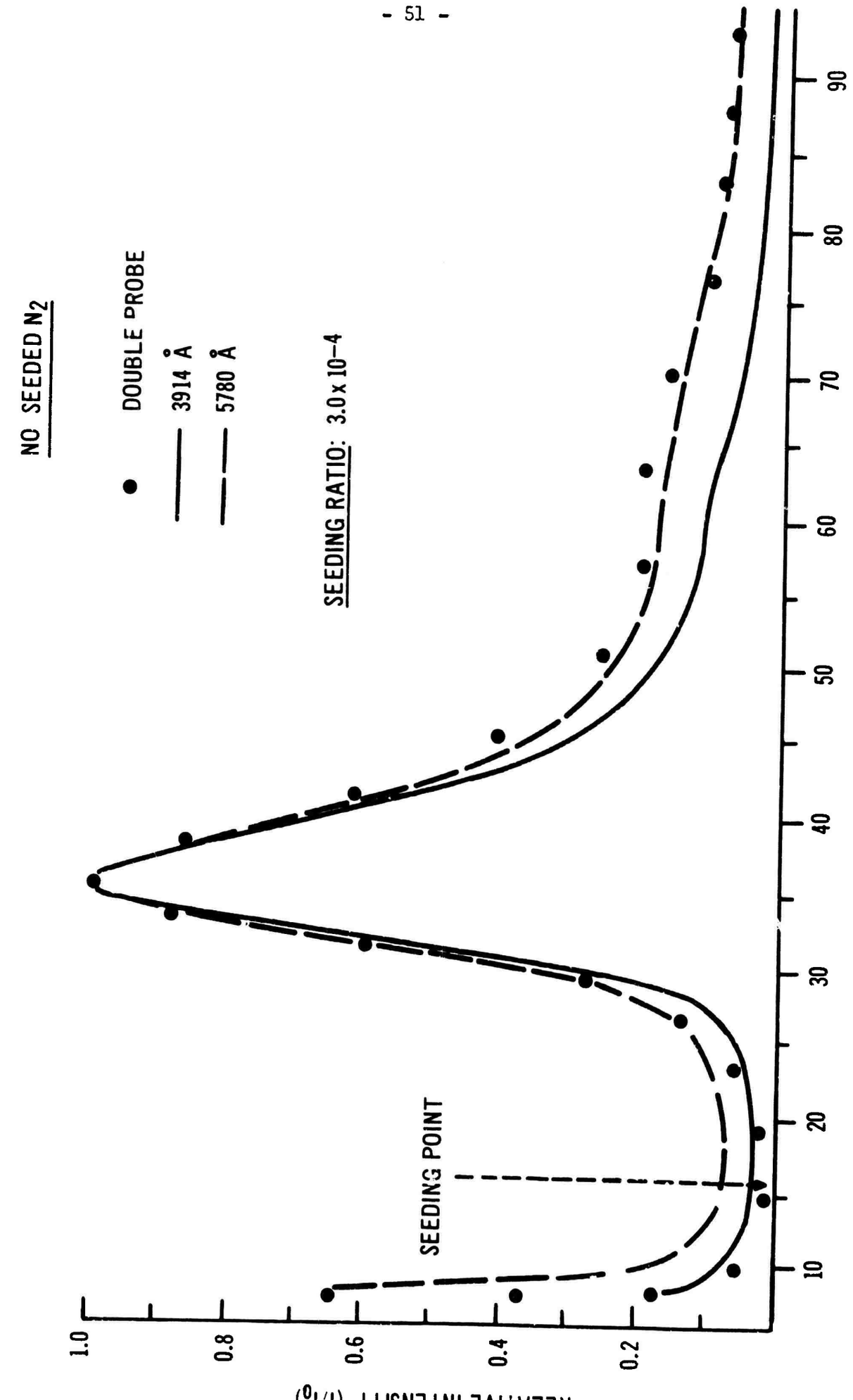

Fig. 13b Comparative plot of the longitudinal distribution of the three investigated systems in the case of an NO/N_2 seeding ratio of 3×10^{-4}. Curves are normalized at their maximum ($p = 3.7$ Torr, flow velocity = 2480 cm/sec)

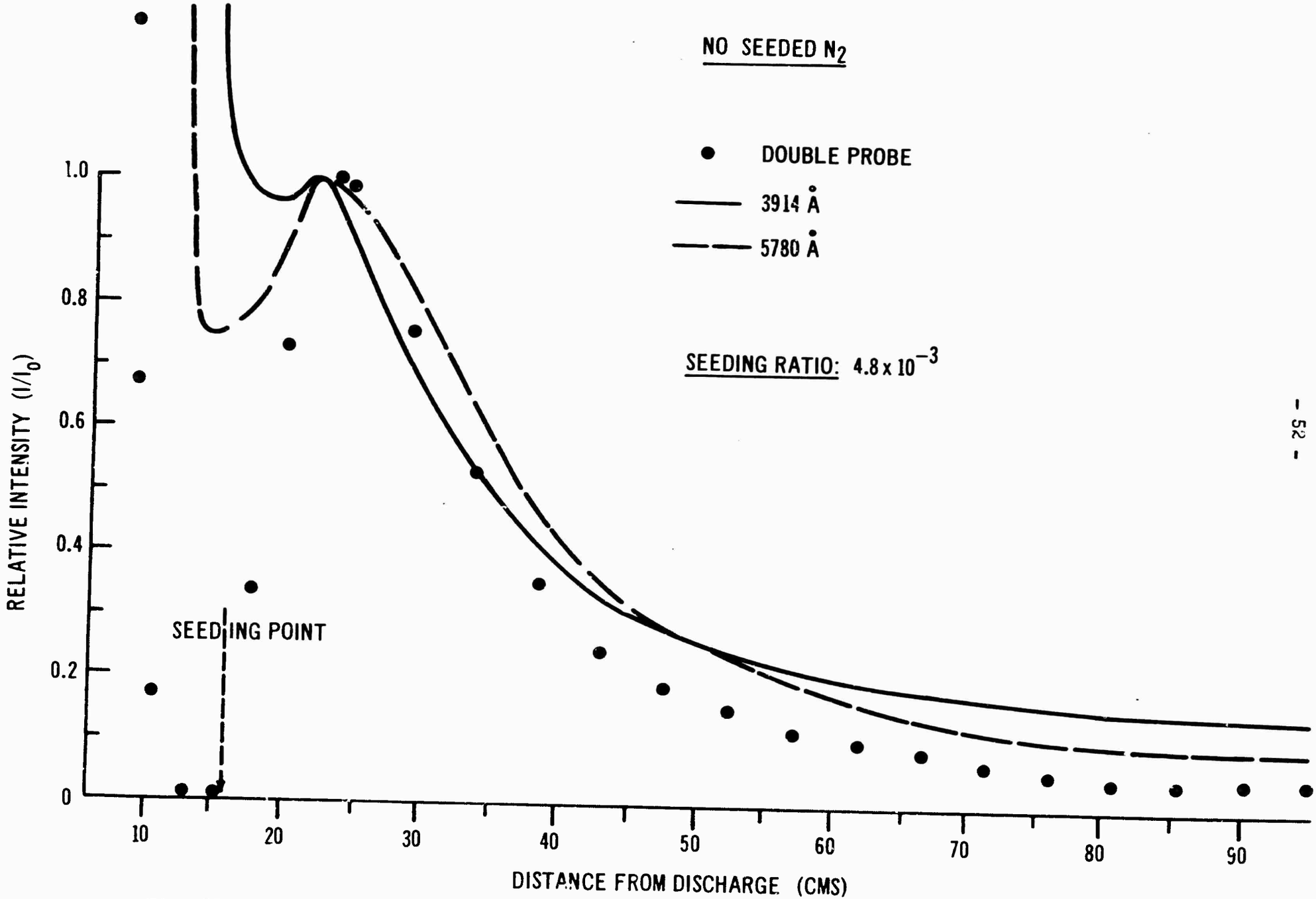

Fig. 13c Comparative plot of the longitudinal distribution of the three investigated systems in the case of an NO/N_2 seeding ratio of 4.8×10^{-3} (titration point). Curves are normalized at their maximum. (p = 3.7 Torr, flow velocity = 2480 cm/sec).

$$N_4 + N \rightarrow N_2(x) + \underset{(1st\ neg)}{N_2^+(B^2)} + e^- + N^* \qquad (2)$$

$$N_4 + N \rightarrow N_2(x) + \underset{(2nd\ pos)}{N_2(C^3)} + N^+ + e^- \qquad (3)$$

$$N_4 + N_2(A^3) \rightarrow N_2(x) + \underset{(2nd\ pos)}{N_2(C^3)} + N + N^* \qquad (4)$$

$$N_4 + N_2(A^3) \rightarrow N_2(x) + 2N + \underset{(1st\ neg)}{N_2^+(B^2)} + e^- \qquad (5)$$

$$N_4 + M(> 1.5\ ev) \rightarrow N_2(x) + N + \underset{(sextet)}{N(3s\ ^6S^0)} + M \qquad (6)$$

$$N_4 + e^- \rightarrow N_2(x) + \underset{(1st\ neg)}{N_2^+(B^2)} + 2e^- \qquad (7)$$

This theory seems also to explain most of the observations made in connection with NO seeding. Indeed, knowing the great affinity of NO for ground-state nitrogen atoms, it is obvious that reactions (2) and (3) will become less and less significant as the N atom concentration is depleted. Therefore, an increased quenching of the first negative and the first positive (by cascade from the second positive) systems as well as of the total ion density should take place for increasing NO seeding rates (Fig.10 and 11). In fact, on the basis of the nearly complete quenching of the pink glow achieved with NO, one seems justified to say that reactions (4) and (5) are much less probable that mechanisms (2) and (3) for the actual conditions of operation.

Some quenching of the total ion density may also be attributed to the electron attachment properties of NO. Measurements by Bradbury (1932) give NO an attachment probability of about 1/10 that of H_2O for the conditions prevailing in the pink glow ($T_e \simeq 10{,}000^\circ K$, p = 3.7 Torr, $E/p \simeq 1.5$). The reaction is of the dissociative type and requires the formation of the

complex $(NO)_2$:

$$2NO \rightarrow (NO)_2$$

$$(NO)_2 + e^- \rightarrow NO^- + NO$$

The electron attachment contributes to the ion quenching in two ways. Firstly, the electrons attaching to $(NO)_2$ are no longer available for reaction (7) and thereby the N_2^+ ion generation is reduced. Secondly, the NO^- negative ion could undergo a charge exchange interaction with a positive ion with a larger cross section than an electron would present for recombination with the same positive ion. The disappearance of mechanism (7) due to electron attachment can account for the faster quenching of the first negative (N_2^+ [B^2]) as observed in Fig.12.

The maxima found close to the NO seeding probe in the case of the total ion and excited neutral N_2(5780 Å) cases (Fig.10 and 11) which also give rise to the maxima shown in Fig.12 are not easily explained. They coincide with this non-uniform transition region created by the streaming NO jet before it can intimately mix with the main flow. Well separated yellow, blue and green emission "strata" are indeed observed in this region showing the presence of excited N_2, NO and NO_2. It is possible that these maxima and the transition region can be reduced considerably by using a seeding probe design that would permit a faster and more efficient mixing. This points up again the need for a careful assessment of the flow geometry when evaluating the results near the mixing region of any seed gas.

The ability of NO for quenching the nitrogen afterglow will be compared in section V with that of other seed gases after the results obtained with these have been described in the following sections.

4.3 O_2 Seeding of N_2

Oxygen was chosen as a seed gas in the present experiments because of the fact that its attachment processes have been studied by many workers over a wide range of energy values and are relatively well-known.

Figure 14(a-e) shows sample longitudinal variation of the intensity of excited ion (N_2^+) emission at 3914 Å, the intensity of excited molecules of emission at 5780 Å and the double probe saturated ion current for different seeding ratios. The results show an appreciable quenching effect.

Figure 15(a-c) shows the normalized plot of intensity of excited ion (3914), excited molecules (5780), and double probe saturated ion current for different seed ratios along the length of the tube. The curves are found to follow each other quite closely.

Figure 16 shows the decay of the intensity of the maximum pink glow for different seed ratios as measured by the three techniques.

From Figure 16, the excited ion intensity is seen to drop more rapidly than the double probe saturated ion current as can be expected because excited ion concentration is not necessarily the same as the total ion concentration. The excited neutral intensity follows the double probe saturated current more closely. However, for a seed ratio of the order of 1%, all curves approach zero indicating a complete quenching of the plasma (pink afterglow).

Oxygen shows a dissociative attachment cross section of $\sim 1.3\times10^{-18} cm^2$ at 6.2 ev. according to a two body process given by

$$e + O_2 \rightarrow O + O^-$$

But considering the electron temperature in the pink glow (10^4K) it seems that the two body attachment is not efficient enough for the removal of electrons and to account for the quenching. However, recent work of Hurst & Bortner (1958) and Chanin et al (1962) have shown a three body process

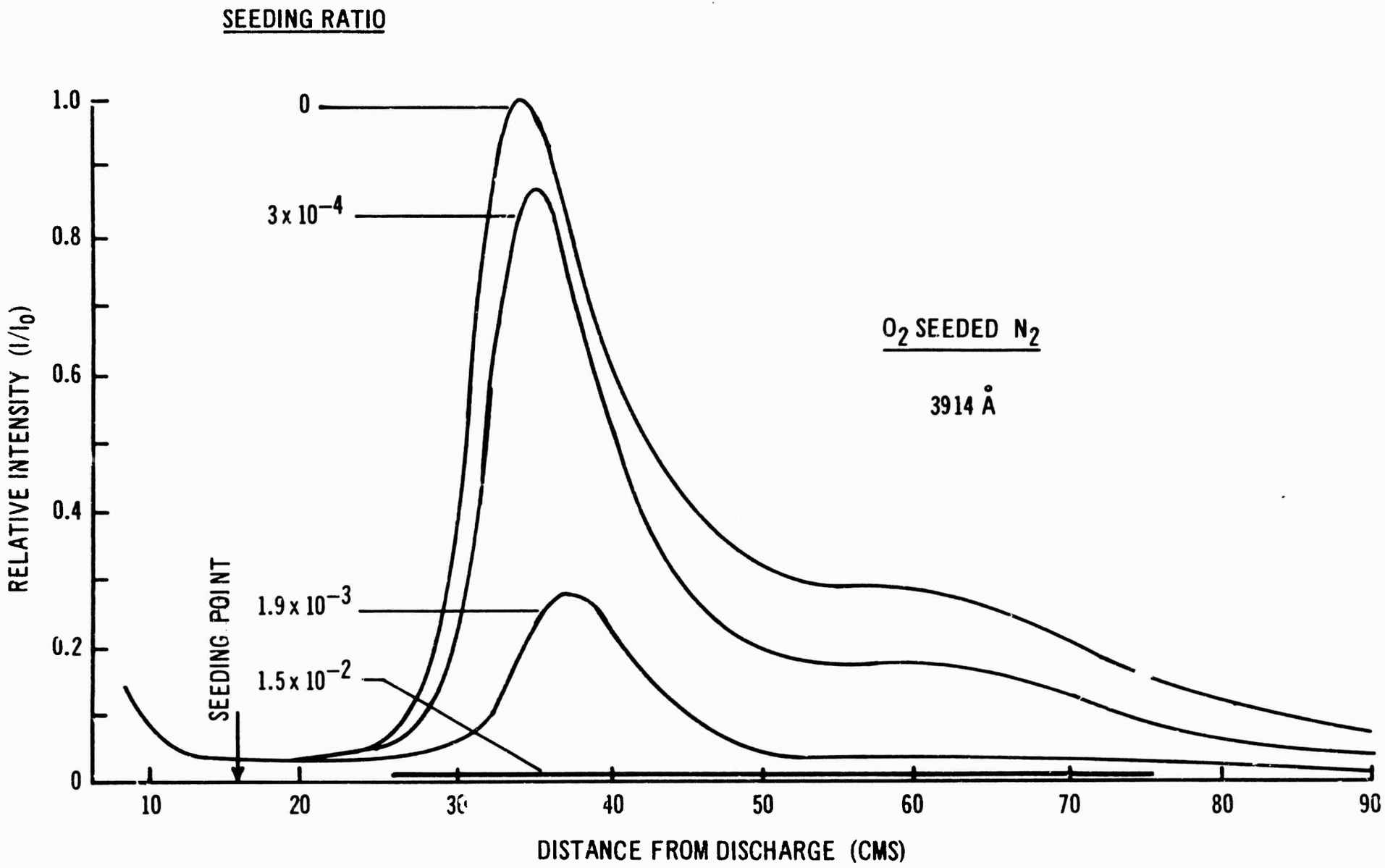

Fig. 14a Relative variation of emission intensity of the (0,0) band of the first negative system (3914 Å) along the spatial display of the afterglow for different O_2/N_2 seeding ratios. (p = 3.7 Torr, flow velocity = 2480 cm/sec).

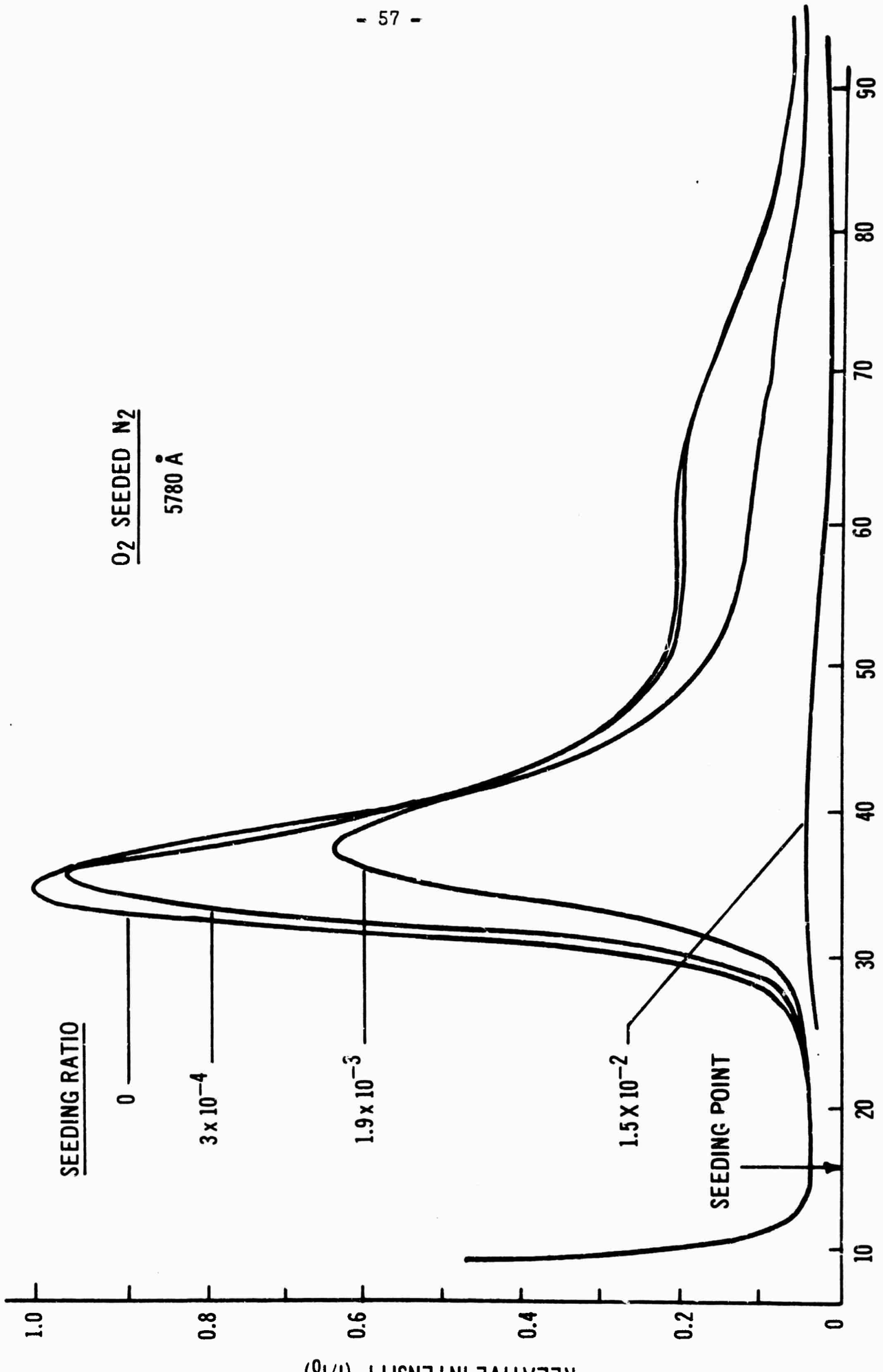

Fig. 14b Relative variation of the emission intensity of 5780 Å in first positive system along the spatial display of the afterglow for different O_2/N_2 seeding ratios. (p = 3.7 Torr, flow velocity = 2480 cm/sec).

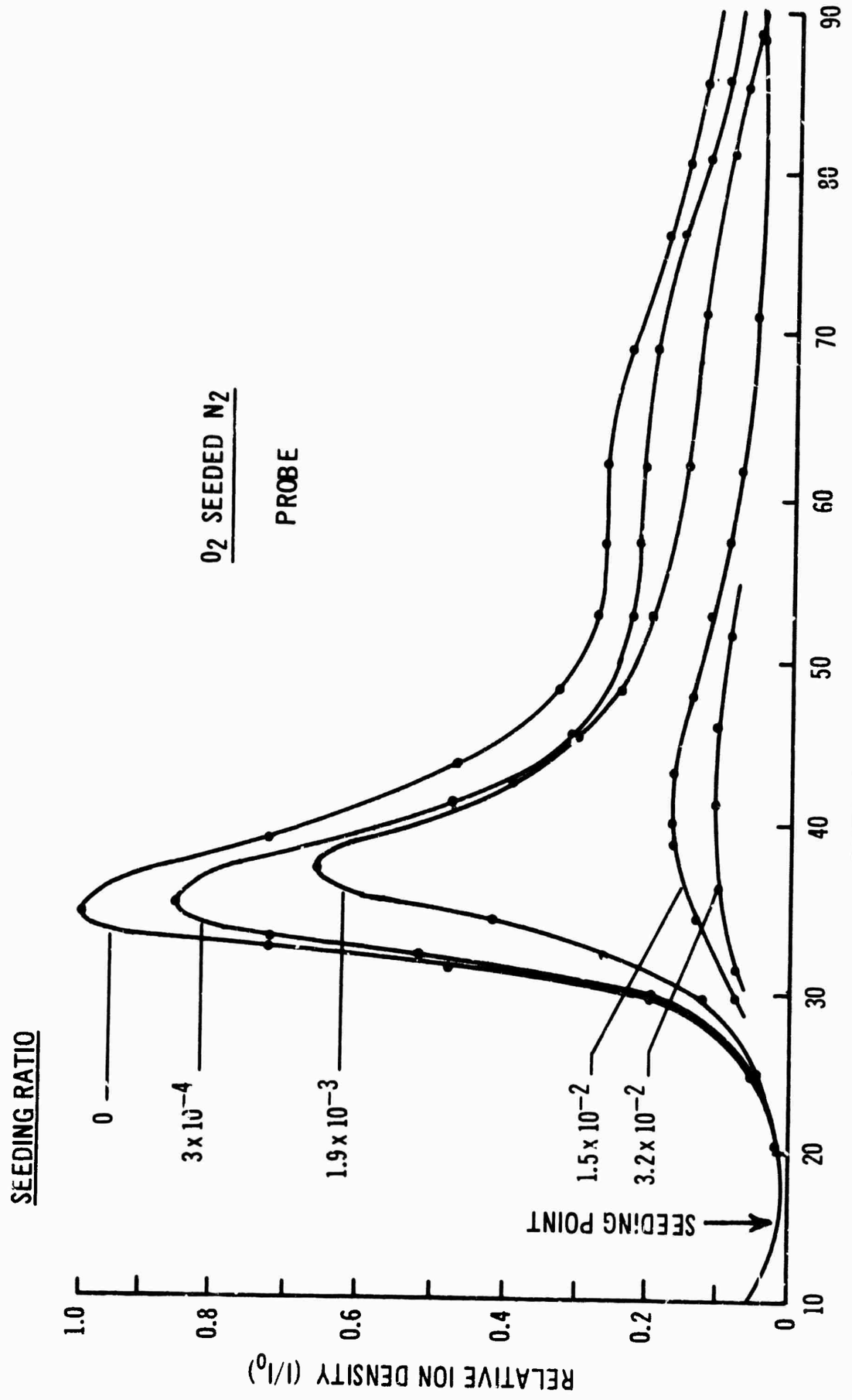

Fig. 14c Relative variation of the double probe saturated ion current along the spatial display of the afterglow for different O_2/N_2 seeding ratios. (p = 3.7 Torr, flow velocity = 2480 cm/sec).

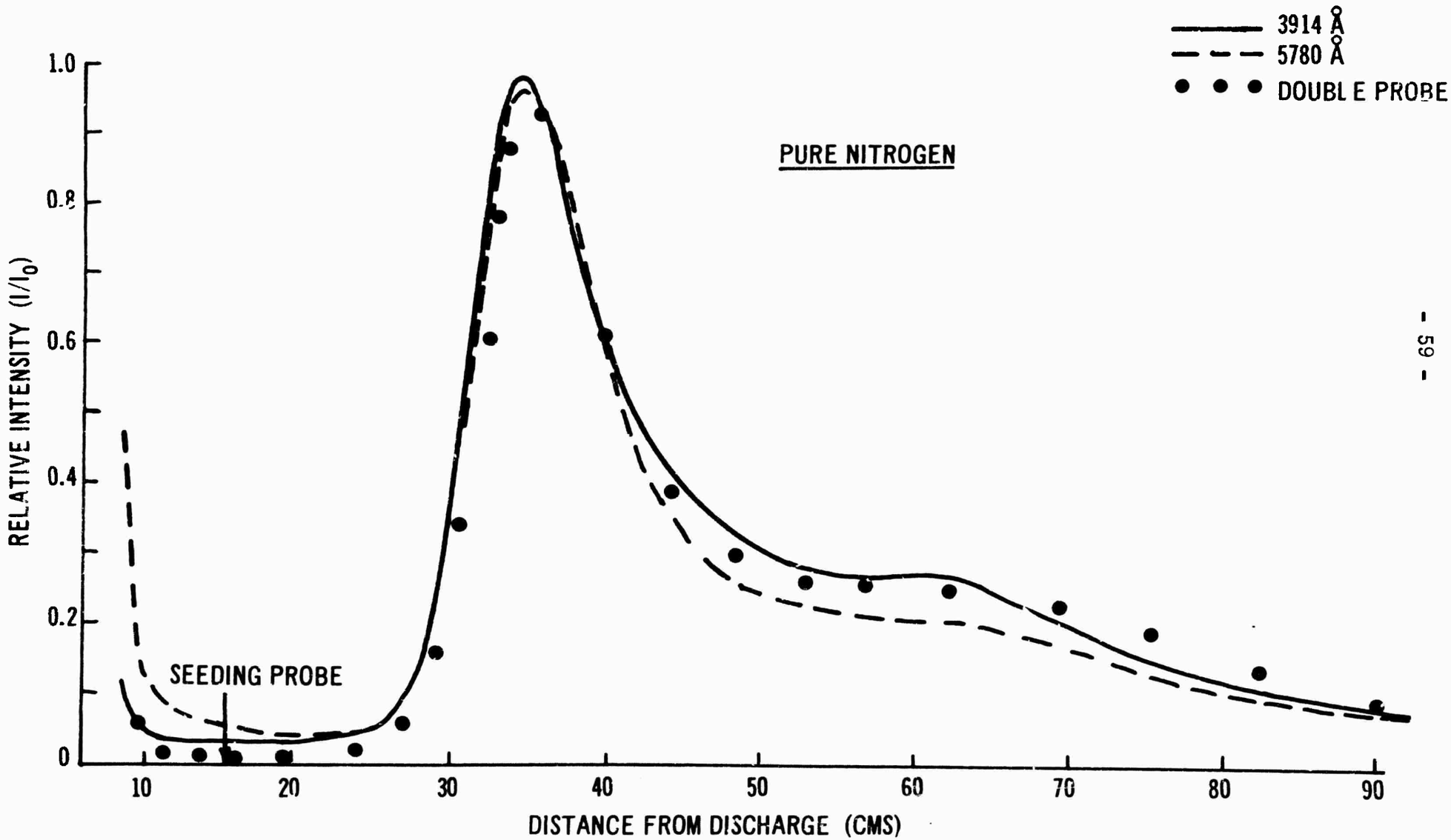

Fig. 15a Normalized plot of the longitudinal variation of 3914 Å, 5780 Å emission intensity and double probe saturation ion current for pure nitrogen afterglow. (p = 3.7 Torr, flow velocity = 2480 cm/sec).

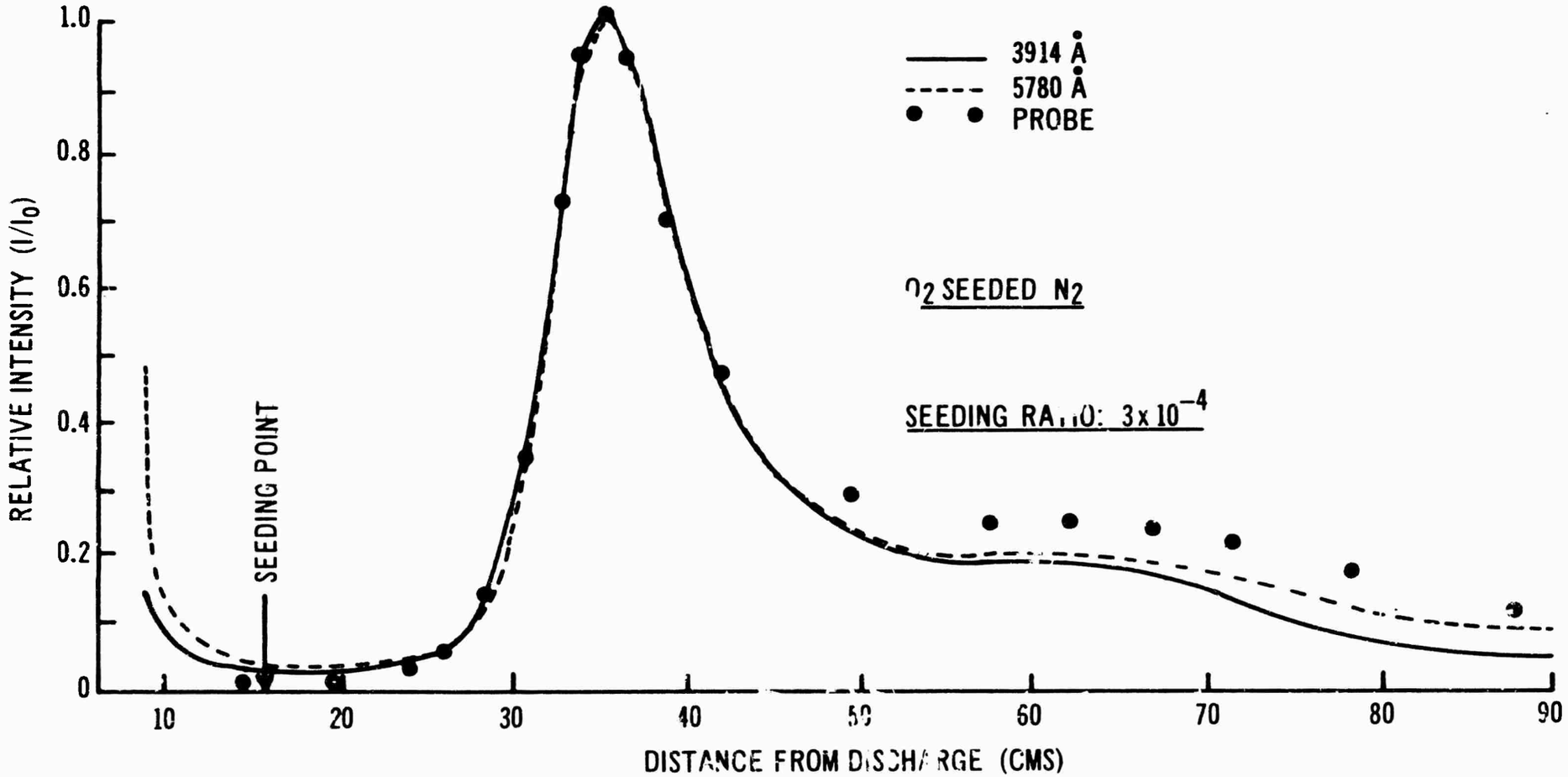

Fig. 15b Normalized plot of the longitudinal variation of 3914 Å, 5780 Å emission intensity and double probe saturation ion current for O_2 seeded afterglow. (Seeding ratio $O_2/N_2=3\times10^{-4}$. Pressure = 3.7 Torr, Flow velocity = 2480 cm/sec).

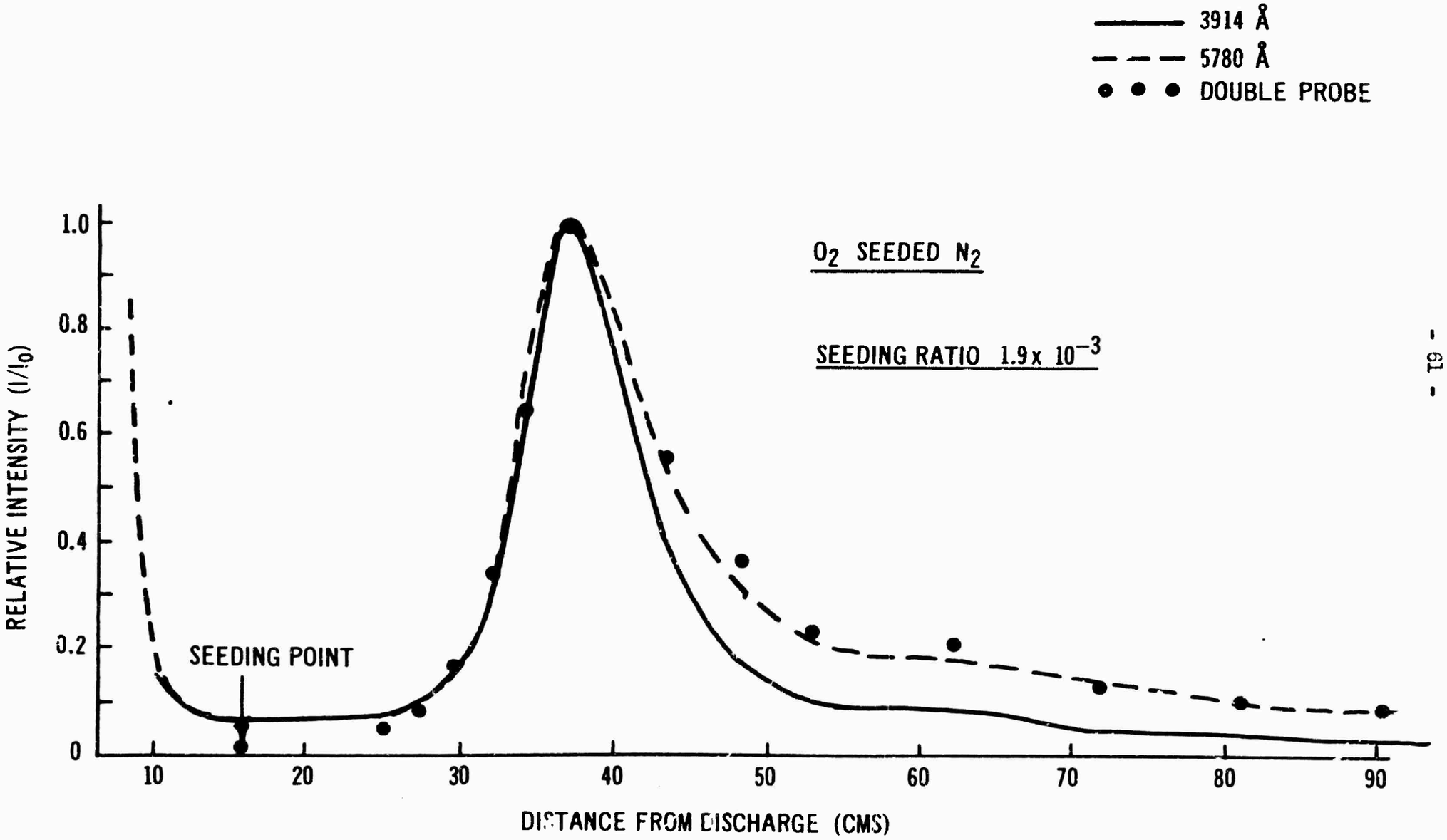

Fig. 15c Normalized plot of the longitudinal variation of 3914 Å, 5780 Å emission intensity and double probe saturation ion current for O_2 seeded afterglow. (Seeding ratio $O_2/N_2 = 1.9 \times 10^{-3}$. p = 3.7 Torr, flow velocity = 2480 cm/sec.)

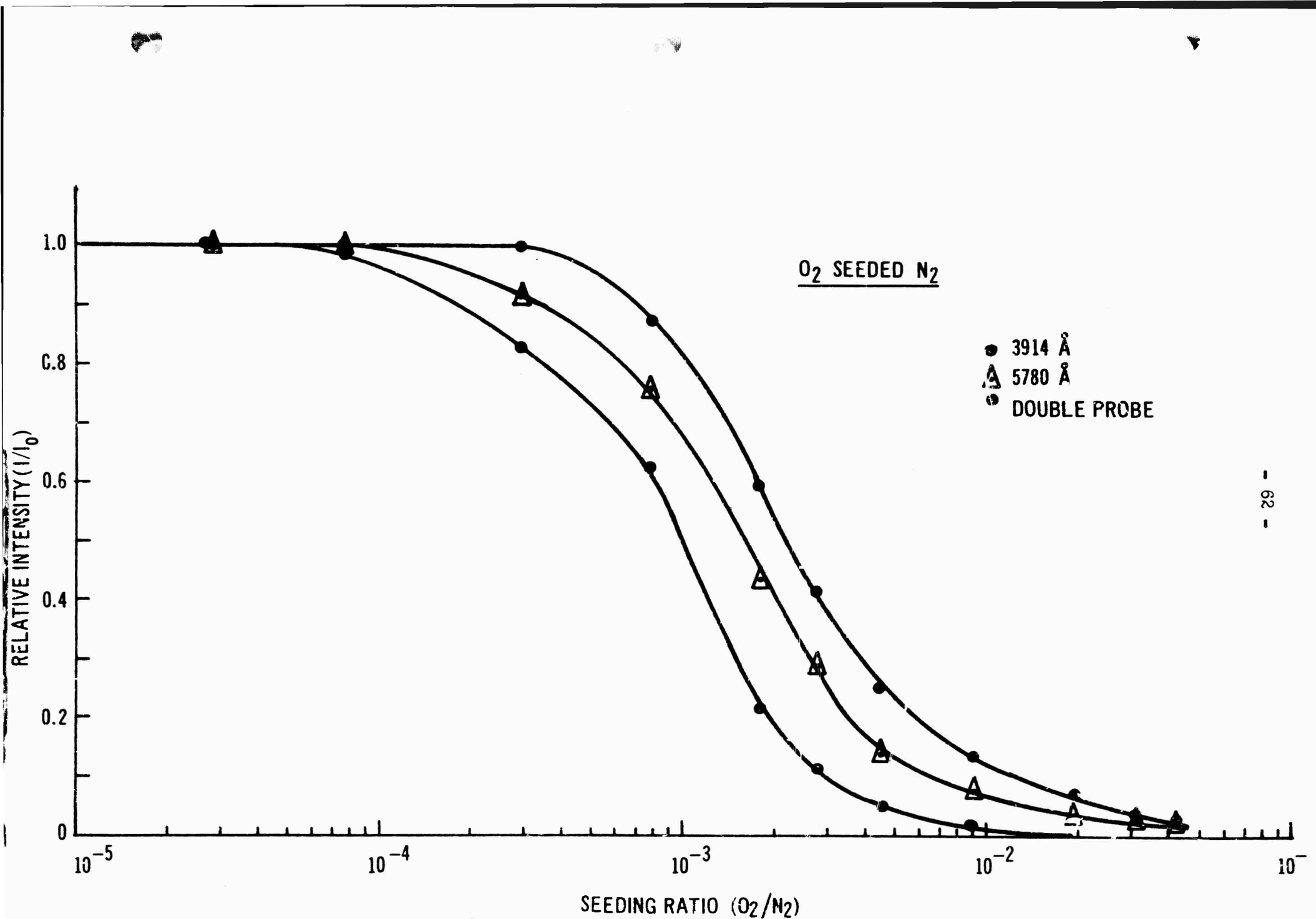

Fig. 16 Comparative plot of 3914 Å, 5780 Å emission intensity and double probe saturation ion current decrease with different O_2/N_2 seeding ratios. (p = 3.7 Torr, flow velocity = 2480 cm/sec)

around 1 ev according to

$$e + O_2 + x(\text{third body}) \rightarrow O_2^- + x$$

Chanin et al (1959) studied the effectiveness of N_2 as the third body in stabilizing attachment for thermal electrons. The value of the attachment coefficient (η/p) in O_2 is found to be quite high for low values of E/p (1.5 $Vcm^{-1}torr^{-1}$) i.e. of the order of 1 ev.

As has been stated before, it may therefore be more meaningful if we compare the attachment coefficient when evaluating the efficiency of quenching for different electronegative gas rather than attachment cross section.

4.4 CO_2 Seeding of N_2

Quenching by CO_2 seeding is of some interest because of the fact that, although the attachment cross section of CO_2 is not very high, a strong quenching was observed with evolution of considerable amount of heat.

Figure 17(a-c) shows the variation of intensity of the excited ion (3914 Å), excited molecule (5780 Å) and the double probe saturated ion current for different seed ratios along the length of the small flow tube.

Figure 18(a-c) shows the normalized plot (i.e. intensities matched at the peak in the afterglow) of the three intensities for different seed ratios.

Figure 19 shows the decay of the intensity of the maximum pink glow for different seed ratios as measured by the three techniques.

From the above results it is seen that CO_2 shows a strong quenching effect and the quantities seem to follow very closely. (Much closer than for O_2 seeding).

The mechanism of attachment in CO_2 is a dissociative attachment according to $CO_2 + e \rightarrow CO + O^-$ which has a maximum cross section of

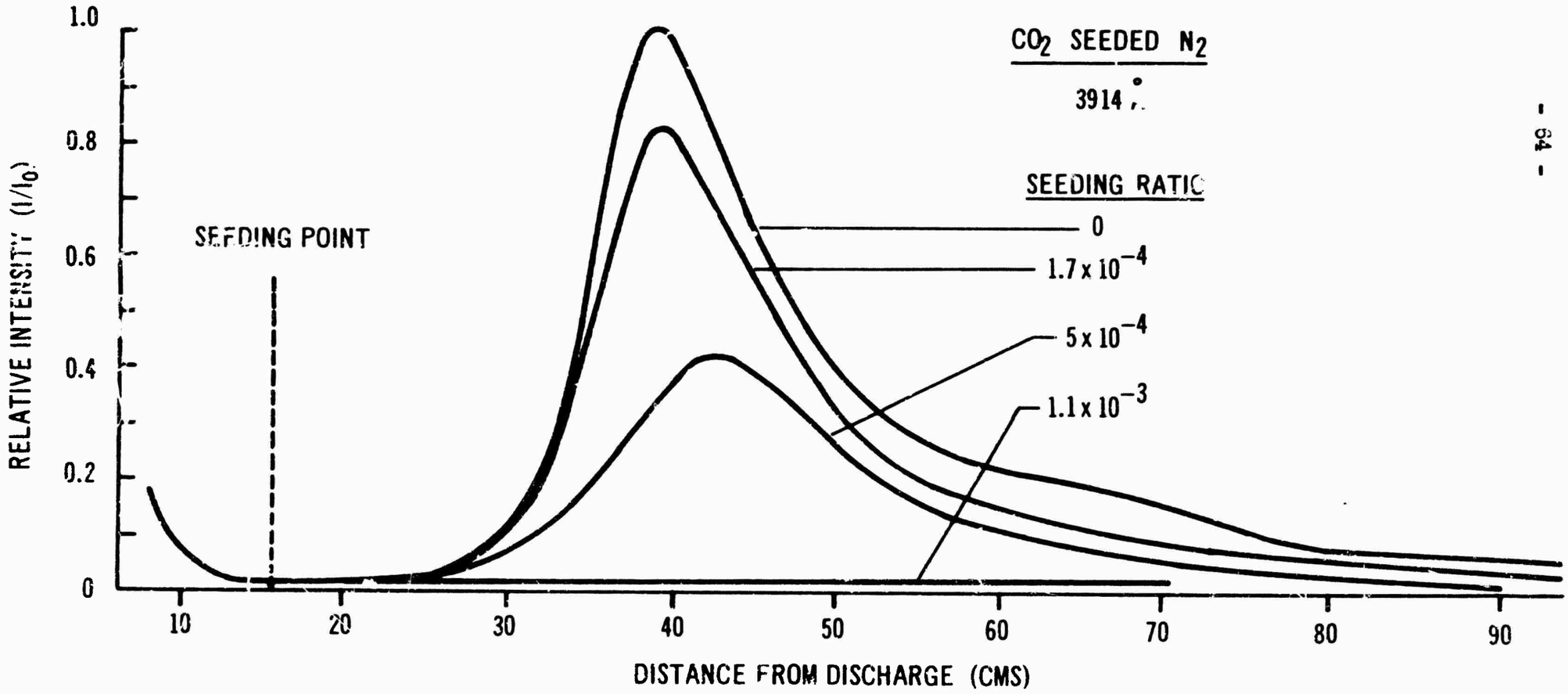

Fig. 17a Relative variation of emission intensity of the (0,0) band of the first negative system (3914 Å) along the spatial display of the afterglow for different CO_2/N_2 seeding ratios. (p = 3.7 Torr. flow velocity = 2480 cm/sec).

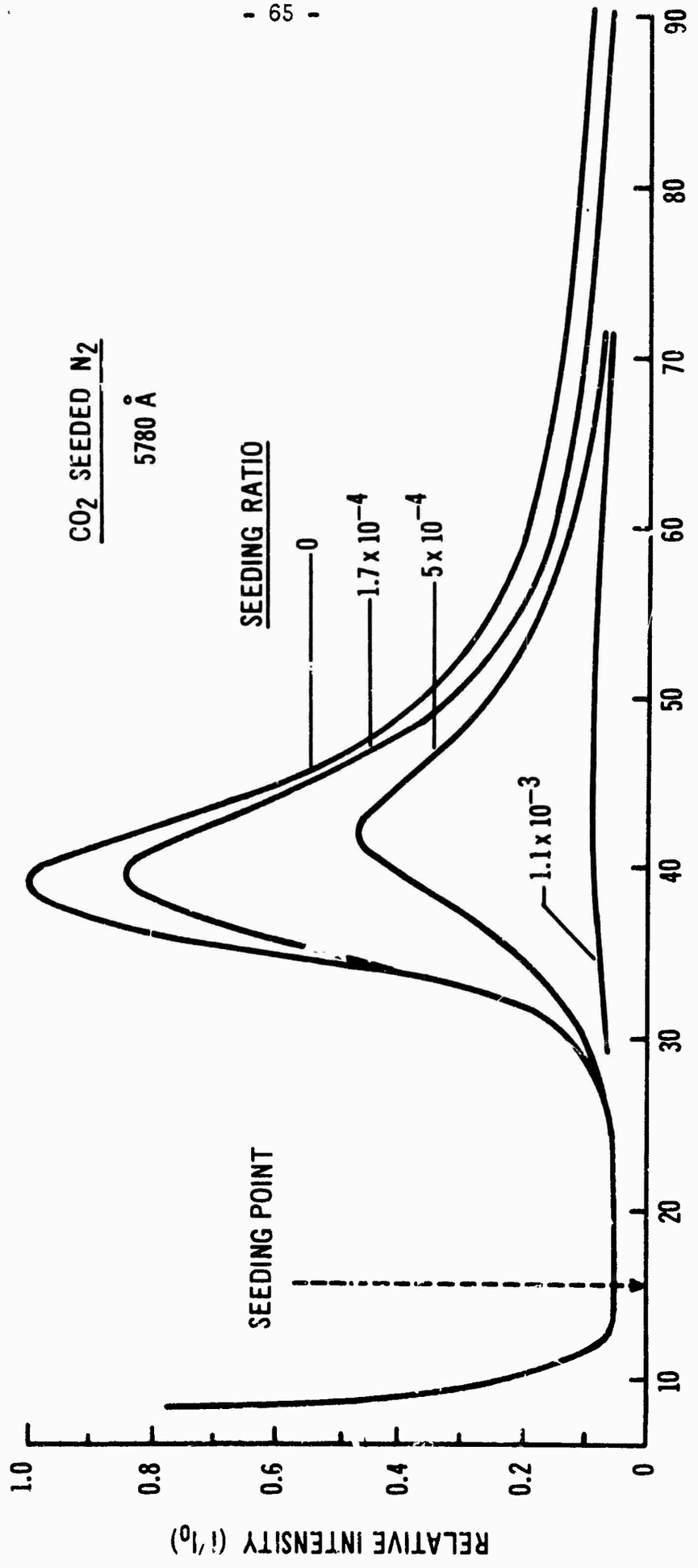

Fig. 17b Relative variation of the emission intensity of 5780 Å in first positive system along the spatial display of the afterglow for different CO_2/N_2 seeding ratios. (p = 3.7 Torr, flow velocity = 2480 cm/sec).

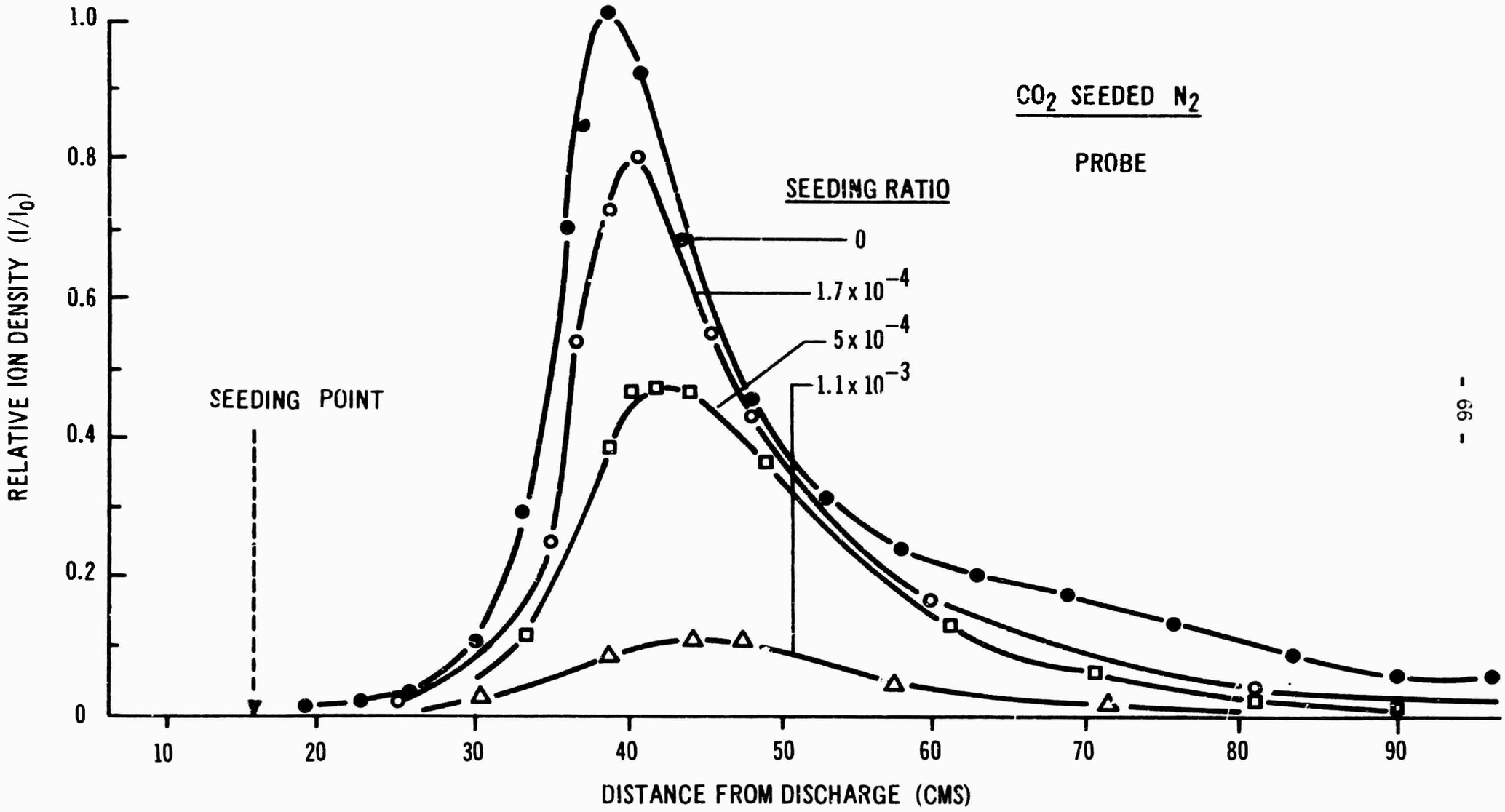

Fig. 17c Relative variation of the double probe saturated ion current along the spatial display of the afterglow for different CO_2/N_2 seeding ratios. (p = 3.7 Torr, flow velocity = 2480 cm/sec).

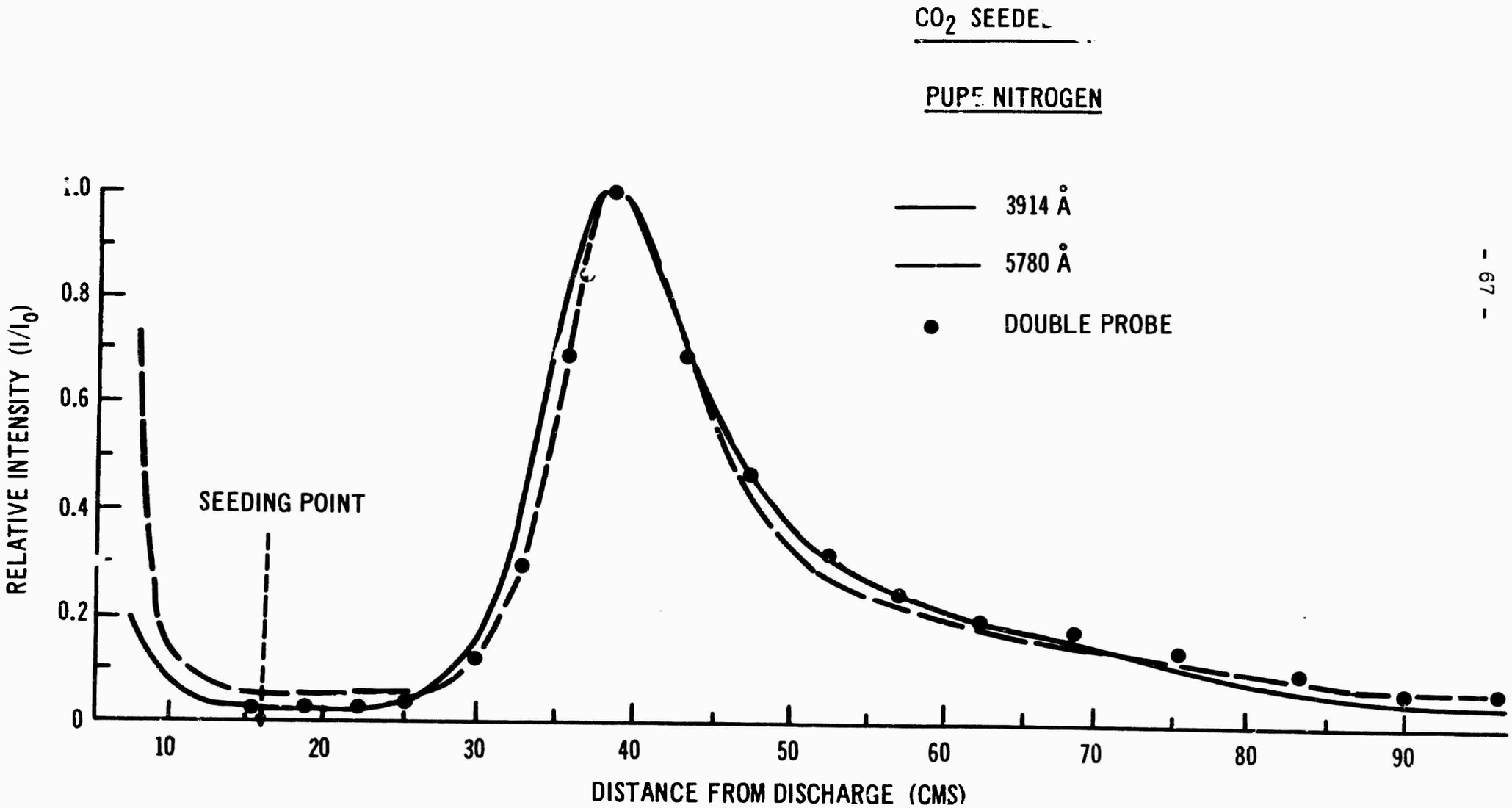

Fig. 18a Normalized plot of the longitudinal variation of 3914 Å, 5780 Å emission intensity and double probe saturation ion current for pure nitrogen afterglow. (p = 3.7 Torr, flow velocity = 2480 cm/sec).

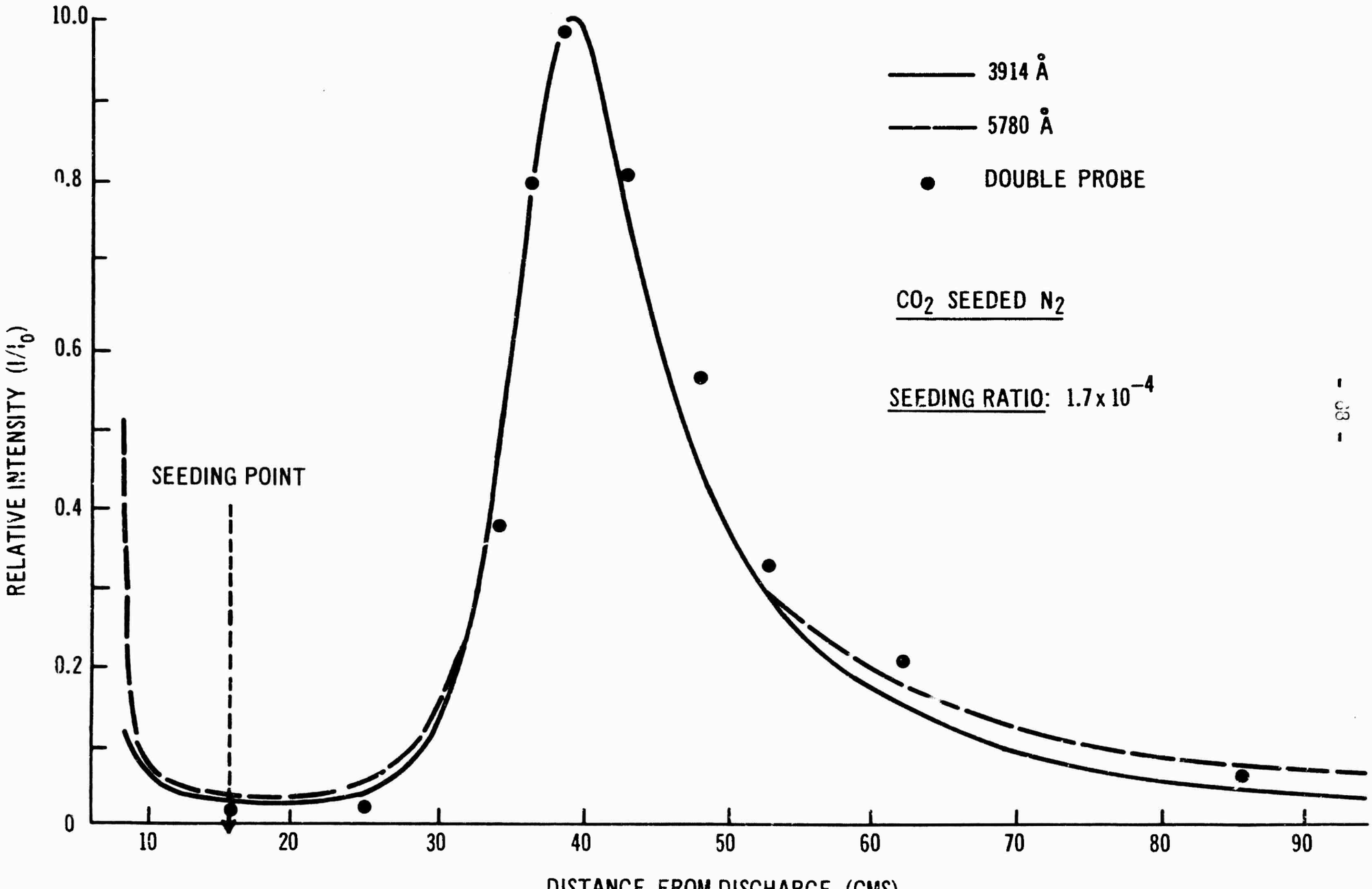

Fig. 18b Normalized plot of the longitudinal variation of 3914 Å, 5780 Å emission intensity and double probe saturation ion current for CO_2 seeded afterglow. Seeding ratio of CO_2/N_2 : 1.7×10^{-4} (p = 3.7 Torr, flow velocity = 2480 cm/sec)

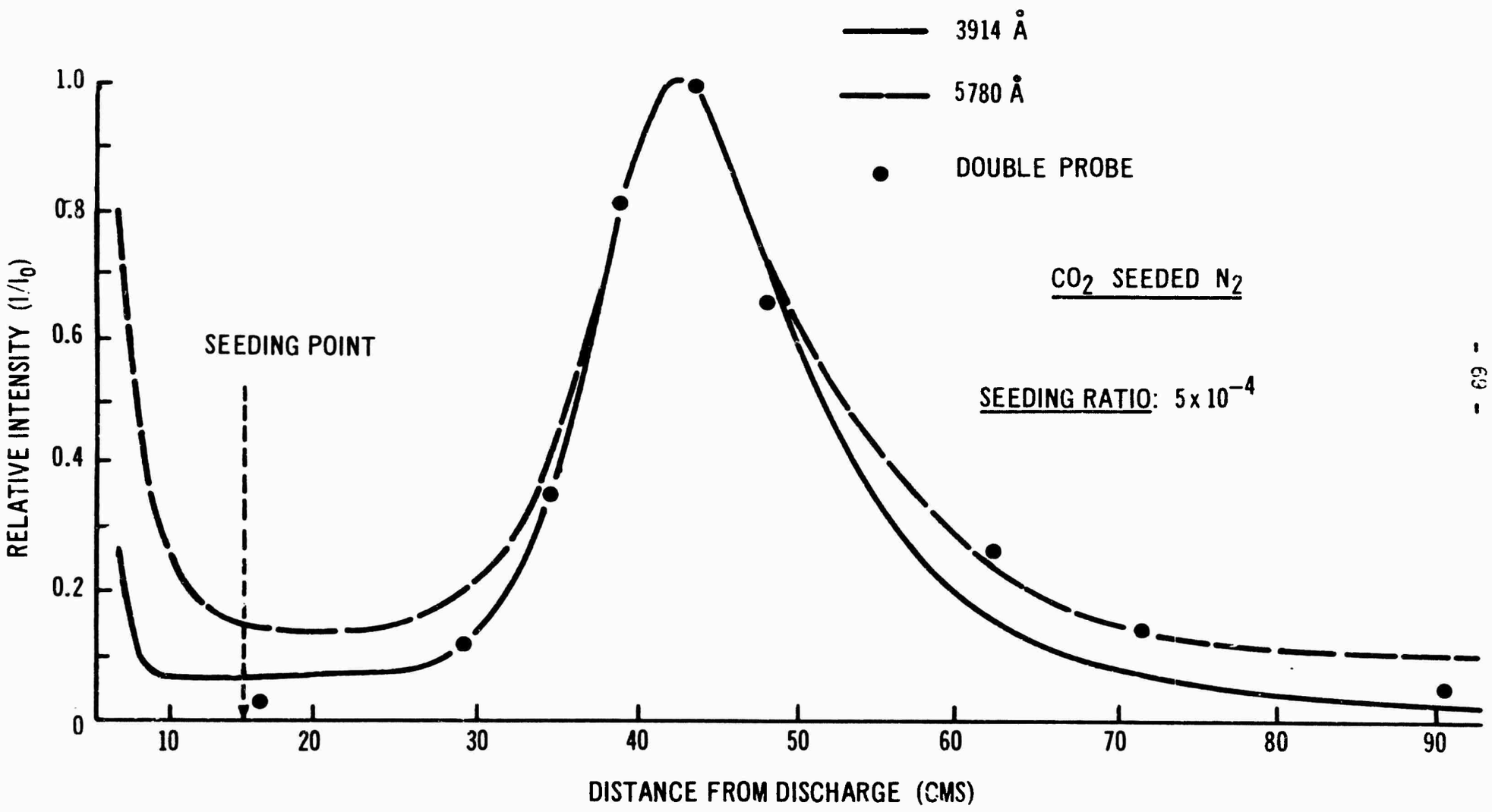

Fig. 18c Normalized plot of the longitudinal variation of 3914 Å, 5780 Å emission intensity and double probe saturation ion current for CO_2 seeded afterglow. (Seeding ratio $CO_2/N_2 = 6 \times 10^{-4}$. p = 3.7 Torr, flow velocity = 2480 cm/sec).

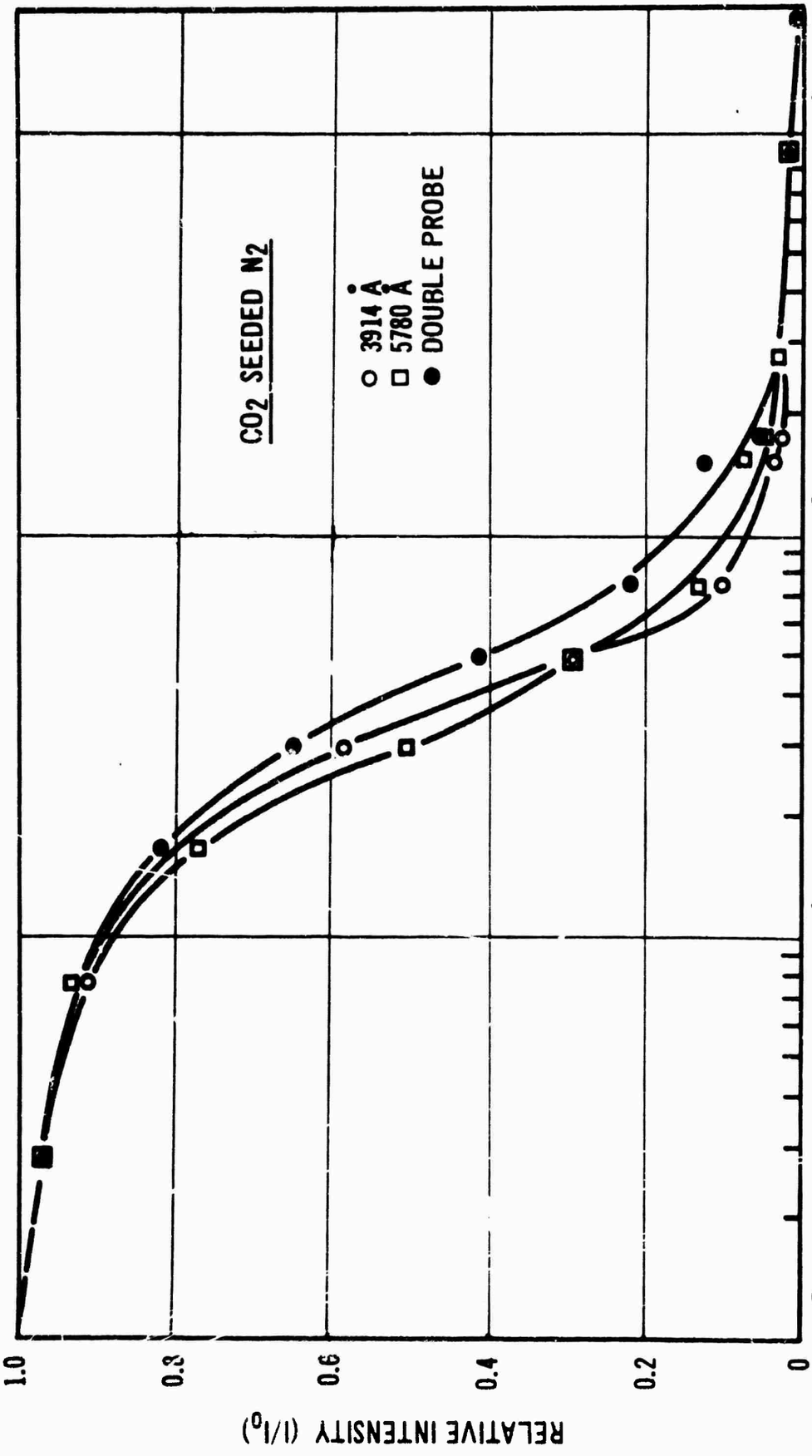

Fig. 19 Comparative plot of 3914 Å, 5780 Å emission intensity and double probe saturation ion current decrease with different CO_2/N_2 seeding ratios. (p = 3.7 Torr, flow velocity = 2480 cm/sec).

$5\times10^{-19}cm^2$ at 7.8 ev. At the thermal condition of the pink afterglow however, ($T_e = 10^4$ K, 1 ev)CO_2 attachment is probably not an efficient enough mechanism to account for the observed quenching. However, the strong quenching was found to be associated with near resonance vibrational energy transfer between the vibrationally excited ground-state of N_2 and the ν_3 vibrational mode of CO_2 (Milne et al (1965)) according to

$$N_2 * + CO_2 \rightarrow N_2 + CO_2 *$$

Absorption studies of N_2 pink afterglow in the vacuum ultraviolet have revealed vibrational excitation up to ν'' = 20,21 (Bass 1964, Nakamura et al 1964).

This vibrational excitation of ground-state N_2 in the pink afterglow is sufficient to exeite vibrational modes of CO_2, and there is a high probability of this type of energy transfer (Rapp et al 1964). This may account for the strong quenching by CO_2 observed in the present experiments.

4.3 <u>H_2O Seeding of N_2</u>

Water vapour as a quenching agent is of considerable interest due to its high attachment coefficient at low E/p (Kuffel, 1959) and its effect on the recombination time (Kuhns 1962). Both mechanisms result in a depletion of the free electrons in the plasma.

The results of the present experiments are shown in the Figures 20 and 21.

The results show a strong quenching of the pink glow - stronger than for either O_2 or CO_2. The decay of excited neutral (5780 Å) intensity seems to follow the double probe saturation current data -(Fig.21) more closely than excited ion intensity as in O_2 and NO.

In these experiments a 10% mixture of water vapour in N_2 was used as the seed gas. It was thought that there might be some "quenching" effect

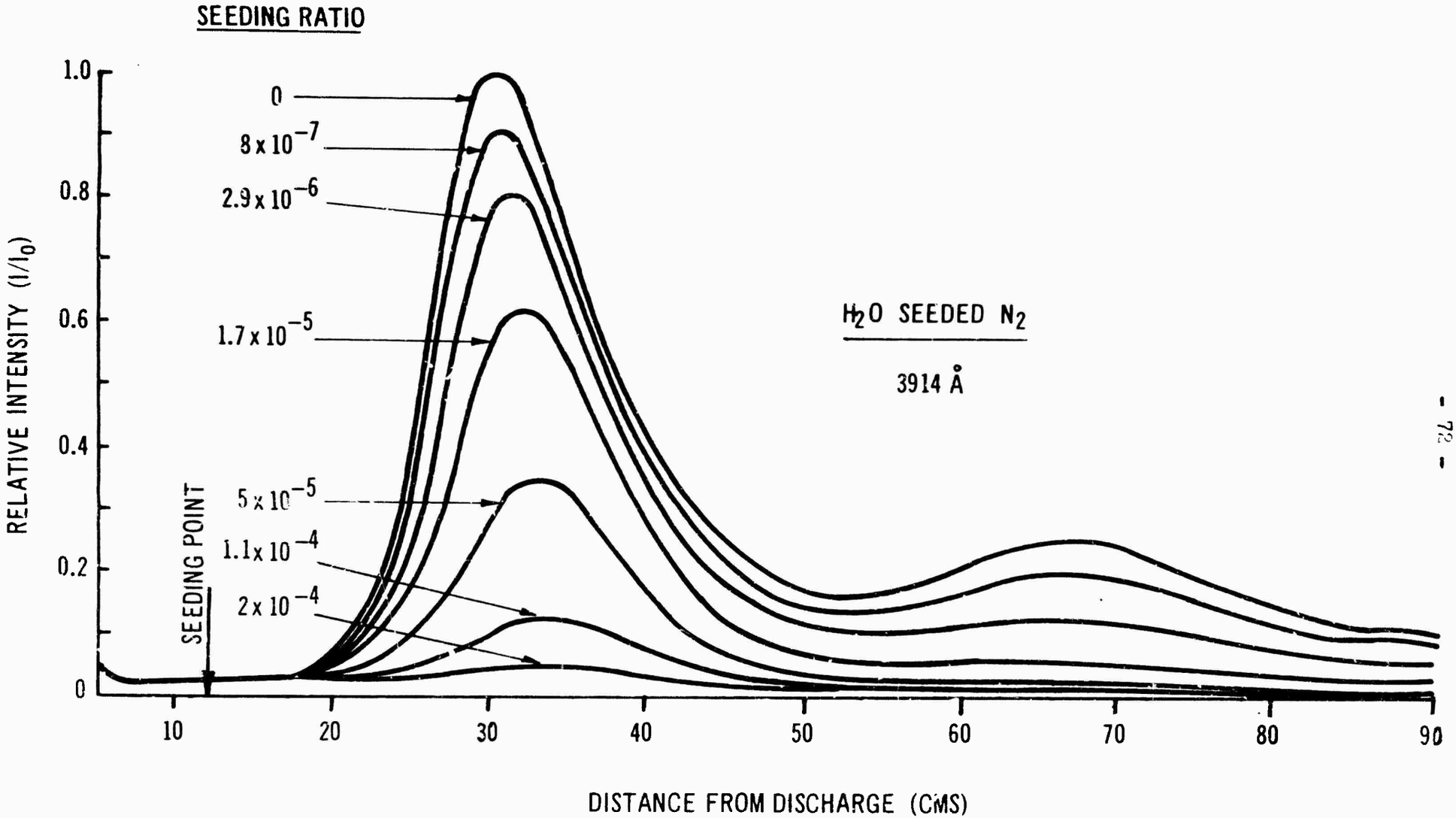

Fig. 20a Relative variation of the emission intensity of the (0,0) band of the first negative system (3914 Å) along the spatial display of the afterglow for different H_2O/N_2 seeding ratios. (p = 3.7 Torr, flow velocity = 2480 cm/sec).

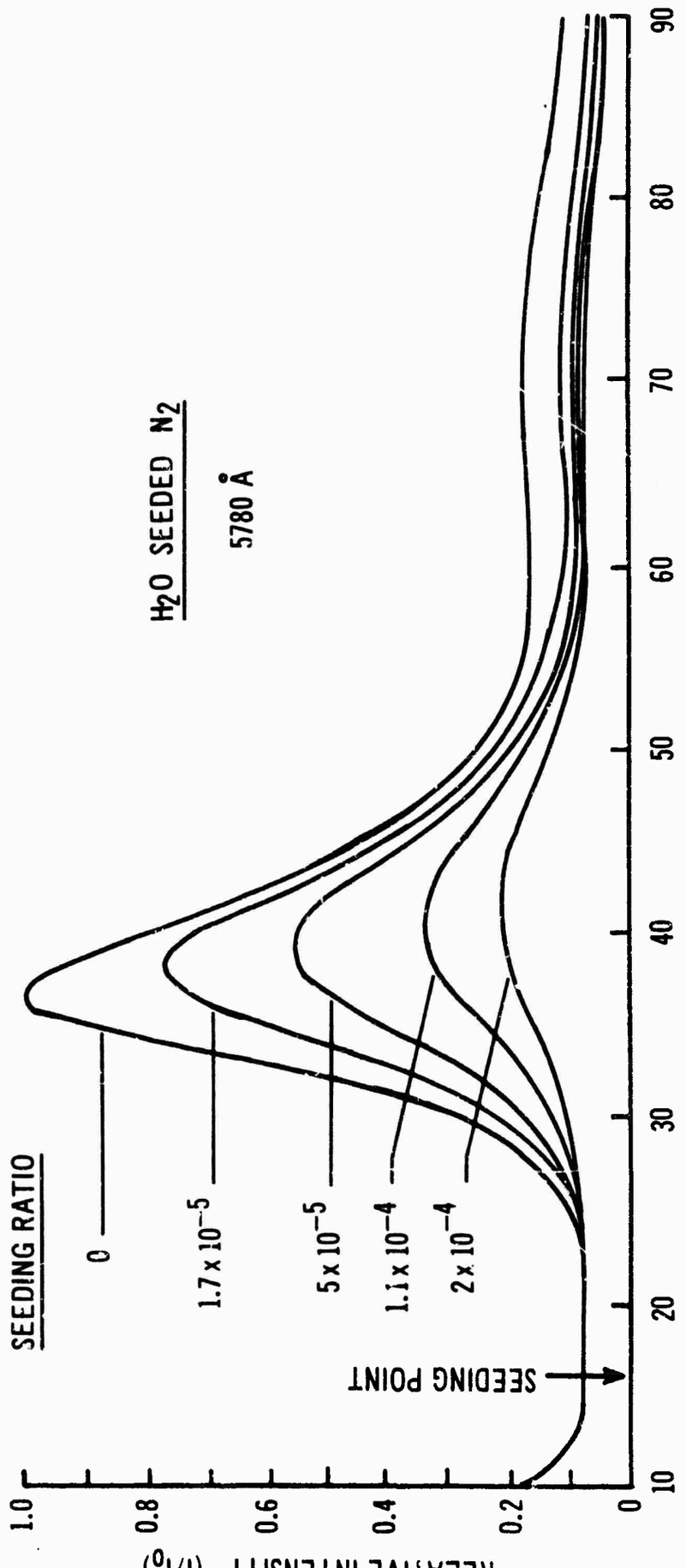

Fig. 20b Relative variation of the emission intensity of 5780 Å in the first positive system along the spatial display of the afterglow for different H_2O/N_2 seeding ratios. (p = 3.7 Torr, flow velocity = 2480 cm/sec).

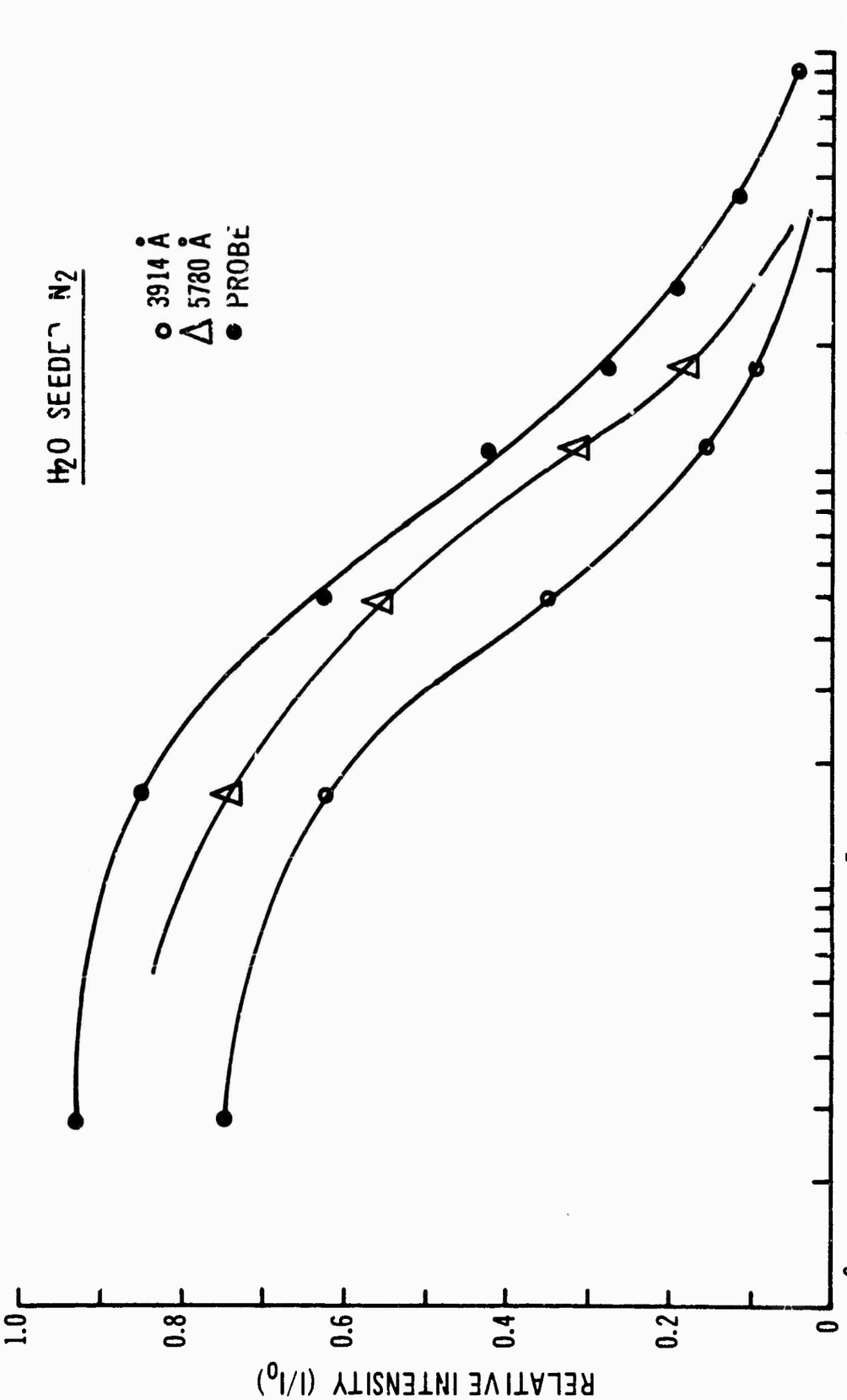

Fig. 21 Comparative plot of 3914 Å, 5780 Å emission intensity and double probe saturation ion current decrease with different H_2O/N_2 seeding ratios. (p = 3.7 Torr, flow velocity = 2480 cm/sec)

due to N_2 by simple cooling of the plasma and would affect the efficiency of water vapour as measured.

To check this, pure N_2 was seeded into the afterglow and a small amount of quenching (Fig.22(a), 22(b), 22(c)) was observed. It was, however, several orders of magnitude smaller than that observed with the H_2O mixtures and much too small to affect the measurements shown in Fig.21 and 22.

For previous measurements (Muschlitz 1957) in water vapour showed production of two types of negative ion H^-, O^- by electron impact on H_2O. OH^- may be produced by secondary reactions. The reactions are:

$$e + H_2O \rightarrow OH + H^- \qquad \text{appearance pot. } 5.7 \text{ ev}$$

$$e + H_2O \rightarrow 2H + O^- \qquad " \qquad " \quad 7.3 \text{ ev}$$

$$H^- + H_2O \rightarrow OH^- + H_2;\ O^- + H_2O \rightarrow OH^- + OH.$$

The electron capture cross section is found to be 4.8×10^{-18} cm^2 at 6.4 ev.

Results of Schulz (1960) involving measurement of negative ion current as a function of electron energy indicated that below 2ev water vapour may not be an efficient gas for attaching electrons. The present results however, indicate a strong quenching at low electron energies (< 2ev) and measurement of the attachment coefficient (η/p) in water vapour at low E/p shows a strong attachment (Kuffel 1959) which may be due to some non-dissociative attachment in water at low energy. According to Kuffel (1959), the relatively high attachment near zero electron energy is due to electron attaching themselves to large clusters of molecules. This idea was also put forward by Bradbury (1934). Thus, the strong quenching measured, could be accounted for by the high attachment coefficient at low energy due to non-dissociative attachment of some sort.

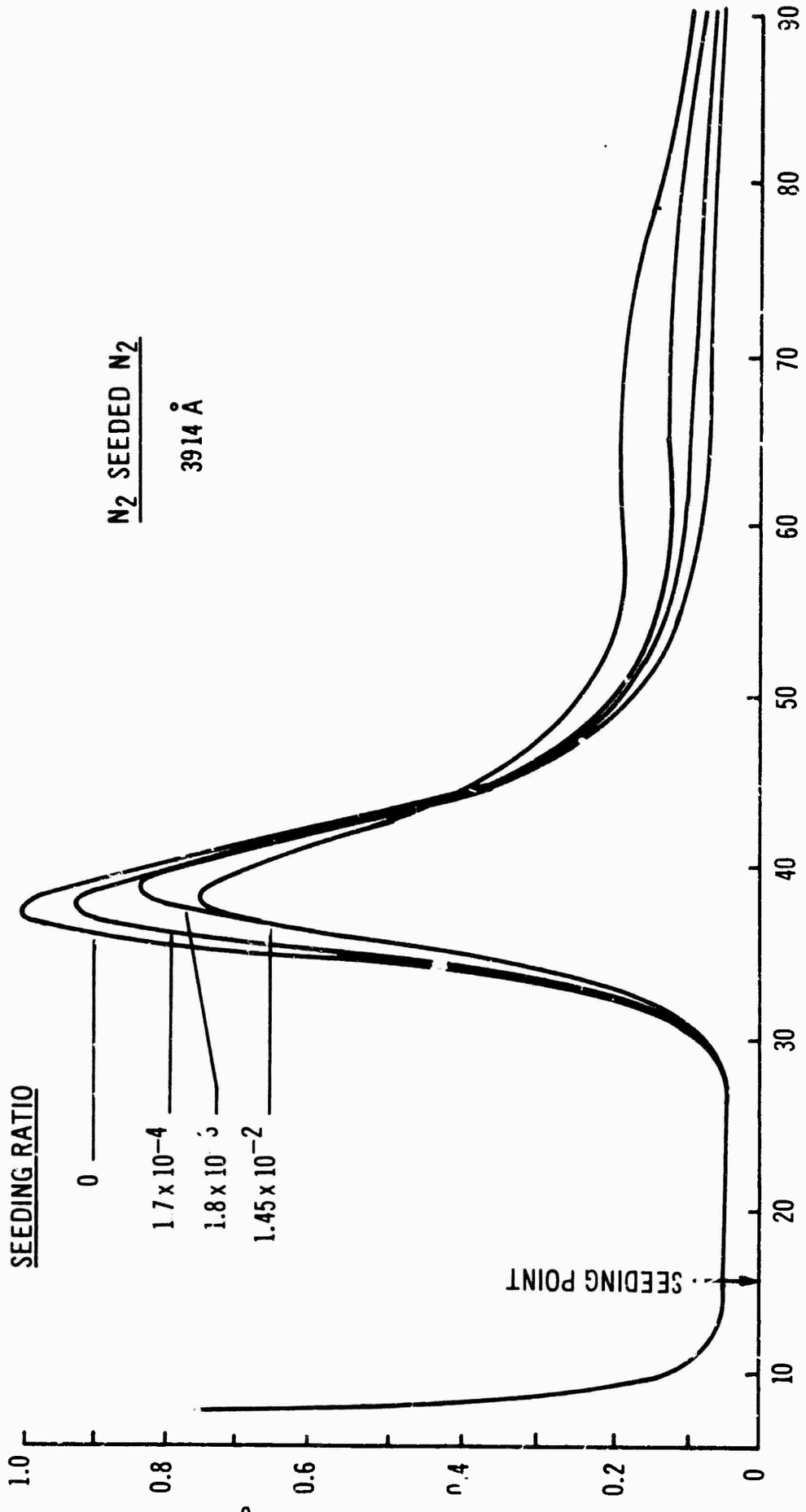

Fig. 22a Relative variation of emission intensity of the (0,0) band of the first negative system (3914 Å) along the spatial display of the afterglow for different N_2/N_2 seeding ratios. (p = 3.7 Torr, flow velocity = 2430 cm/sec).

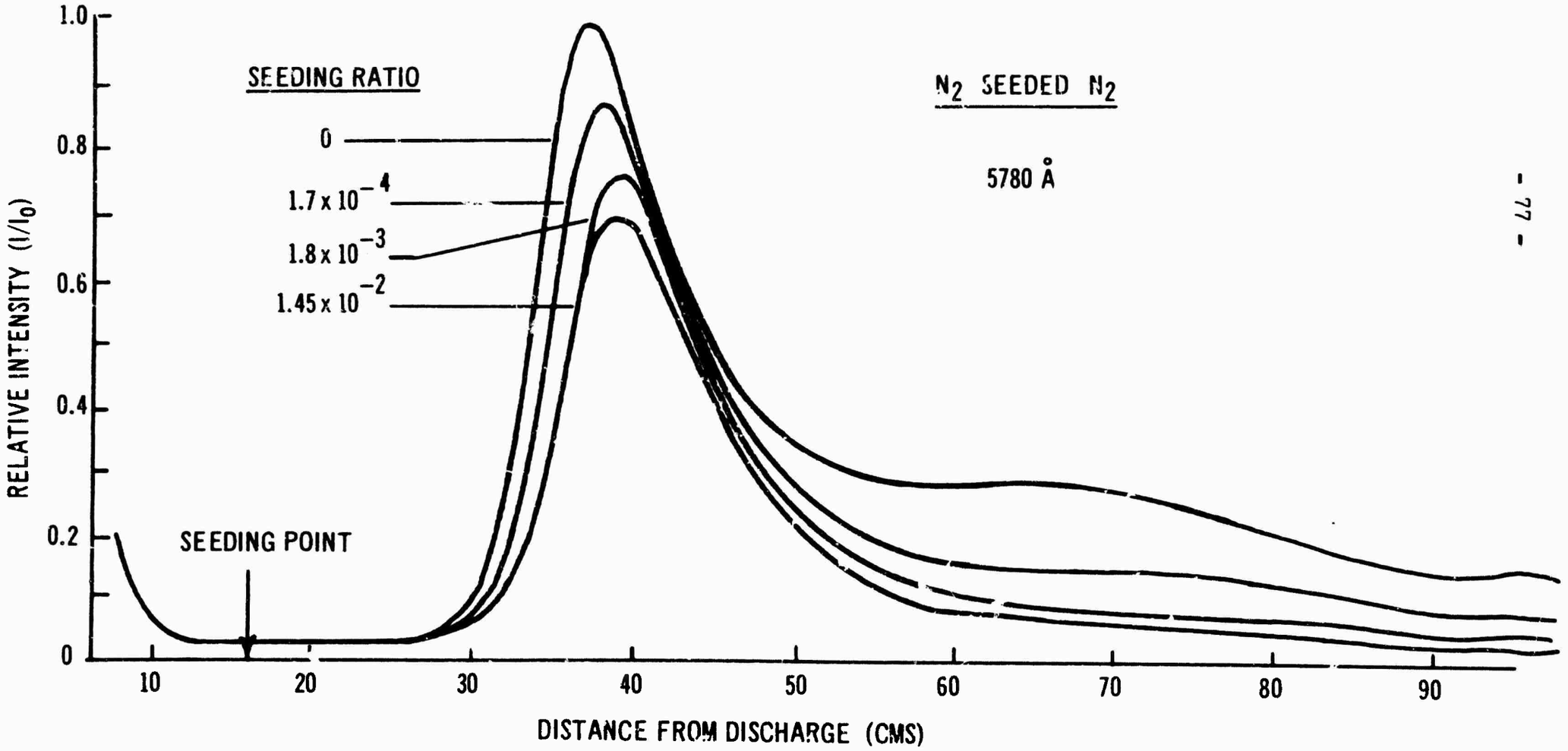

Fig. 22b Relative variation of the emission intensity of 5780 Å in the first positive system along the spatial display of the afterglow for different N_2/N_2 seeding ratios. (p = 3.7 Torr, flow velocity = 2480 cm/sec).

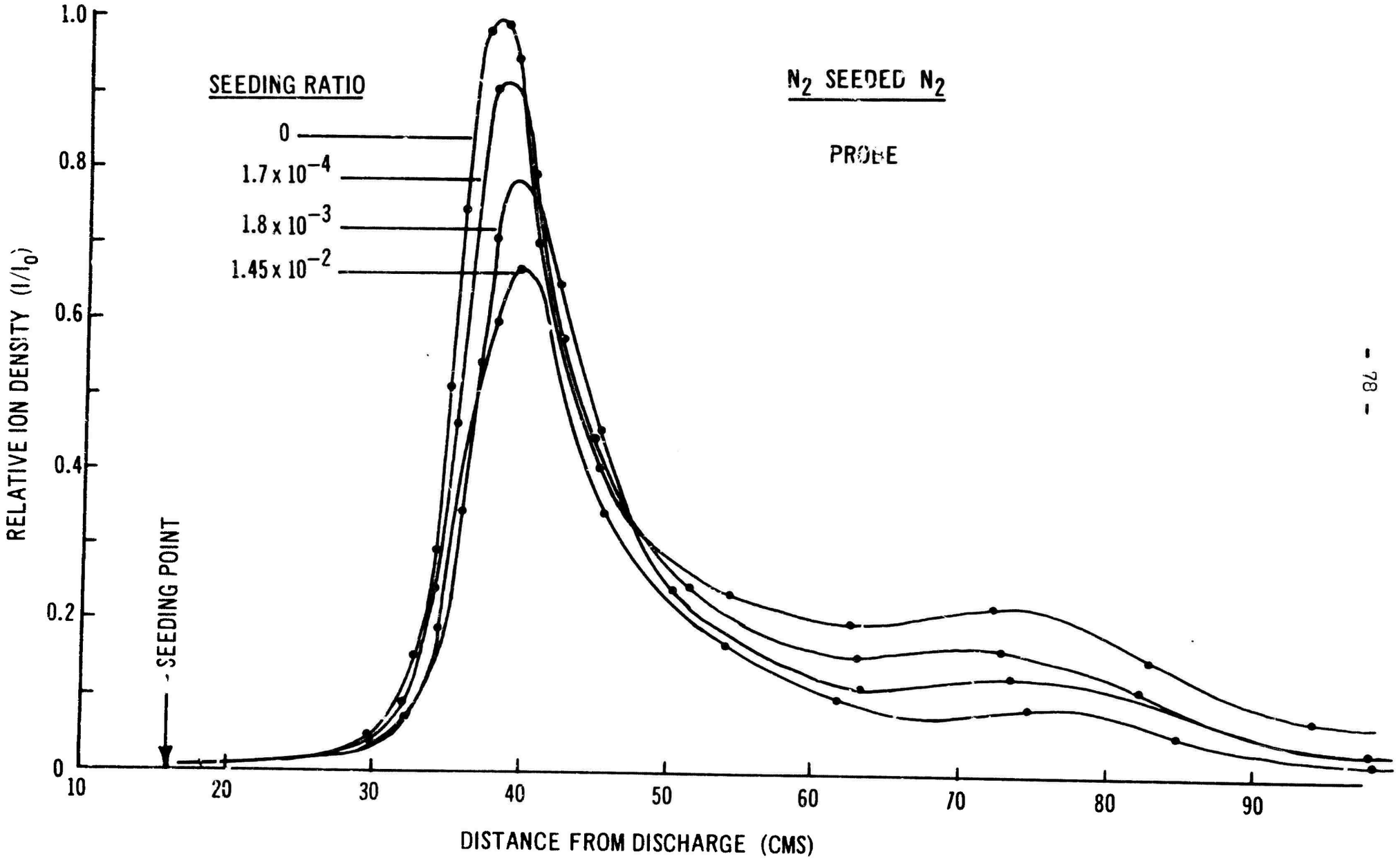

Fig. 22c Relative variation of the double probe saturated ion current along the spatial display of the afterglow for different N_2/N_2 seeding ratios. (p = 3.7 Torr, flow velocity = 2480 cm/sec).

4.5 SF_6 Seeding of N_2

Because of its very large electron capture cross section ($\sim 5\times10^{-16}cm^2$) near zero electron energy, SF_6 is expected to be a very efficient seed gas for plasma quenching and very encouraging results have been obtained previously in argon plasmas. (Carswell & Cloutier 1964).

A strong quenching is expected in the pink glow because of the more favorable thermal condition (i.e. lower temperatures) for SF_6 in attaching electrons. Results of experiments done at 3.7 Torr, are shown in the Figs. 23 and 24 where it is seen that complete quenching is achieved for a seeding ratio of about 10^{-5}.

The attachment coefficient for low values of $E/p(2\ Vcm^{-1}torr^{-1})$ in SF_6 is ~ 2 (McAfee 1955). Hickam and Fox (1956) have used the RPD technique to study SF_6 attachment from 0 to 2 ev. SF_6^- was observed to be formed in a resonance capture process with a cross section of $\sim 10^{-15}cm^2$ below .1 ev. A dissociative attachment of SF_6 peaked at about .1 ev was also observed with a cross section of $10^{-17}cm^2$.

Although the capture cross section of SF_6 is maximum around .1 ev, its efficiency of quenching at relatively high temperature plasma ($\sim 7\times10^4K$) was found to be quite high (Carswell et al 1964). This, however, can be explained from the fact that overall attachment coefficient is relatively high at large values of E/p (Geballe & Reeves 1953, Bhalla & Craggs 1962). Hence, SF_6 may be a very efficient seed gas for quenching over a wide thermal condition of plasma.

One interesting additional phenomenon observed with SF_6 seeding was the fact that after the experiment when the seeding valve was closed, there was an enhancement of the intensity of the pink glow - particularly of the second maximum (Fig.3). This is probably due to wall conditioning which is a very important factor in determining the properties of the pink glow.

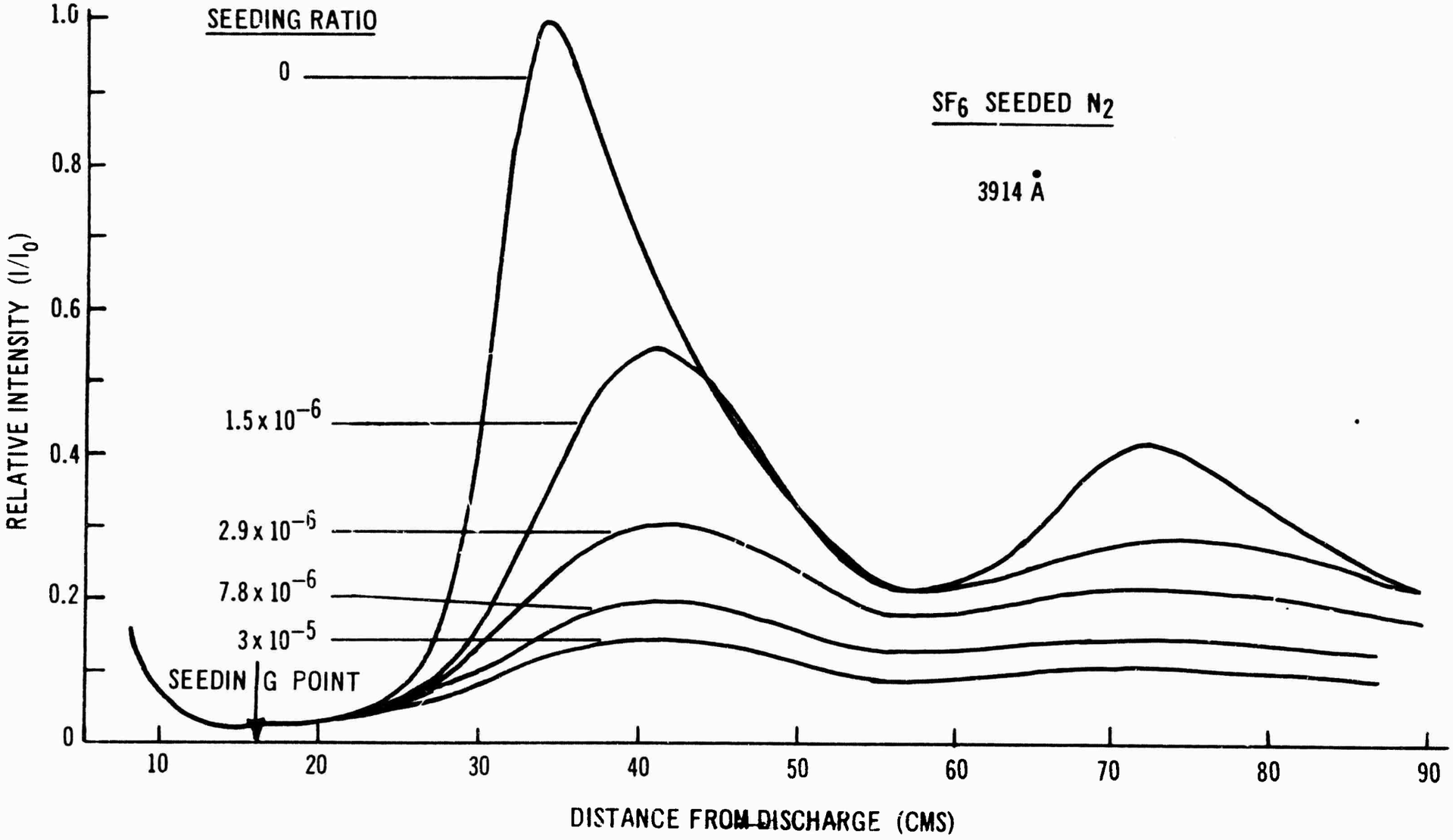

Fig. 23a Relative variation of emission intensity of the (0,0) band of the first negative system (3914 Å) along the spatial display of the afterglow for different SF_6/N_2 seeding ratios. (p = 3.7 Torr, flow velocity = 2480 cm/sec).

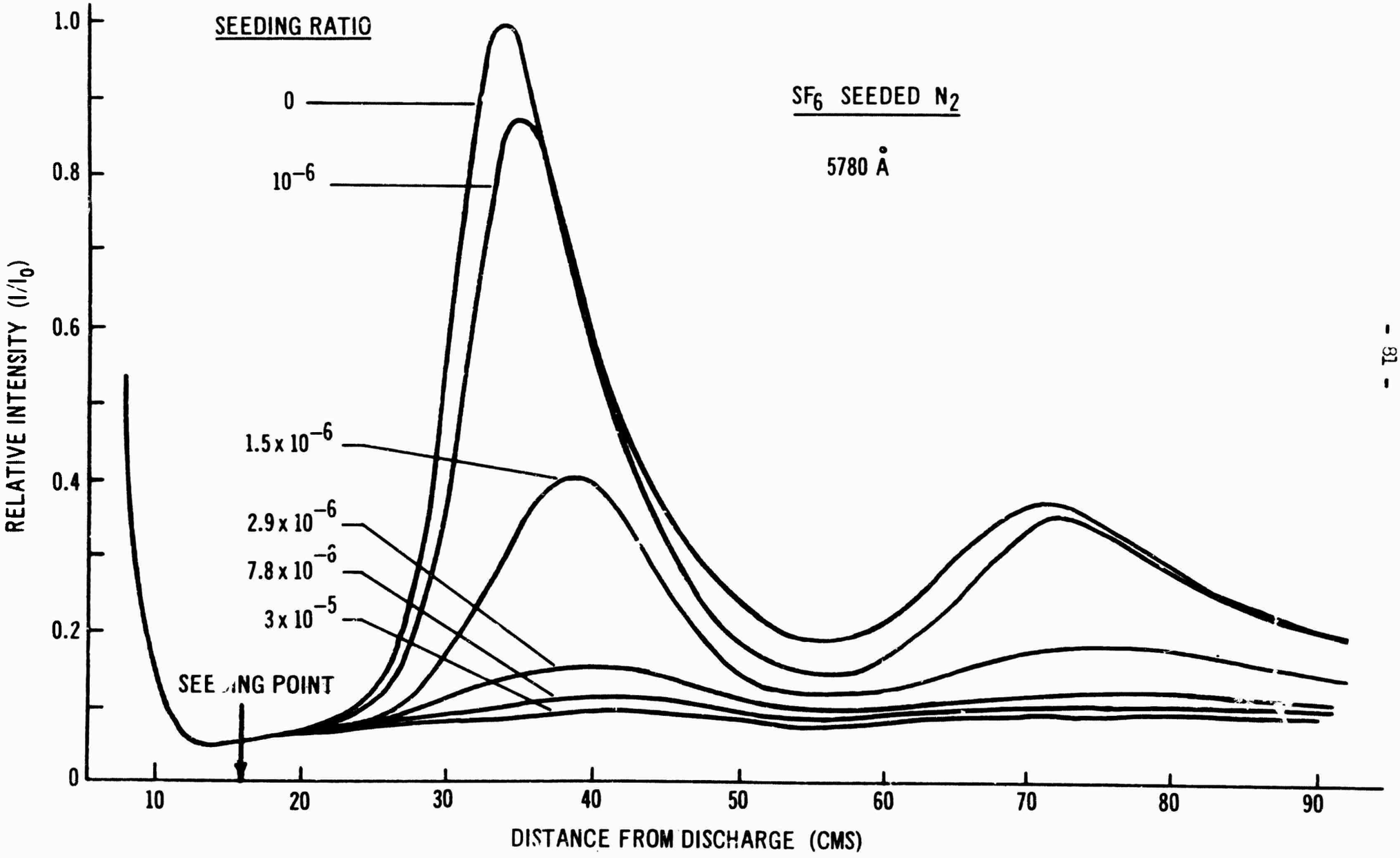

Fig. 23b Relative variation of the emission intensity of 5780 Å in the first positive system along the spatial display of the afterglow for different SF_6/N_2 seeding ratios. (p = 3.7 Torr, flow velocity = 2480 cm/sec).

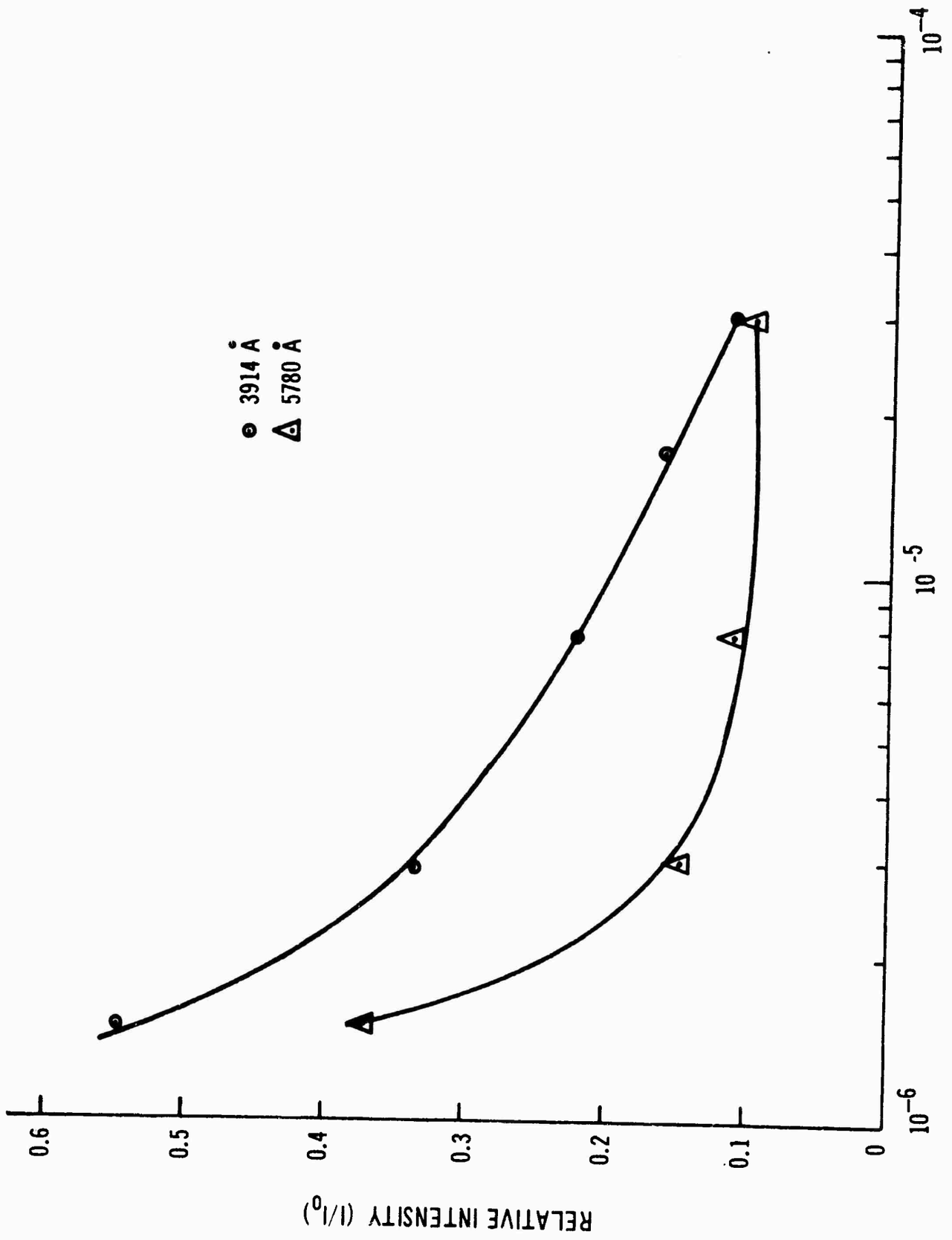

Fig. 24 Comparative plot of 3914 Å and 5780 Å emission intensity decrease with different SF_6/N_2 seeding ratios. (p = 3.7 Torr, flow velocity = 2480 cm/sec).

V DISCUSSION

As already mentioned in Section 4.1, the relative efficiency of a seed gas for quenching can be compared on the basis of the attachment coefficient rather than the attachment cross section. This is because the attachment coefficient is a measure of the overall electron loss no matter what the process of attachment is. Cross sections are usually known for dissociative attachment which may be insignificant under some conditions of the plasma energy distribution. With this in mind, a plot (Fig.25) is given of the attachment coefficient (η/p) as a function of E/p ($Vcm^{-1}torr^{-1}$) for the different gases that have been studied. From the figure, it is shown that although O_2 and H_2O do not show significant dissociative attachment at low energy, non-dissociative attachment of some sort is significant enough to account for a large attachment coefficient (η/p) at low energy values.

Figure 26 shows a plot of the afterglow reduction as a function of seeding ratio for the seed gases used in the present investigations. This plot indicates the relative "efficiencies" of the "seed" gases for plasma quenching based on the measurements given in Section IV. SF_6 is found to be the most effective quenching gas which is obviously due to its large cross section and attachment coefficient at low energy. H_2O vapour also acts as a good seed gas for quenching and this is no doubt due to its high attachment coefficient of some non-dissociative processes at low energy (Fig.25). On a "per-molecule" basis, SF_6 is apparently more efficient than H_2O, but on the basis of quenching per unit mass, H_2O becomes equally attractive since its molecular weight is only 18 compared to 146 for SF_6.

CO_2, O_2 and NO show some degree of quenching efficiency although the mechanism of quenching for NO may be partly due to its unique property

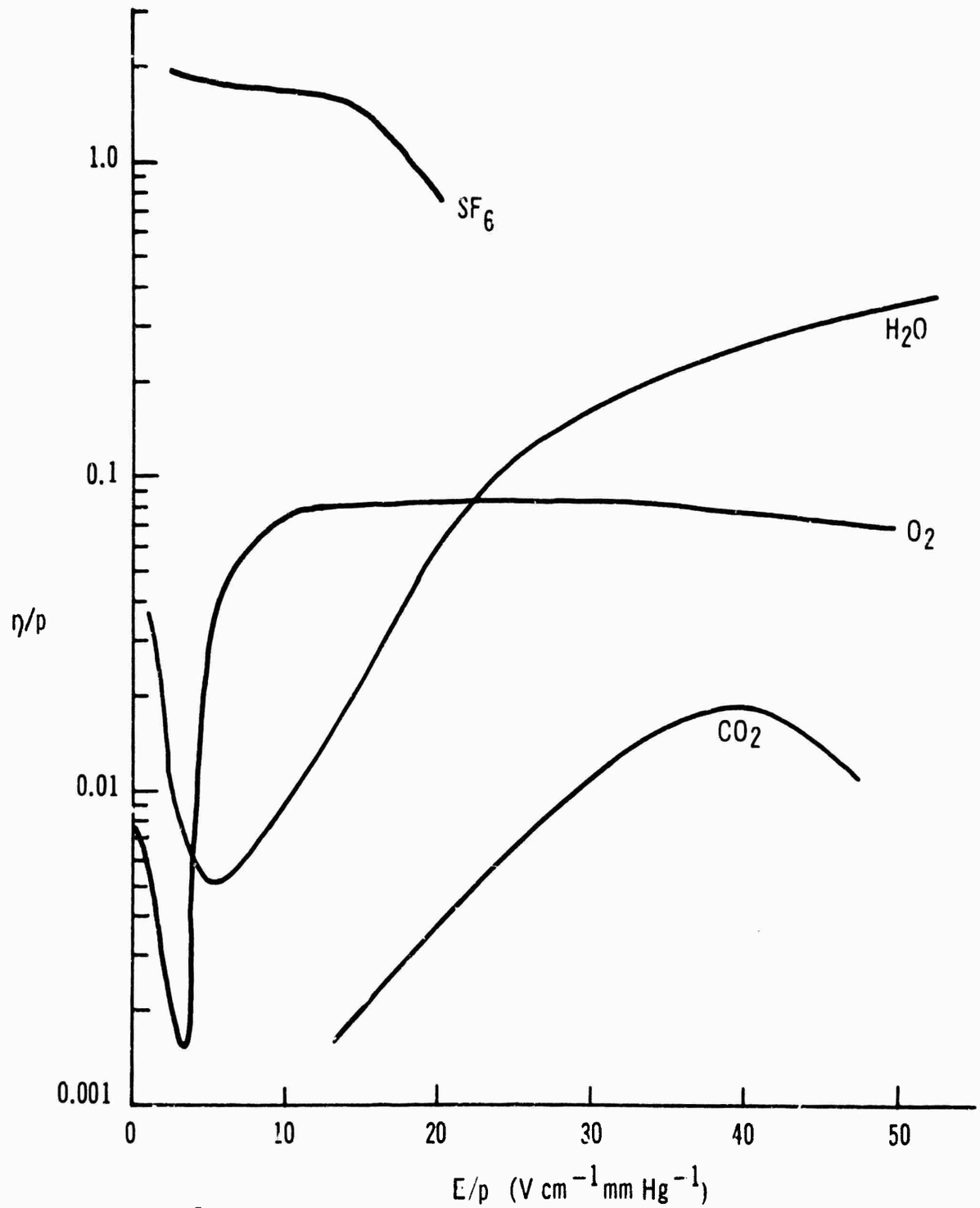

Fig. 25 Variation of attachment coefficients (η/p) for different gases as a function of E/p (V cm^{-1} $torr^{-1}$).

of absorbing the ground-state atomic nitrogen which acts as a reactant in producing pink glow (Prag & Clark 1963). This has been discussed in detail in connection with NO seeding (see Section 4.2).

CO_2 has been observed to be a slightly better quenching agent than O_2 although its attachment coefficient is smaller than oxygen. This can probably be attributed in part to the near resonance vibrational energy transfer between the N_2 ($X^1\Sigma g^+$) and the ν_3 mode of CO_2 (Milne 1965), but the exact mechanism of quenching the afterglow ionization is not fully understood.

It must be emphasized however, that attachment is not the only property of the seed gas which determines its quenching efficiency. It should be borne in mind that , in addition to "attachment", the seed gas can have an effect on the electron-ion recombination time in the afterglow as has been observed by Kuhns (1962) in water vapour. The seed gas may act as an efficient third body for the volume recombination of the plasma, leading to a sharp quenching.

The effect of the seed gas on the recombination time must therefore be studied with care before a quantitative assessment is made.

Another point to be mentioned in connection with the present experimental results, is the fact that all seeding was done in the so-called dark space between the discharge and the pink glow. This dark space contains many high energy carriers (atoms & molecules) which are responsible for the pink glow. The seed gas may have some collisional energy exchange with them and thereby augment the quenching of the pink glow. Hence, additional measurements will be required over a wide range of plasma conditions to establish the relative efficiencies of the seed gases more accurately.

As has been mentioned before, it would appear that the capture of electrons in the plasma by an electronegative gas is probably followed

by a charge exchange interaction between the positive ions and the negative ions which leads to complete neutralisation of the plasma (Carswell et al 1964)

Depending on the pressure in the discharge chamber the interaction may be a two body process or a three body process.

In the two body process, a reaction of the form

$$X^+ + Y^- \rightarrow X + Y$$

can take place both with atomic and molecular ions with high probability under certain conditions. The excess energy is distributed as kinetic energy among the collision products. The coulomb attraction between the reactants distorts the potential energy curve leading to a pseudo-crossing. The cross section for the single pseudo-crossover at a nuclear separation R_x for an exothermic collision of energy defect ΔE ev is of the form (Hasted 1964)

$$\sigma = 4\pi R_x^2 \, I(\eta)$$

where $R_x = 27.2/\Delta E$ and

$$I(\eta) = \int_1^\infty \exp(-\eta x)[1 - \exp(-\eta x)]x^{-3} \, dx$$

$$\eta = \frac{247 \mu^{\frac{1}{2}} \Delta\mu^2}{\Delta E^2 \, E_p^{\frac{1}{2}}}$$

where $\Delta\mu$ = energy separation at crossover

μ = reduced mass and E_p = energy of impact

The cross section reaches a maximum at $E_p \approx 100$ ev, but is not negligible at thermal energies. Yeung & Sayers (1958) have computed the cross section for iodine by radiofrequency absorption techniques and have found it to be of the order of 3×10^{-13} cm^2. In pure halogen vapour afterglows, the free electrons are captured in 100 μsec and the recombination coefficient was found to be independent of pressure up to 1 Torr.

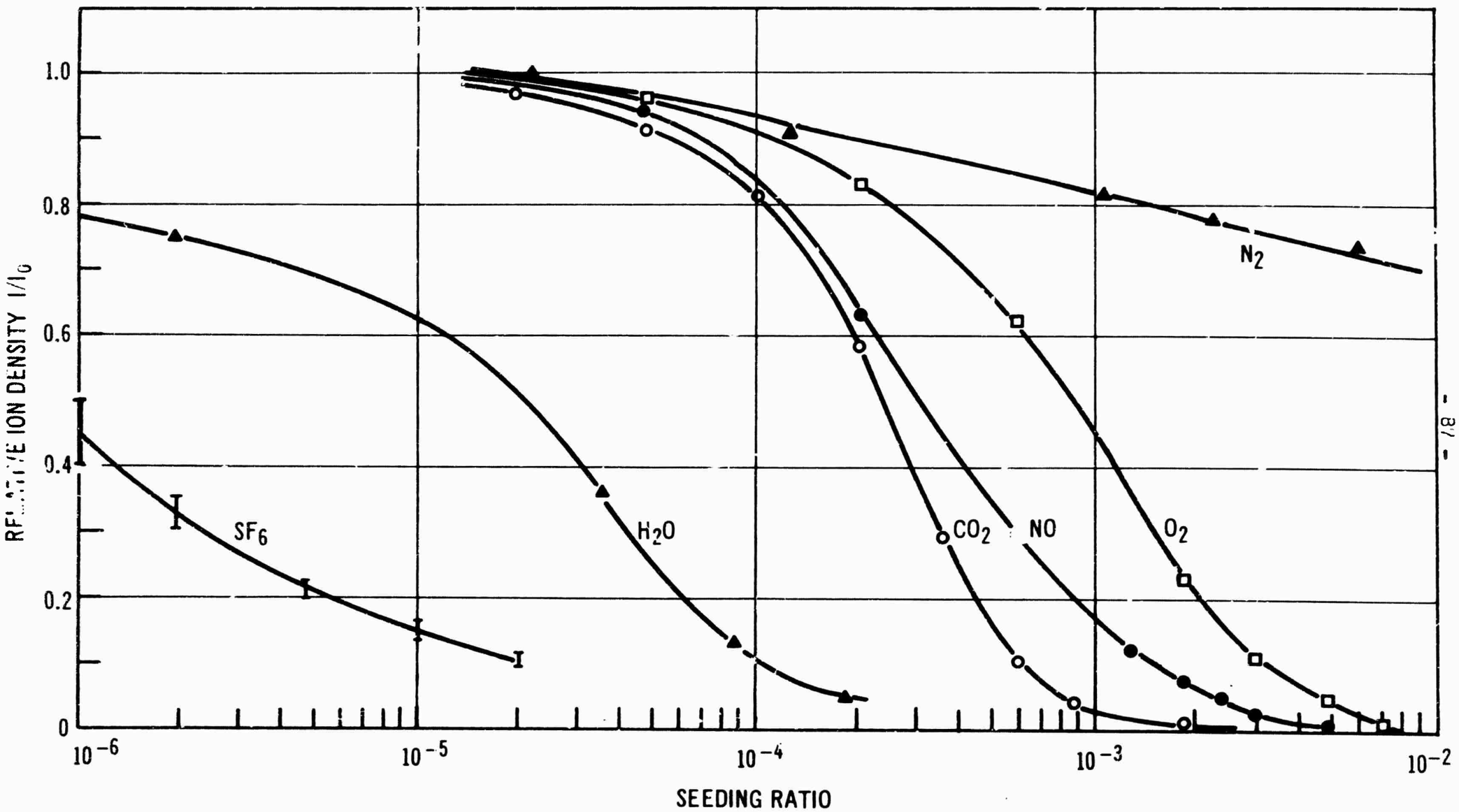

Fig. 26 Sample results showing the quenching of N_2 afterglows by various seed gases. The ratio I/I_0 expresses the ratio of the ion densities in the seeded and unseeded systems as shown by the 3914 Å emission.

At higher pressure, presumably a three body recombination is more predominant

$$X^+ + Y^- + Z \rightleftharpoons X + Y + Z$$

the third body taking the excess energy. The theory for this process has been worked out by Thomson & Langevin at low pressure and high pressure respectively. Recently, Natason (1959) has given a unified theory which agrees with Thomson at low pressure and with Langevin at high pressure. As for the experimental results, Bayers (1938) and Gardner (1938) have made some probe measurements which agreed quite well with Thomson's at low pressure.

Hence, in the present systems, the exact quenching processes could only be decided by making measurements of the attachments and recombination coefficients for the different seed gases. However, from the practical point of view, it may not be necessary to determine the processes exactly. Results such as those of Fig.26, when determined over the appropriate range of plasma conditions, should serve to define the relative quenching efficiencies of the various seed gases.

REFERENCES

Bachynski, M.P. - "Electromagnetic wave penetration of re-entry plasma sheaths" RadioScience Jour. of Research. NBS/USNC-URSI Vol.69 D No.2, 147 Feb.(1965).

Bass, A.M. - Absorption spectrum of the "pink" afterglow of nitrogen in vacuum ultraviolet. J.Chem.Phys. 40 695 (1964)

Beale, G.E.& Broida, H.P. - Spectral study of a visible short duration afterglow in nitrogen. J.ChemPhys. 31 1031 (1959)

Bhalla, M.S. & Craggs, J.D. - "Measurement of Ionization & Attachment Coefficients in Sulphur Hexafluoride in Uniform Fields" Proc. Phys.Soc. (Lond) 80 151 (1962)

Bortner, F.E. & Hurst, G.S. - Health Phys. 1 39 (1958).

Bradbury, N.E. - Phys.Rev. 40 980 (1932).

Bradbury, N.E. - J.Chem.Phys. 2 835 (1934).

Carswell, A.I. & Cloutier, G.G. - "Supersonic Plasma Streams Seeded with Electronegative Gases" Phys.Fluids 7 No.4 602 (1964)

Carswell, A.I. & Richard, C. - "Electrochemical Properties of Seeded Plasma Flow Fields" RCA Victor Res.Rep. 7-801-34 (Dec. 1964).

Chanin, L.M., Phelps, A.V. & Biondi, M.A. - Measurement of the attachment of slow electrons in oxygen. Phys.Rev.Letters 2 344 (1959)

Chanin, L.M., Phelps, A.V. & Biondi, M.A. - Measurement of the attachment of low-energy electrons to oxygen molecules. Phys.Rev. 128 219 (1962)

Clark, K.C. & Fairchild, C.E. - "Resonance Absorption by Nitrogen Atoms in Afterglows" Proc. of the 3rd Int.Conf. on the Physics of Electronic and Atomic Collisions (London) 1963, 581.Atomic Collision Processes. J. Wiley & Sons N.Y. (1964).

Cloutier, G.G. & Carswell, A.I. - Plasma quenching by electronegative gas seeding. Phys.Rev.Letters. 10 No.8 327 (1963).

Gardner, M.E. - Phys.Rev. 53 75 (1938).

Geballe, R. & Reeves, M.L. - "A condition on uniform field breakdown in electron-attaching gases" Phys.Rev. 92 867 (1953).

Hasted, J.B. - Phys. of Atomic Collisions, 271 (1964) Butterworth Advanced Physics Series.

Hickam, W.M. & Fox, R.E. - Electron attachment in Sulphur Hexafluoride using Monoenergetic Electrons, J.Chem.Phys. 25 No.4 642 (1956)

Harteck, K.P., Reeves, R.R. & Mannella, G. - Rate of Recombination of Nitrogen Atoms" J.Chem.Phys. Vol.29 608 (1958).

Innes, F.R. & Oldenberg, O. - Metastable atoms and the Auroral Afterglow of Nitrogen. J.Chem. Phys. 37 2427 (1962).

Johnson, E.O. & Malter, L. - A Floating Double Probe Method for Measurements in Gas Discharges" Phys.Rev. 80 58 (1950).

Kaufman, F. & Kelso, J.R. - J.Chem.Phys. 27 1209 (1957).

Kuffel, E. - "Electron Attachment Coefficients in Oxygen, Dry Air, Humid Air, and Water Vapour" Proc.Phys.Soc. 74 297 (1959).

Kuhns, P.W. - Microwave Measurements of Steady-state and Decaying Plasmas - IRE Trans. Space Electronics Telemetry SET-8, No.2 173.

Malter, L. & Webster, W.M. - "Rapid determination of gas discharge constants from probe data" RCA Rev. 191 (June 1951).

McAfee, J.R. K.B. - Pulse Technique for measurement of the probability of formation and mobility of negative ions. J.Chem.Phys. 23 No.8 (1955)

McDaniel, E.W. - Collision pheno. in ionised gases. 382 J.Wiley & Sons (1964)

Milne, E.L., Steinberg, M. & Broida, H.P. - Vibra luminescence of CO_2 and N_2O in Active Nitrogen. J.Chem.Phys. 42 No.7 2615 (1965).

Muschlitz Jr., E.E. - Formation of Negative ions in Gases by Secondary Collision Processes. J.Appl.Phys. 28 1414 (1957)

Nakamura, M., Tanaka, Y. Jursa, G.S. & Innes, F.R. - Bull.Am.Phys.Soc. 9 183 (1964)

Natason, G.L. - Zh.Tekh.Fiz 29 1373 (1959).

Prag, A.B. & Clark, K.C. - Excitation Mechanism for the Nitrogen Pink Afterglow. J.Chem.Phys. 39 No.3 799, 1963.

Repp, D. & Englander-Golden, P. - J.Chem.Phys. 40 573 (1964).

Sayers, J. - Proc.Roy.Soc. A 169 83 (1938).

Yeung, T.H.Y. & Sayers, J. - Recombination Coefficients for Positive and Negative Ions" Proc.Phys.Soc. (Lond) 71 341 (1958).

APPENDIX -A

Afterglow Studies in Non-Flowing Nitrogen Discharges

As has been stated earlier in the report, the pulsed afterglow study was initially undertaken in a non-flow condition in order to have a cross-check of some of the results in the flowing system which gives a spatial display of the afterglow pattern. It was hoped that this comparative study would supply more accurate data on the recombination times and help in establishing the time scale of the multiple peaks observed in the flowing system.

It turned out that the study revealed some very important aspects of the afterglow so far undetected in a non-flowing system.

The "small" system was used and in this series of measurements, a photomultiplier was placed in front of the discharge to receive the light emitted. The pressure was kept constant at a particular value under no-flow condition. The afterglow intensity of 3914 Å and 5780 Å emission (using interference filters) was photographed by switching the discharge off. This was done for different pressures, wall temperature and "wall conditioning". The system was given 2 minute flushing time between each shot at a moderate pressure (4-5 Torr).

Figure A1 and Figure A2 show the effect of pressure on the afterglow emission for 3914 Å and 5780 Å respectively. The general behaviour of both the 3914 Å and 5780 Å emission pattern is found to be similar. At low pressure (2 Torr) the peak occurred around 15 ms; while at higher pressures (5 Torr), multiple peaks were observed at about 3 ms, 15 ms and 24 ms.

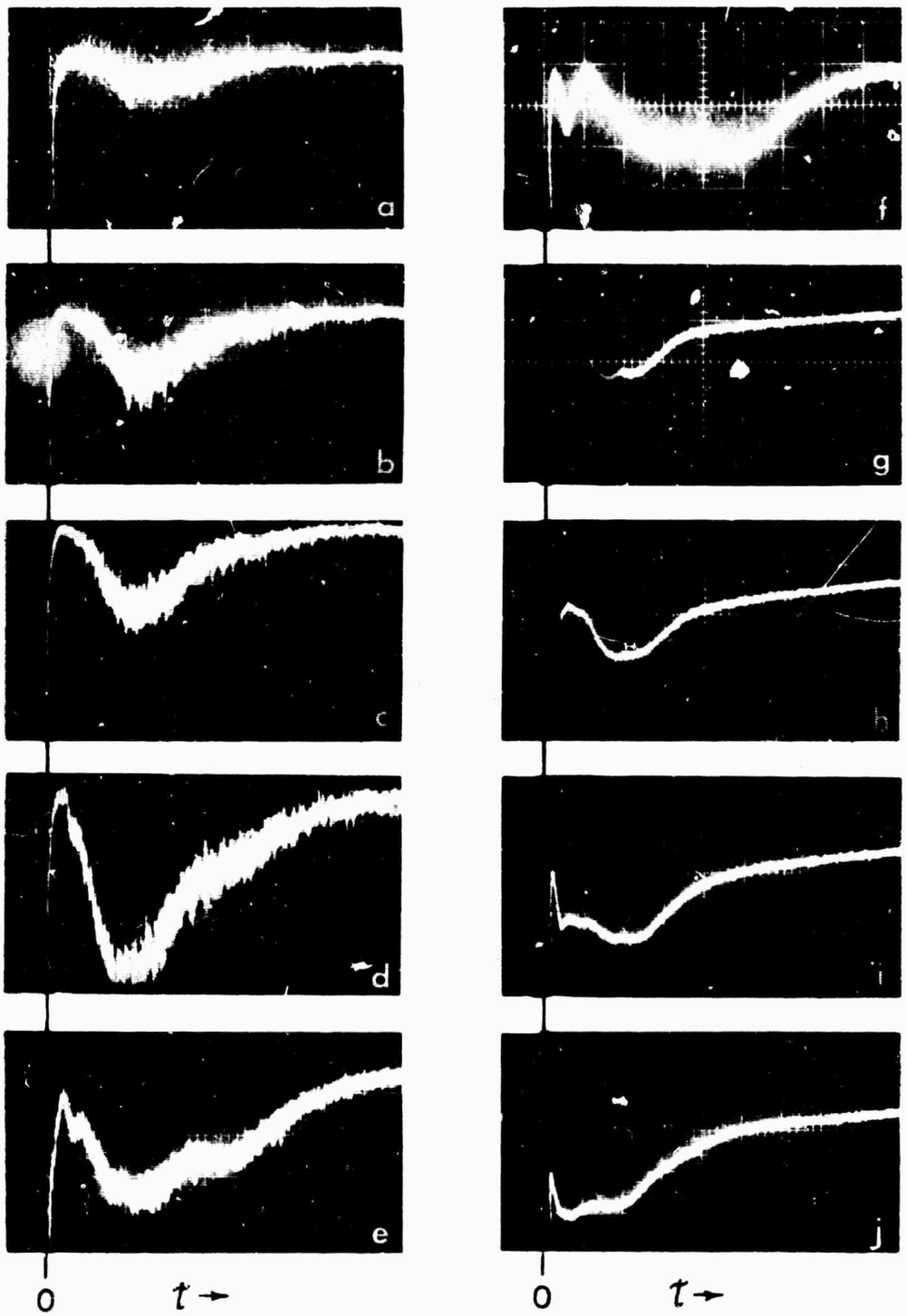

Fig. A1 Sample photographs showing variation of the afterglow 3914 Å emission with pressure. (Light intensity increases downward.) Horizontal sweep (a)-(f) 5ms/div. (g)-(j) 10ms/div. vertical gain (a)-(d) 5mv/div. (e) 20mv/div. (f) 50mv/div. (g)-(j) 100mv/div. (a) 1.0 torr; (b) 1.7 torr; (c) 2.0 torr; (d) 3.0 torr; (e) 4.0 torr; (f) 5.0 torr; (g) 6.0 torr; (h) 7.0 torr; (i) 8.0 torr; (j) 9.0 torr.

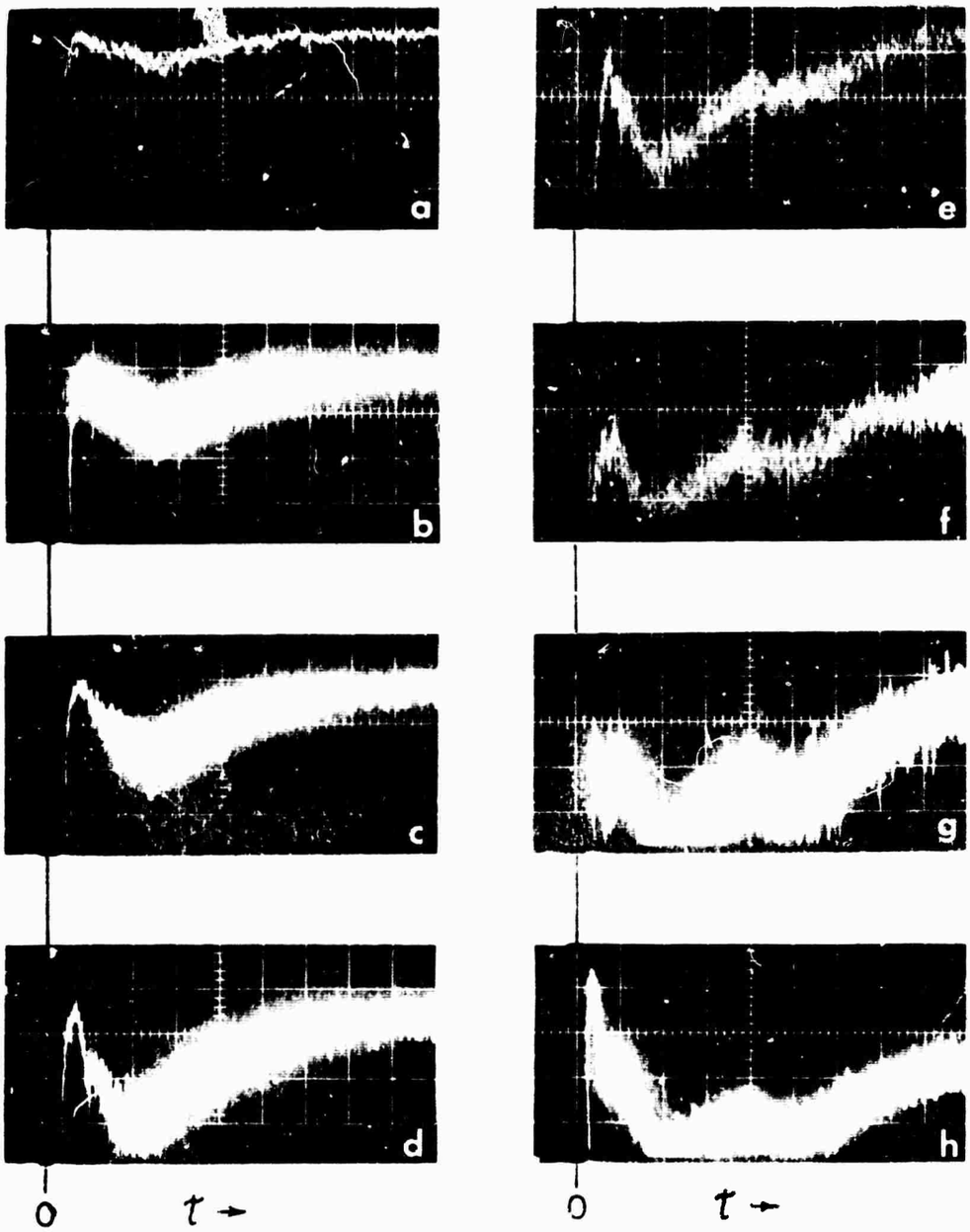

Fig. A2 Sample photographs showing variation of the afterglow 5780 Å emission with pressure. (Light intensity increases downward.) Horizontal sweep 5ms/div. vertical gain (a)-(g) 5mv/div. (h) 10mv/div. Pressure (a) 1.0 torr; (b) 1.5 torr; (c) 2.0 torr; (d) 3.0 torr; (e) 4.0 torr; (f) 4.5 torr; (g) 5.0 torr; (h) 6.0 torr.

Figure A3 shows the effect of wall temperature on the afterglow intensity pattern. (The temperature was monitored by an external thermocouple on the pyrex tube.) A negative temperature effect was observed as the temperature increased. It was found that at a wall temperature of about 150°C, the afterglow disappeared completely. In fact, brief heating of pink afterglow in a flowing system did decrease the brightness of the pink (Beale & Broida 1959).

Figure A4 shows an interesting effect, probably due to "wall conditioning". It was found that when the discharge was first turned on after a long interval of time (e.g. over night), the afterglow pattern continuously changed with successive "firings". Every time the discharge was on for 5 secs and then switched off. The system was flushed for two minutes between each shot. It was found that after 10-12 "firings", the afterglow pattern attained a steady structure at a particular pressure and a sort of "equilibrium" condition was reached. Initially the afterglow showed an early spike (5 ms) which then disappeared as a peak at 13 ms "built up" at the equilibrium condition . This peculiar behaviour is attributed to the effect of "wall conditioning" which had already been pointed out as being an important parameter in obtaining a pink afterglow in a flow system.

Another peculiar behaviour of the afterglow pattern was that it varied from position to position in the discharge. The best position in obtaining a multiple peaked afterglow pattern was not the mid-point between the electrodes of the discharge, but rather a few centimeters upstream in the blue region. The "midpoint" of the discharge showed an earlier spike. As the photomultiplier was moved further "downstream", the peak was found to disappear gradually.

It is to be noted carefully that before any measurement was made, the system was flushed for about 2 minutes at a pressure of 4 to 5 Torr. This

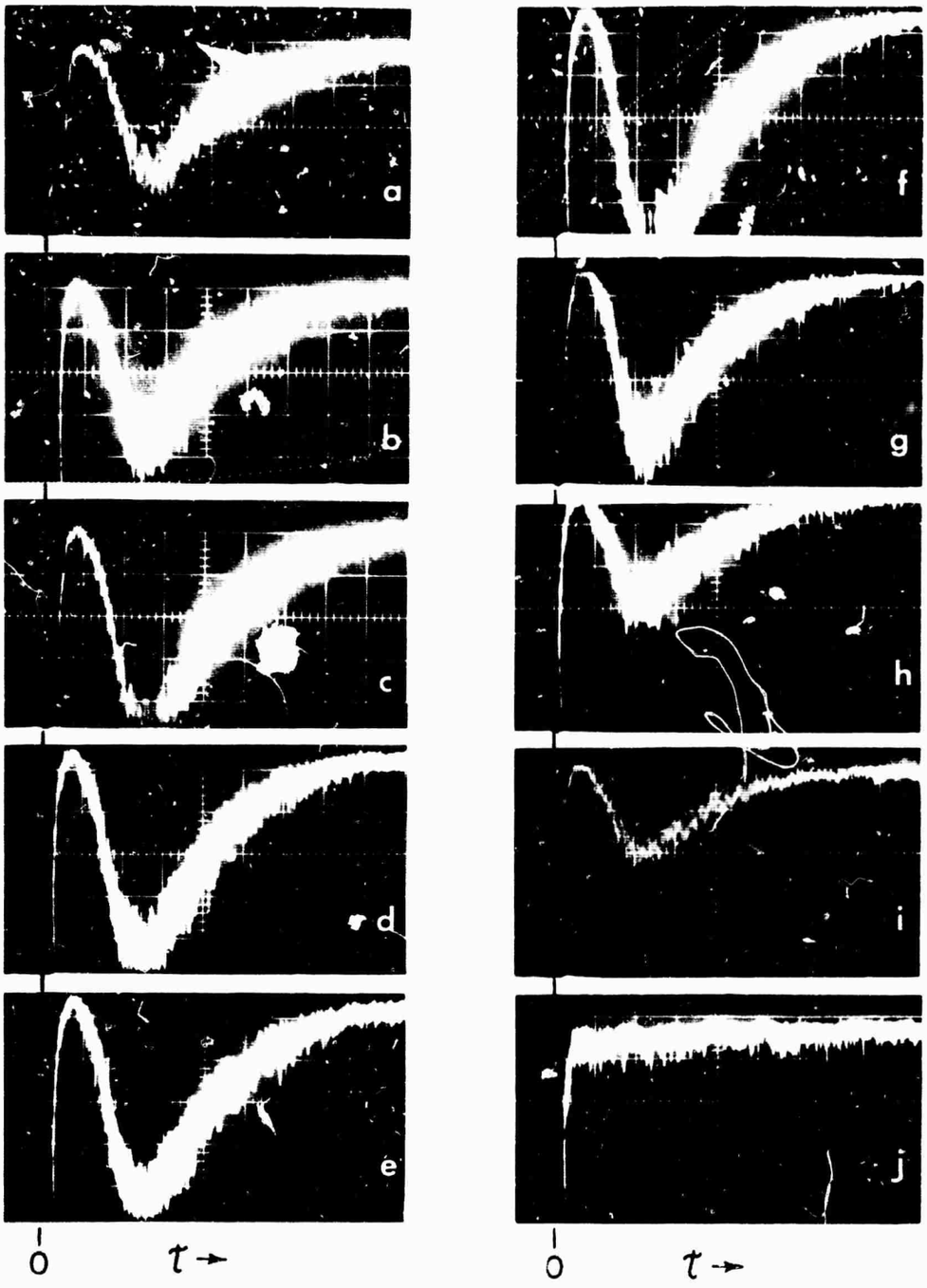

Fig. A3 Sample photographs showing the variation of afterglow 3914 Å emission with discharge tube wall temperature. (Light intensity increases downward.) Pressure 2 torr. Horizontal sweep 5ms/div. vertical gain (a)-(i) 5mv/div. (j) 2mv/div. (a) 33°C; (b) 38°C; (c) 40°C; (d) 55°C; (e) 60°C; (f) 65°C; (g) 70°C; (h) 80°C; (i) 90°C; (j) 150°C.

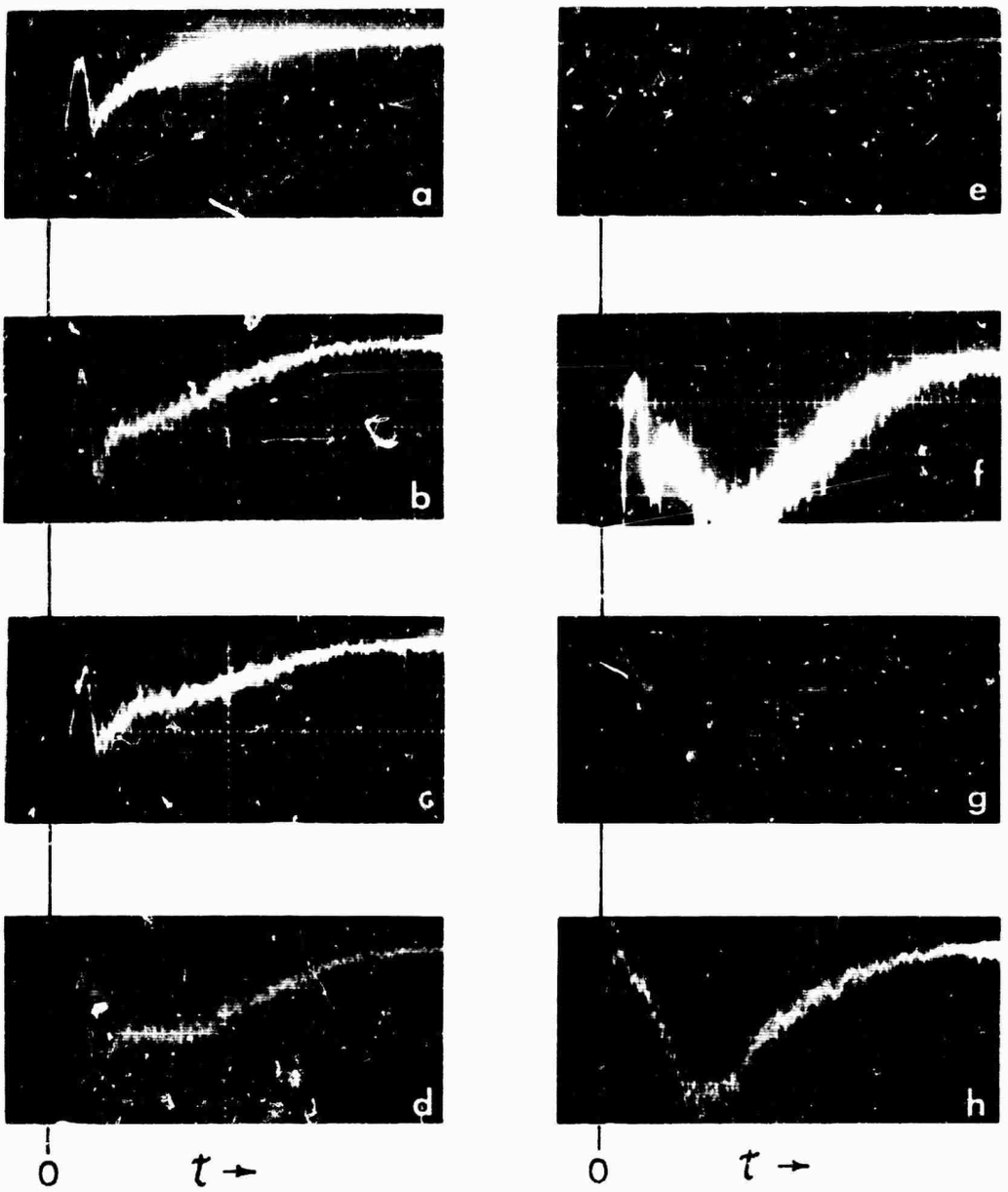

Fig. A4 Sample photographs showing variation of the afterglow 3914 Å emission. (Light intensity increases downward.) Due to wall conditioning. Pressure 2 torr. Horizontal sweep 5ms/div. (a)-(e) vertical gain 10mv/div. (f)-(h) vertical gain 5mv/div. The series from (a) to (h) shows the changes occurring from first discharge in the tube to "equilibrium" condition.

was an important measure in connection with the reproducibility of the results. It was found that without this "flushing", the afterglow pattern was lost after three or four "firings". Thus, the flushing may be serving to drive out some impurity or acting to provide a favourable wall "conditioning".

These results reveal some very interesting phenomena in connection with the pink glow which has been described by so many authors as "temperamental".

The multiple peaks confirm the complicated nature of the recombination processes involved. Variation in the value of the afterglow time quoted by different authors in a supposed "identical" condition can probably be explained from the effect of "wall conditionings" and wall temperature which may change with the method of production of the primary discharge that means either rf discharge, microwave discharge or D.C. discharge.

The peaks in the afterglow pattern obviously indicate some sort of repetitive production mechanisms along with the loss due to recombination and diffusion. Without specifying the actual species involved in the recombination processes of such a complicated nature, one can write the recombination equation involving the loss and production processes for a cylindrical geometry

$$\frac{dn}{dt} = -\alpha n^2 + \alpha \delta n + Q(t) + \frac{D_a}{r}\frac{\partial}{\partial r}\left(r\frac{\partial n}{\partial r}\right)$$

where δ = non-zero net charge density

α = electron ion recombination coefficient

D_a = ambipolar diffusion coefficient

$Q(t)$ = a production term; that is an ionizing source when the actual discharge is off.

$\delta = 0$ in most of the occasions.

Kunkel (1951) solved this equation neglecting diffusion and assuming an ionizing source of exponentially decay form

$$Q(t) = b e^{-\beta t}$$

and he obtained a solution of the form

g".

$$n \simeq \frac{1-e^{-\beta t}}{\alpha t+\beta/b}$$

which can explain one peak in the afterglow.

A qualitative explanation of a process w'th single peak can be given as follows.

Initially, the ionizing source (Q(t)) is most efficient in producing ions and electrons, and loss due to recombination is negligible due to lack of concentration. Hence, production will increase until the concentration is large enough to make recombination an efficient mechanism. As soon as sufficient concentration of ions and electrons are formed they will recombine and the concentration will decrease. The multiple nature of the peaks is difficult to explain unless some sort of oscillatory reactions are involved. Reaction schemes suggested by Prag & Clark (1963) may fulfil the Rice's oscillatory criterion (Rice 1960) as has been proposed by Young (1962) for his own set of reactions. In fact, Prag & Clark (1963) did suggest some sort of cyclic process for their own set of reactions in causing repetitive dissociation and formation of N_4 molecule which is believed to be the main energy carrier in producing pink afterglow.

In this connection also, reference should be made to the work of Fite et al (1962) who found in their studies of pulsed N_2 afterglows that the various nitrogen ion species (N^+, N_2^+, N_3^+ and N_4^+) exhibited a "peaked" distribution in the afterglow and that the various species reached their maximum abundance at different times in the afterglow.

As a result of the present pulsed studies, the complex nature of the short duration afterglow of N_2 has been further emphasized. The maxima at times less than 5 millisec, shown in the figures are very sharp and do not seem to have been reported previously. The peaks at 10-15 m sec correspond to those we have observed in the flow system as shown in Sections III and IV. Because of the complicated interplay of temperature, pressure, impurity and wall-effects, any experimental investigation of the detailed structure of the afterglow will have to be performed with great care if meaningful results are to be obtained.

REFERENCES FOR APPENDIX A

1. Beale, G.E. & Broida, H.P. - "Spectral Study of a Visible, Short Duration Afterglow in Nitrogen" J.ChemPhys. 31 1030 (1959)
2. Fite, W.L., Rutherford, J.A., Snow, W.R. & Van Lint, V. - Disc. Faraday Soc. 33 264 (1962)
3. Kunkel, W.B. - "Analysis of Ionic Recombination Including Ion Production during Measurement". Phys.Rev. 84 218 (1951)
4. Prag, A.B. & Clark, K.C. - "Excitation Mechanism of Nitrogen Pink Afterglow" J.Chem.Phys. 39 No.3 799 (1963)
5. Rice, O.K. - "Condition for a Steady State in Chemical Kinetics". J.Phys.Chem. 64 1851 (1960)
6. Young, R.A. - "Observations on the Pink Nitrogen Afterglow" J.Chem.Phys. 36 No.11 2854 (1962)

APPENDIX B

Velocity Measurements in Afterglow Flow Systems

The flow velocities quoted in the results given in this report represent only average values. As discussed earlier (Section III), because of the complex nature of the nitrogen afterglow, temperature and pressure gradients are generated in the flow and the velocity becomes a function of spatial position in the flow system.

In an attempt to improve the accuracy of the velocity values obtained and possibly to observe the spatial dependence of this velocity in the flow systems, measurements were carried out using a pulse technique. Generally speaking, it consisted of switching off the discharge in the flowing gas at a known instant and monitoring the subsequent behaviour of the afterglow at various positions downstream, with the help of photomultipliers.

The composite photograph in Fig. B1 presents a selection of traces extracted from a series of such measurements illustrating the time history of the afterglow at discrete positions along the tube from the moment the discharge is switched off. The bottom and the top traces show the time dependence of the rf power and afterglow intensity respectively. The rf signal was monitored from an antenna located in the vicinity of the discharge, rectified, detected through an R.C. circuit and fed into the oscilloscope. The rather long decay time for the rf. signal shown on the pictures (~ 1 millisec) is that of the R.C. circuit. The actual decay time, measured without filter, is of the order of 25 μsec, - that is to say, instantaneous, compared to the time scale of the afterglow. The discharge rf was turned off

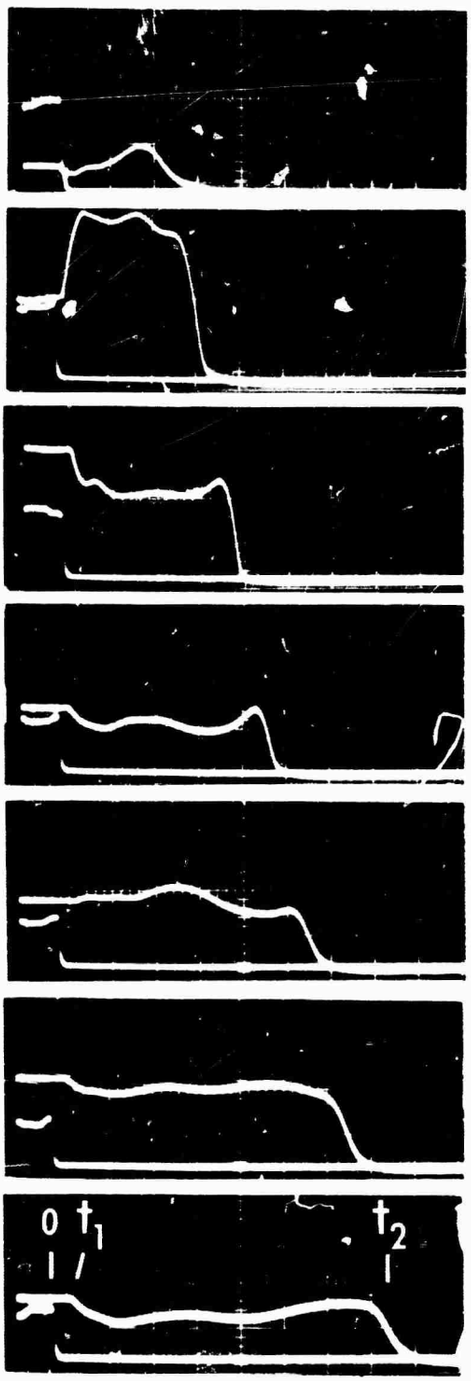

Fig. B1 Sample photographs showing photomultiplier response (upper trace) when the R.F. (lower trace) is switched off (t=0) for different photomultiplier distances (d) from the discharge. Horizontal sweep 5ms/div. Pressure 1.5 torr. Top to bottom d: 19cm; 25cm; 31cm; 41cm; 51cm; 61cm; 71cm.
t_1: Time to receive the first response
t_2: Time required for final decay.

by a delayed relay operated manually by a switch which at the same time triggered the oscilloscope.

The rf signal trace is self explanatory. Three different regions can be observed in the afterglow emission trace. Firstly, before switch-off, a continuous horizontal line showing the steady state nature of the afterglow in the flow. Then a sudden break of the equilibrium (more or less pronounced, depending on the position of the photomultiplier), leading to a region of undulating structure marked generally by a slight decrease of the average intensity and, in a few cases, by an appreciable increase. Finally, a rapid intensity decay coinciding with the disappearance of the glow. The final decay is preceded in all cases by a short intensity maximum.

The flow velocity can be found by dividing the discharge-to-photomultiplier distance by the time interval between the discharge rf cut-off and the afterglow decay (t_2). Because of the appreciable extent of the discharge, there is some uncertainty about both the effective size and location of the afterglow source. The position of the source was, as a result, fixed arbitrarily at the downstream end of the discharge electrode and the graph of time (t_2) against position was plotted in Fig. B2 from the same series of traces as those shown in Fig. B1.

As a consequence of both the finite size of the source and the finite decay time of the glow, the afterglow intensity does not present a sharp cut-off and there exists some doubt as to where t_2 should be measured. Therefore, three values of time, corresponding respectively to those measured at the last maximum, halfway down the decay slope and at the intensity zero, were recorded. And in Fig.B2, the vertical lines at each position indicate the spread of these times. It is apparent from the figure that the t_2 values determine a fairly good straight line indicating a rather constant value of the velocity as determined in this manner. Extrapolation of this

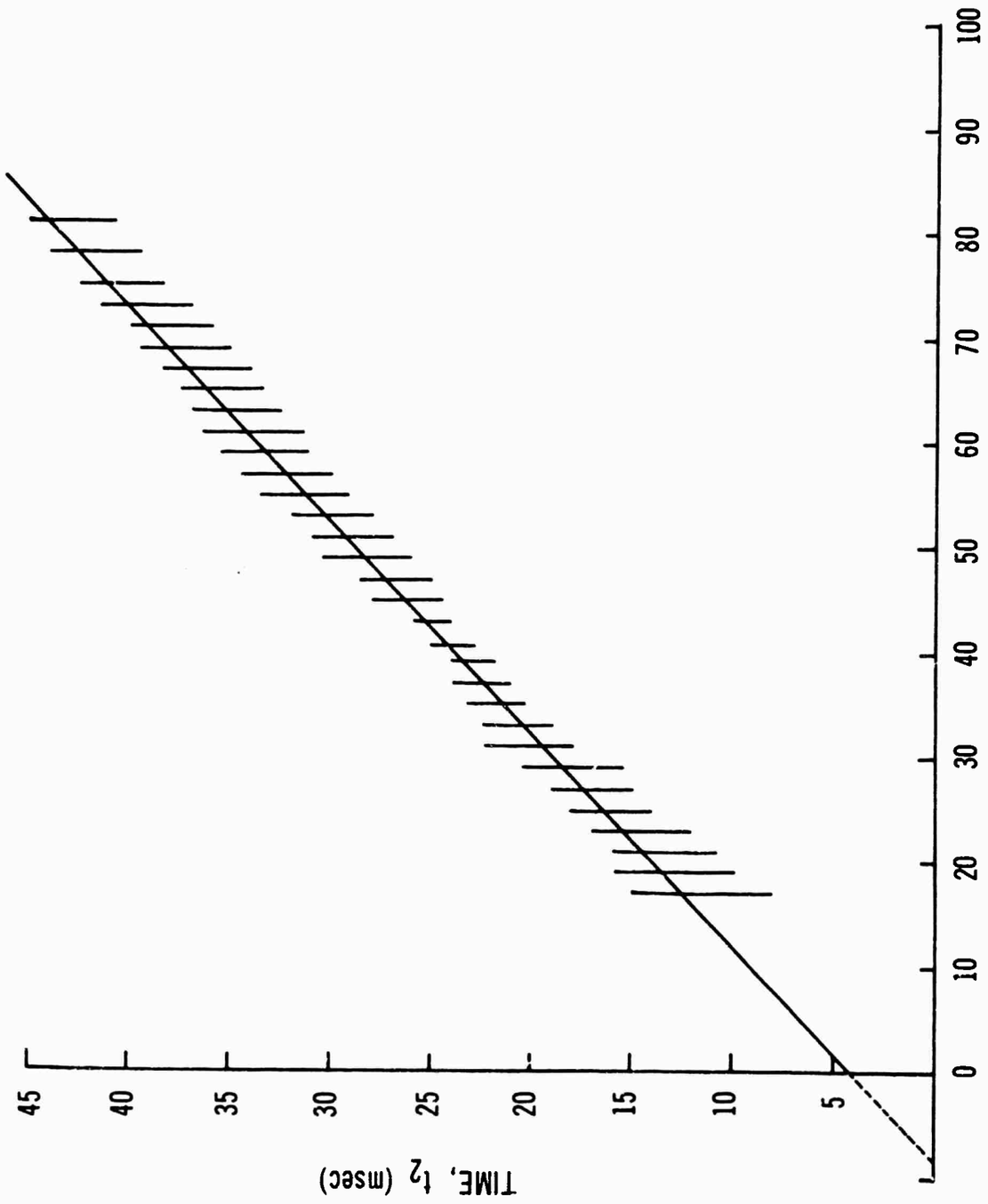

Fig. B2 Plot of the time interval (t_2) between switch off of the rf discharge and decay of the afterglow intensity as function of position downstream, leading to measurement of the flow velocity. ($p = 1.5$ Torr).

line down to the distance axis locates the effective position of the source relative to the arbitrarily chosen value. The velocity calculated from the curve of Fig.B2 is found to be 2040 cm/sec.

Another interesting phenomenon occurs on switch-off of the rf discharge. It consists of a signal travelling down the tube at the speed of sound and believed to be caused by a pressure disturbance due to the sudden gas cooling accompanying the cut off of the discharge. The phenomenon corresponds to the first break occurring on the downstream photomultiplier traces (i.e.t_1 in Fig.B1. It is observed that the time t_1 increases as the photomultiplier is moved down the tube.

When the time t_1 is plotted against position, the slope of the straight line so obtained gives the propagation velocity of the signal. This is done in Figure B3 for two different flow conditions in nitrogen. We see that the velocity of propagation of this signal is independent of the gas pressure. A speed of 3.5×10^4 cm/sec was calculated from Fig.B3 and as an average value it agrees very well with the calculated velocity of sound in nitrogen at 300°K. Thus, knowing the temperature dependence of sound velocity, the measured velocity can be used to calculate the effective gas temperature. This temperature may then be employed in the calculation of the flow velocity from measurements of the flow volume.

This disturbance taking place at the source and travelling rapidly downstream in the afterglow is closely related to the undulating structure of the trace in the second region of Fig.B1. When the rf is cut off, the "instantaneous" replacement of the hot gas in the discharge region by cool (300°K) incoming gas generates a pressure rarefaction which propagates down the tube, creating instabilities and generating oscillations of the afterglow intensity.

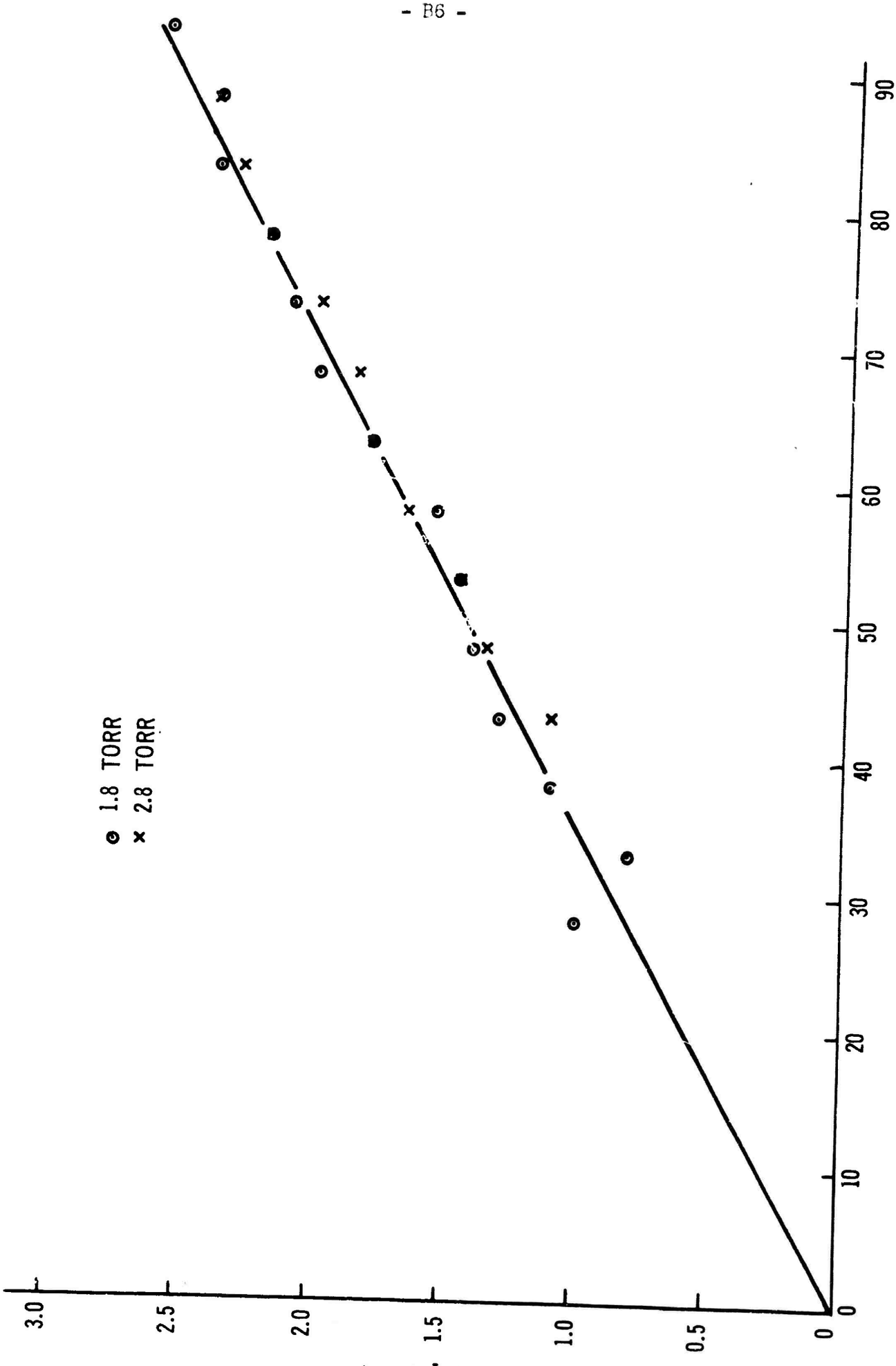

Fig. B3 Plot of the time interval (t_1) between the switch off of the rf discharge and the setting up of an undulating afterglow intensity as function of position downstream illustrating the propagation of a disturbance at the velocity of sound (p = 1.5 Torr).

One of the immediate effects produced by the disturbance is observable in the sample photographs of Fig.B1. It is apparent that some downstream photomultiplier traces undergo a rise in intensity (25 cm, 51 cm) while the others suffer a drop right after the break point (t_1). The reason for this can be found by referring to Fig.B4 where an axial scan of the afterglow is shown for steady state conditions. Also indicated by vertical lines, are the photomultiplier positions corresponding to time history photographs of Fig.B1. We observe that if the whole curve is shifted upstream (i.e. to the left) by a few centimeters, the amplitudes given by the new crossing points have undergone a variation in the same direction as that following the break on the corresponding photograph. Hence, the photomultiplier at 25 cm is affected by a big rise and position 31 cm by a rather large drop on both Fig. B1 and Fig. B4. It therefore appears that the immediate result of turning off the discharge is to shift the afterglow pattern upstream. (This "backward" motion can actually be observed visually when the pink glow has sufficient intensity).

In order to check this result and find out how fast this displacement was taking place, curves of Fig. B5 were constructed using the series of photographs whose samples appear in Fig. B1. From the time history taking place at discrete positions down the afterglow (~ every 2 cm) the spatial intensity distribution of the afterglow is reconstructed with time as the parameter. The shift is well illustrated and the motion is seen to start with the passage of the "sound wave" and be achieved in less than 2 milliseconds.

This plot is most instructive for following the time variation of the distribution. After the rapid backward (upstream) motion of the afterglow, the unexcited, cold gas moves downstream and begins to diminish the afterglow intensity at the upstream end. As shown in Fig. B5, this removal of the afterglow occurs as an "eating-away" of the upstream edge with the downstream

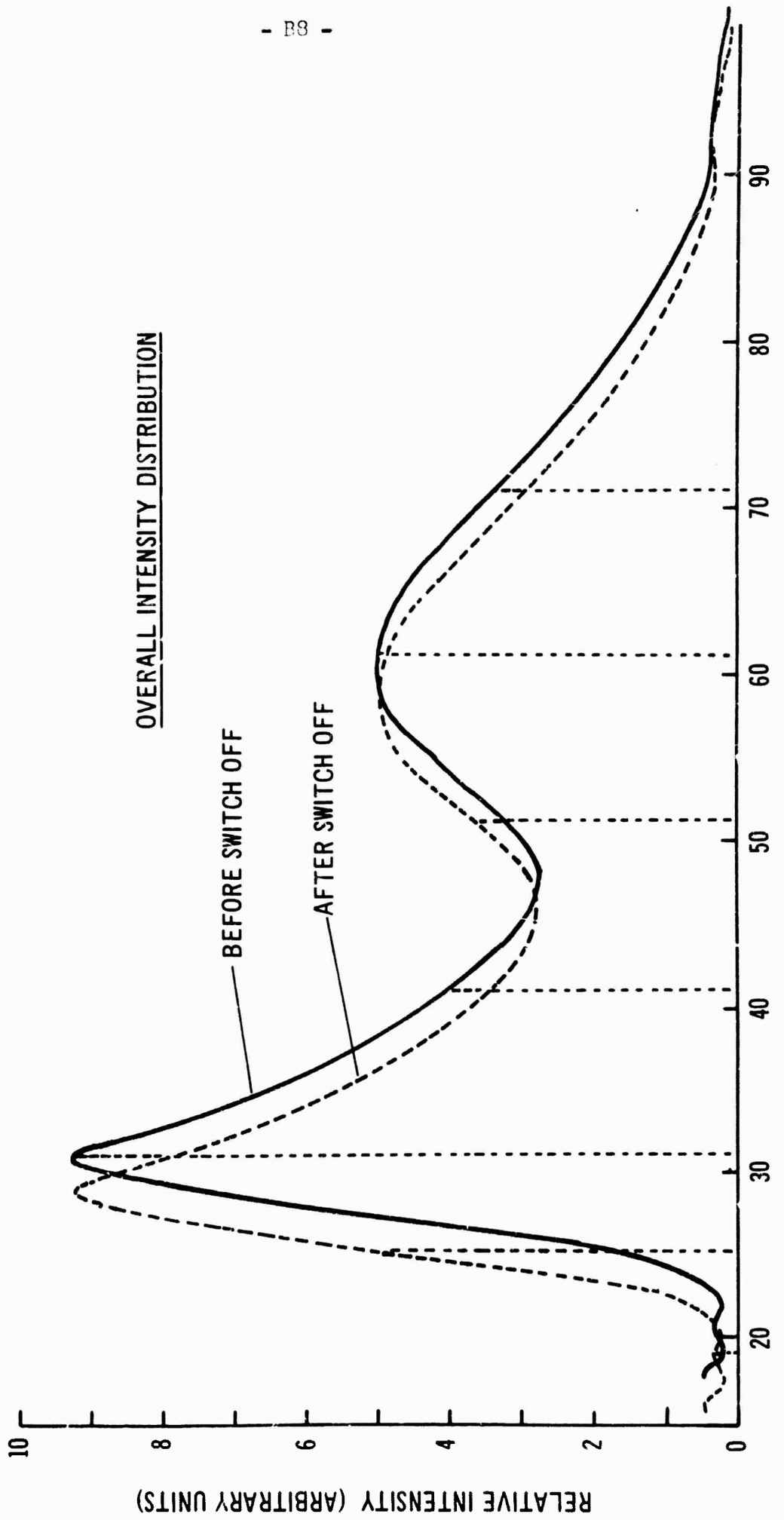

Fig. B4 Illustration of the rapid upstream shift of the afterglow that is believed to take place on switch off, and the corresponding rise or drop of the intensity depending on the position.

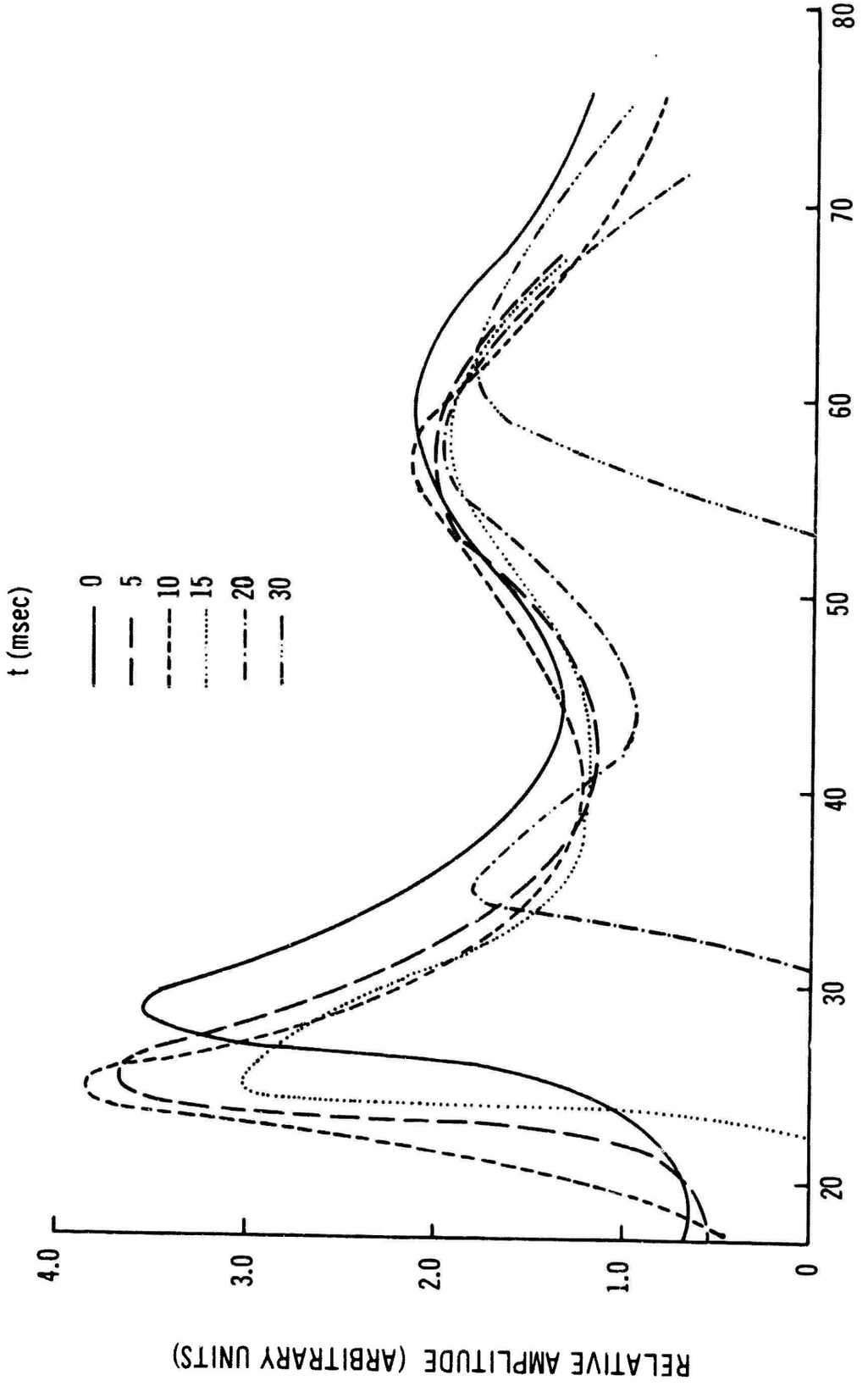

Fig. B5 Plot of the afterglow intensity distributions for different times after switch off.

portion of the afterglow distribution remaining essentially intact and at rest with respect to the flow tube. This type of behaviour can be explained from the fact that at any given position in the flow system, the afterglow conditions first adjust rapidly (in a time t_1) to the new pressure and velocity conditions and then remain in a steady-state flow condition (apart from the small undulations) until the unexcited gas reaches that position (time t_2) and removes the excited species.

In an attempt to improve the accuracy of the pulsed method for measuring flow velocity, a different arrangement was employed. This time, two photomultipliers separated by a known distance, were located at different positions downstream and their output was fed into a dual beam oscilloscope. The discharge rf power cut off was carried out in the same manner as described previously and so was the 'scope triggering. Fig. B6 shows sample photographs of the simultaneous responses of the photomultipliers for a separation of 15 cm and distances (upstream photomultiplier) of 20, 48 and 82 cm respectively from the discharge. From the photomultiplier separation and time interval between decays as measured on the photographs, the flow velocity can be found. In principle, by reducing the inter photomultiplier distance it is possible to increase the resolution (i.e. decrease the distance averaged velocity) and establish the flow velocity distribution down the tube. However, it is found in practice that this method of measurement is of limited accuracy because of the irregular nature of the decay portions of the intensity curves. Also, as a result of phenomena such as those shown in Fig. B5, any use of pulsing techniques, provides a measure of the velocity after the pulse and not of the original steady-state flow. This is true whether one or several photomultipliers are used. This effect has been observed with the two photomultipliers arrangement. Using traces such as those shown in Fig. B6, the flow velocity was measured for several flow conditions and simultaneously the

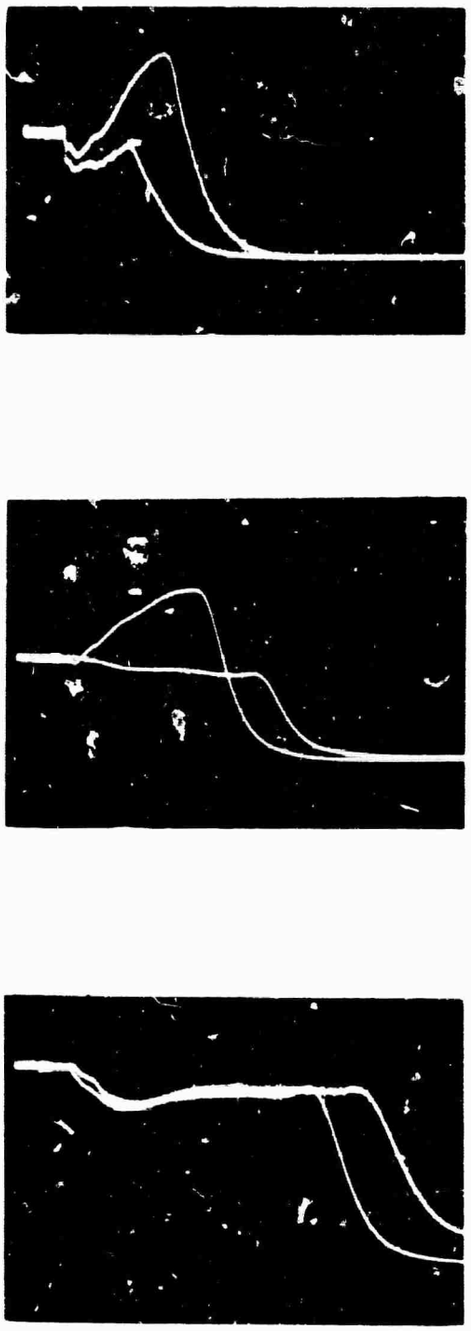

Fig. B6 Sample photographs showing the simultaneous response of two photomultipliers at different distances from the source, Horizontal sweep 5ms.div. Pressure 3.5 torr. Separation between the two photomultipliers is: 15cm (fixed). Distance (d) of the first photomultiplier from the discharges is: 20cm; 48cm; 82cm.

total volume flow was recorded to provide a second velocity measurement. The results are summarized in Table I below:

Table I - Comparative Flow Velocities

Pressure	Vel. from Photomult.	Vel. from Vol.flow(300°K)	Vel. from Vol.flow (400°K)
1.5 Torr	1970 cm/sec	2060	2780
2.0 "	2270 "	2360	3150
3.5 "	2230 "	2320	3100

To compute the velocity from the volume flow it is necessary to know the gas temperature in the flow tube. From the thermocouple measurements (e.g. Fig.7) it is known that the temperature of the afterglow is of the order of 400°K. In order to get reasonable agreement in Table I however, a temperature of about 300°K must be used indicating that the flow velocity measured by the "switching-off" technique corresponds to the temperature of the inflowing room temperature gas. (In agreement with the velocity of sound measurement from t_1 of Fig.B1). This is quite reasonable in view of the rapid velocity reduction on switch-off shown by the upstream motion of the afterglow pattern in Fig. B5.

In conclusion it can be stated that it was found that the pulse method with switch-off of the discharge source and downstream intensity monitoring photomultipliers does not constitute an accurate means for the determination of the steady state afterglow. The arrangement using two downstream photomultipliers can however, be employed advantageously for a rapid determination of the order of magnitude of the flow velocity. Perhaps the most interesting aspect of this study is the observation of the "sound" wave propagated down

the tube on switch-off which is followed by a rapid reduction in the flow velocity. The sound wave can be used to find an average afterglow temperature that can also be employed in the calculation of the average flow velocity by measurement of the flow exhaust.

APPENDIX C

Double Probes in Plasmas

Dr. T.W. Johnston

INTRODUCTION

Double probe investigation of a plasma is very useful in cases where the current drawn from the plasma must be kept to a minimum. In practical cases the positive ion current variation to the probe elements is not negligible, and simple theory, based on this neglect, is inadequate. Several people have dealt with this problem in collisionless plasmas with varying degrees of success. (Allen, Boyd and Reynolds (1957); Bernstein & Rabinowitz (1959); Hall (1961,1964), Lam (1965), Chen (1965)).

Recently Laframboise (1964) has calculated very convenient numerical results for cylindrical (and spherical) probes in stationary Maxwellian collisionless plasmas with one type of positive ion and one type of negative ion with arbitrary charge and mass.

This last feature allows one to construct the Langmuir single probe characteristic and, from it, the double probe characteristic for any two-component plasma of interest.

In this appendix, this has been done for the cases of interest in the present study: N_2^+ and $e^-(T_e >> T_{N_2})$, and N_2^+ and $SF_6^-(T_{N_2} = T_{SF_6})$. From the results a simple procedure is derived for obtaining moderately accurate results quickly from the probe characteristics.

A basic conclusion is that, while double probes are adequate for determining the positive ion density, they are almost useless for determining the composition of the negative charge species (i.e. the relative proportions of electrons and negative ions).

CONSTRUCTION OF PROBE CHARACTERISTICS

The determining parameter is the root of the ratio of the masses of the charge species. For the N_2^+, e^- system $\sqrt{m_+/m_e}$ is 227, for the N_2^+, SF_6^- system $\sqrt{m_-/m_+}$ is 1.58. Laframboise's normalized curves are shown in Fig.1 for the attracted particles for various ratios of probe radius r_p to Debye length λ_D. The repelled particle current is merely $\exp(-eV_p/kT)$, where V_p is the voltage relative to the plasma potential.

The convenient normalizing current per unit probe area to use is the random current at the greater temperature of the species, normalized to whatever species mass is convenient.

For the N_2^+, e^- system, since the ion current was of interest and the ion temperature was low, the normalizing current was

$$I_{o+} = n_+ e\,(2\pi r_p L_p)\left(\frac{kT_e}{2\pi m_+}\right)^{\frac{1}{2}} = n_+ e\,A_p\left(\frac{kT_e}{2\pi m_+}\right)^{\frac{1}{2}} \qquad (1)$$

r_p, L_p and A_p are the probe radius, length and area. The other symbols have their usual meaning. The electron temperature was used in the voltage scale. The characteristics are given in Figs. C2 to C7.

For the N_2^+, SF_6^- system the temperatures T were assumed equal, and the current was again normalized to the heavier species (SF_6^-) mass. The results are given in Figs. C8 to C10.

Particle Flow

The particle flow curves were constructed by using the curves of Fig.C1 directly for the normalizing species and multiplying the other

mirror-reversed curve by the mass ratio as given in Figs.C2, C8. Note that only the retarding part of the electron current is required, because of the extreme mass ratio, for the double probe result, but that the full characteristic is required when the species are of comparable mass.

Single Probe

The relevant portions of the single Langmuir probe characteristics are now constructed by simple subtraction of the ion current from electron current. The rectified version of the Langmuir characteristics (i.e. negative current shown positive) is given in Figs.C3,C9. Note that in the electron-ion plasma, the floating (zero-current) potential is quite negative, and moves negatively as the probe is made larger. In the ion-ion plasma the floating potential is slightly positive and does not move.

Double Probe

The double probe curves (for both probes identical, but isolated in the same plasma) are constructed from the rectified single probe curves by choosing a current and obtaining the voltage difference at that current between the positive and negative parts of the characteristics. This normalized probe current is plotted against the normalized voltage difference in Figs.C4 and C10. These curves are the upper right hand quarter of the usual S-type double-probe characteristic. To facilitate discussion and comparison with experiment, the electron-ion curves were normalized (by division by suitable α factors) to allow the lower part of the characteristics to be superimposed, giving Fig.C5.

Thus Figs.C5 and C10 are the theoretical standards for fitting the experimental results. Given these curves, the probe dimensions, plasma composition, and the experimental current-voltage characteristics, the plasma density and temperature are to be deduced.

TEMPERATURE AND NUMBER DENSITY

A basic problem in this diagnostic technique is that the normalising factors of the current and voltage variables are what is unknown. An obvious way to use the experimental data is to fit the experimental probe characteristics to the normalized plots by horizontal and vertical scaling factors. The normalizing factors appear immediately. One finds by the fit what voltage corresponds to kT/e and then what probe current fits the appropriate random current and thus determining what the ion density must be. The value of r_p/l_D can then be calculated and the curve for that value compared with the actual probe curve as an experimental consistency check. A short cut for this somewhat tedious procedure is obviously desirable.

Since the N_2^+, e^- curves had to be normalized to be superimposed, this second normalization must be considered as well, so the treatment of that system differs somewhat from the N_2^+, SF_6^- case .

N_2^+, e^-

In Fig.6 the normalization constant α, of Figs.C4, C5 is plotted as a function of r_p/l_D, as well as a useful parameter S, the ratio of the slope of the saturated part of the characteristic to the slope of the zero voltage difference region. This last parameter is independent of the vertical and horizontal scale factors. From S, on an experimental curve, one can roughly estimate r_p/l_D from Fig.C6. In Fig.C7, S is plotted against α so that α can also be obtained directly from S. The diagnostic prescription now is as follows:

1. In the usual fashion draw saturation asymptotes and the slope line L_o through $V_d = 0$. The intersection of L_o and L_s gives the break point voltage V_b which can be taken to be twice the electron energy i.e. $eV_b = 2kT_e$. The current I_b at the intersection is between 1 and 1.1αI_{o+}. The ratios

of the slopes of L_o and L_s determine α from Fig.C7. I_{o+} is defined above. Thus

$$kT_e/e = \tfrac{1}{2} V_b \qquad (2a)$$

In MKS units

$$I_{o+} = n_{MKS} A_{MKS} \left(\frac{kT_e}{2\pi m_+}\right)^{\frac{1}{2}} e = (nA)_{MKS} V_b^{\frac{1}{2}} \left(\frac{e}{2\pi m_+}\right)^{\frac{1}{2}} e$$

$$= nAV_b^{\frac{1}{2}} \left(\frac{m_e}{m_+}\right)^{\frac{1}{2}} 1.9\times10^{-14} \text{ amps}$$

$$n_{+MKS} = \frac{I_b (m_+/m_e)^{\frac{1}{2}}}{1.1\alpha\ A\ V_b^{\frac{1}{2}}} \frac{10^{14}}{1.9} = \frac{I_b}{\alpha\ A_{MKS} V_b^{\frac{1}{2}}} \times 227\times4.8\times10^{13} \text{ electrons/m}^3$$

In cgs units

$$n_+ = \frac{I_b}{\alpha\ AV_b^{\frac{1}{2}}} \times 227\times4.8\times10^{+11} = \frac{I_b}{\alpha\ AV_b^{\frac{1}{2}}} \times 1.09\times10^{+14} \text{ electrons/cc} \qquad (2b)$$

<u>$N_2^+ SF_6^-$</u>

No second normalization was necessary so Fig.C10 can be used directly. It should be noted that the curves do not show the clear saturation of the $N_2^+ e^-$ curves, so the drawing of the saturation line L_s is somewhat arbitrary. The (L_o, L_s) intersection voltage V_b is 1.8 to 2.3 and current I_b is 1.6 to 2.1. For nominal accuracy (better than 20%) it is enough to take the intersection voltage V_b as $2kT_e/e$. Because of the larger variation in I_b it is better to take the value at V_b of I (which only varies from 1.2 to 1.4) as 1.3. Thus we have

$$kT/e = \tfrac{1}{2} V_b \qquad (3a)$$

$$n_+ = \frac{I_{(V_b)}}{1.3AV_b^{\frac{1}{2}}} \left(\frac{m_+}{m_e}\right)^{\frac{1}{2}} \times 4.8\times10^{11} = \frac{I_{(V_b)}}{AV_b^{\frac{1}{2}}} 1.32\times10^{14} \text{ electrons/cc} \qquad (3b)$$

Since the saturated slope is somewhat uncertain, probably the best consistency check is to calculate l_D from $l_D = 6.9(T/n)^{\frac{1}{2}}$ and plot

a few experimental points on Fig. C10 to see if they fit the appropriate r_p/l_D curve. If the fit is fairly good the accuracy of the measurement may be increased by re-fitting the curve more carefully, but usually the first attempt accuracy is more than enough considering other sources of error.

DISCUSSION

The general similarity of Figs. C5 and C10 and formulas 2 and 3 indicates that for comparable r_p/l_D ratios the difference in electron-positive-ion or negative-positive-ion plasma double probe characteristic is not striking. The double probe is much more a detector of total ion density normalized to the heaviest species and highest temperature of opposite sign particles which determine the saturation current.

In order to determine whether electrons or heavy negative ions are involved one must use an auxiliary diagnostic. This could be the full Langmuir probe. If the current drain is unacceptable or no fixed plasma potential current be established, a convenient radio-wave method such as microwave transmission, resonance or stripline resonance may be the next best solution.

If the double probe characteristics do not fit these curves, The likely reasons are as follows:

(1) Probes too close and hence not independent.

(2) Collisions - if frequent, diffusion theory must be used.

(3) Non-Maxwellian distribution.

Of these (1) and (2) can be checked by rough calculation but (3) can only be determined by a complete single probe measurement which may not be possible.

The fact that normalized curves are given enables one to decide

if the slope fits the theory - a consistency check not usually available.

To sum up: The ideal collisionless Maxwellian cylindrical double probe characteristics for two plasmas (N_2^+, $e^-(T_+ << T_e)$; N_2^+, $SF_6^-(T_+ = T_-)$) have been given together with a procedure for determining the temperature and number density. Some limitations have been indicated which should be explored further in any future work on the topic.

REFERENCES

J.E. Allen, R.L.F. Boyd, P. Reynolds "The Collection of Positive Ions by a Probe Immersed in a Plasma" Proc.Phys.Soc. B70, 297-304 (1957)

I.B. Bernstein, I.N. Rabinowitz "Theory of Electrostatic Probes in a Low-Density Plasma" Phys.Fluids 2, 112-121 (1959)

F.F. Chen "Numerical Computations for Ion Probe Characteristics in a Collisionless Plasma" J.Nuclear Energy C7, 47-67 (1965)

L.S. Hall "Probes and Magnetic Pumping in Plasma" UCRL 6535 (1961) "The Computation of Self-Consistent Potential Distributions in a Collisionless Plasma" UCRL-7660-T (1964) (Univ.Calif.Rad.Lab. (Livermore) unpublished reports)

S.H. Lam "The Langmuir Probe in a Collisionless Plasma" Phys.Fluids 8, 73-86 (1965), "Plasma Diagnostics with Moderately Large Langmuir Probes" Phys.Fluids 8, 1001-1004 (1965)

J. Laframboise "Theory of Spherical and Cylindrical Langmuir Probes in a Collisionless Plasma at Rest" paper given at 4th Int.Symp. on Rarefied Gas Dynamics, Toronto, July 14-17 (1964) to be published (Academic Press, J.H. de Leeuw, ed.)

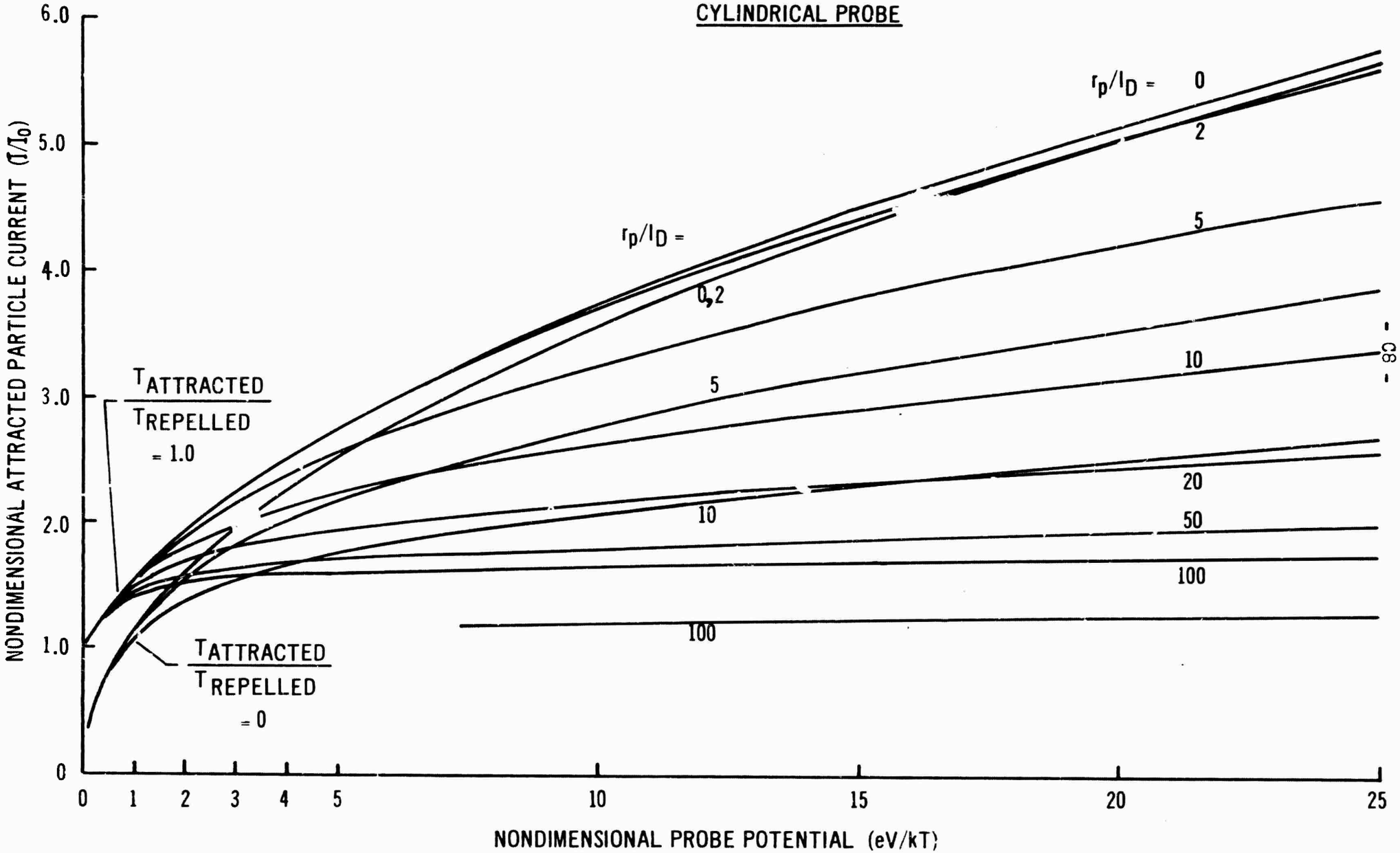

Fig. C1 Normalized cylindrical probe current-voltage characteristics for attracted particles, normalized with repelled particle temperature for random attracted current and Debye length. From these curves, probe characteristics can be constructed for any mass ratio and temperature ratios of zero and 1. (e.g. Fig.s C2-C4, C8-C10).

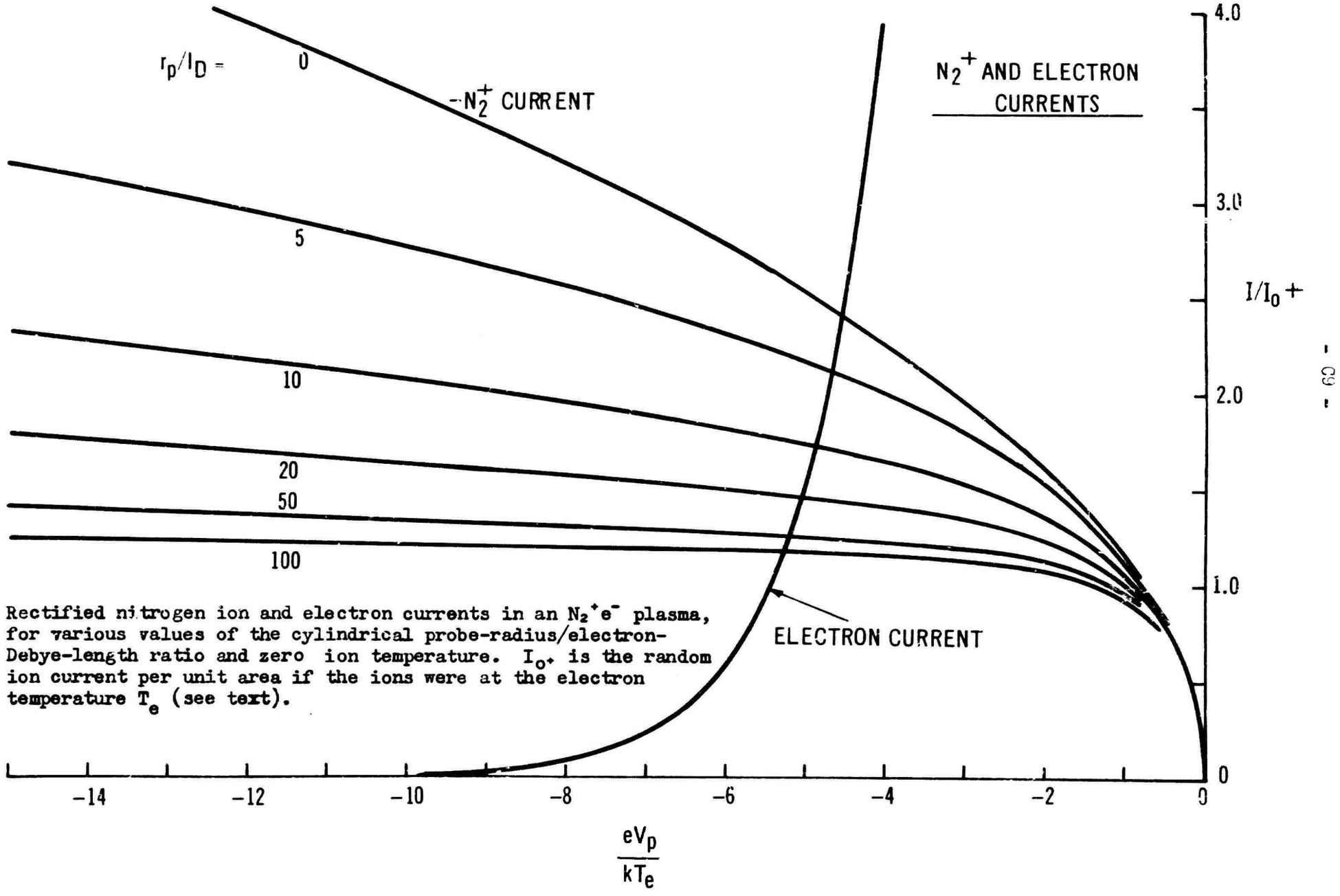

Fig. C2 Rectified nitrogen ion and electron currents in an $N_2^+e^-$ plasma, for various values of the cylindrical probe-radius/electron-Debye-length ratio and zero ion temperature. I_{o+} is the random ion current per unit area if the ions were at the electron temperature T_e (see text).

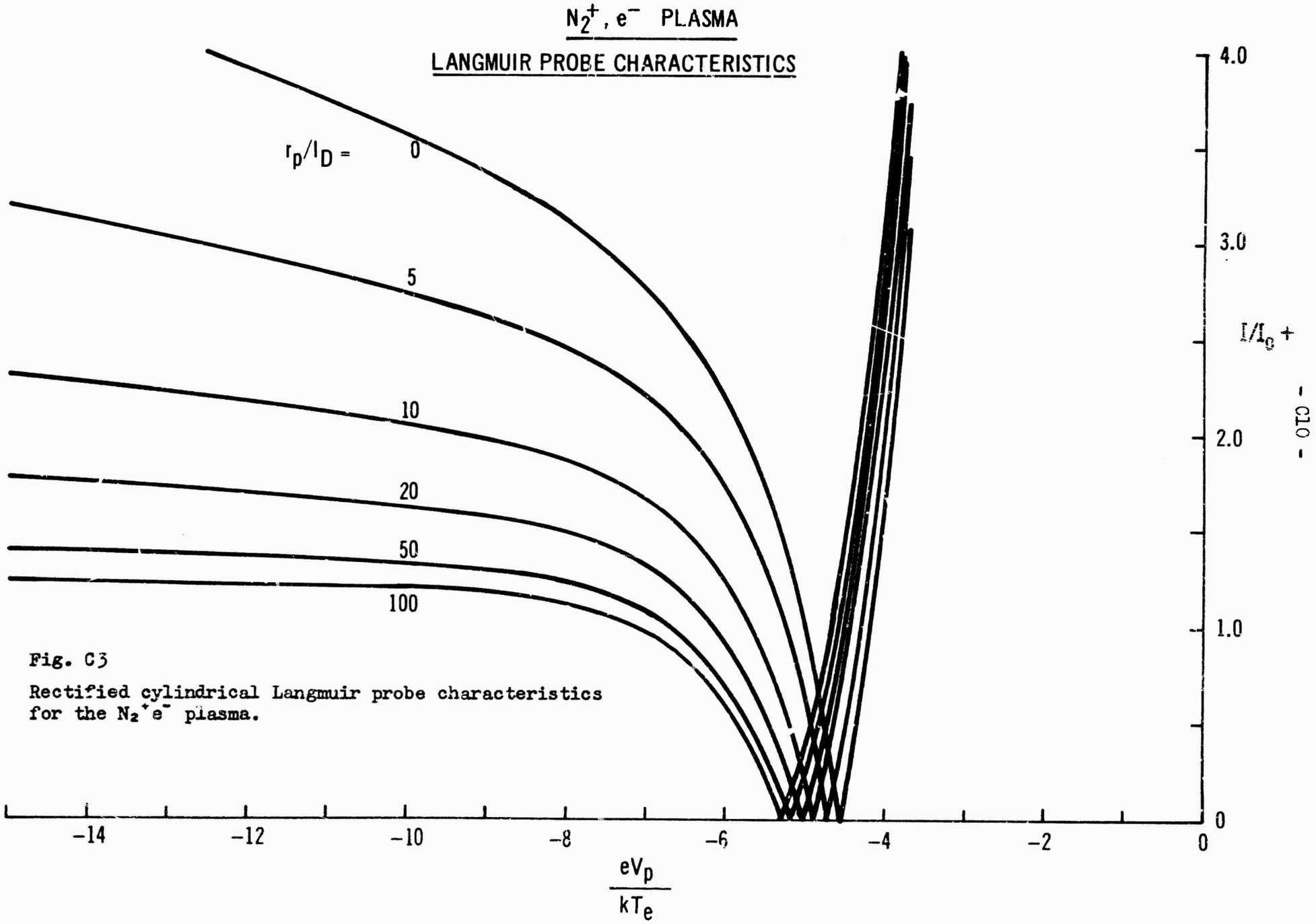

Fig. C3

Rectified cylindrical Langmuir probe characteristics for the $N_2^+e^-$ plasma.

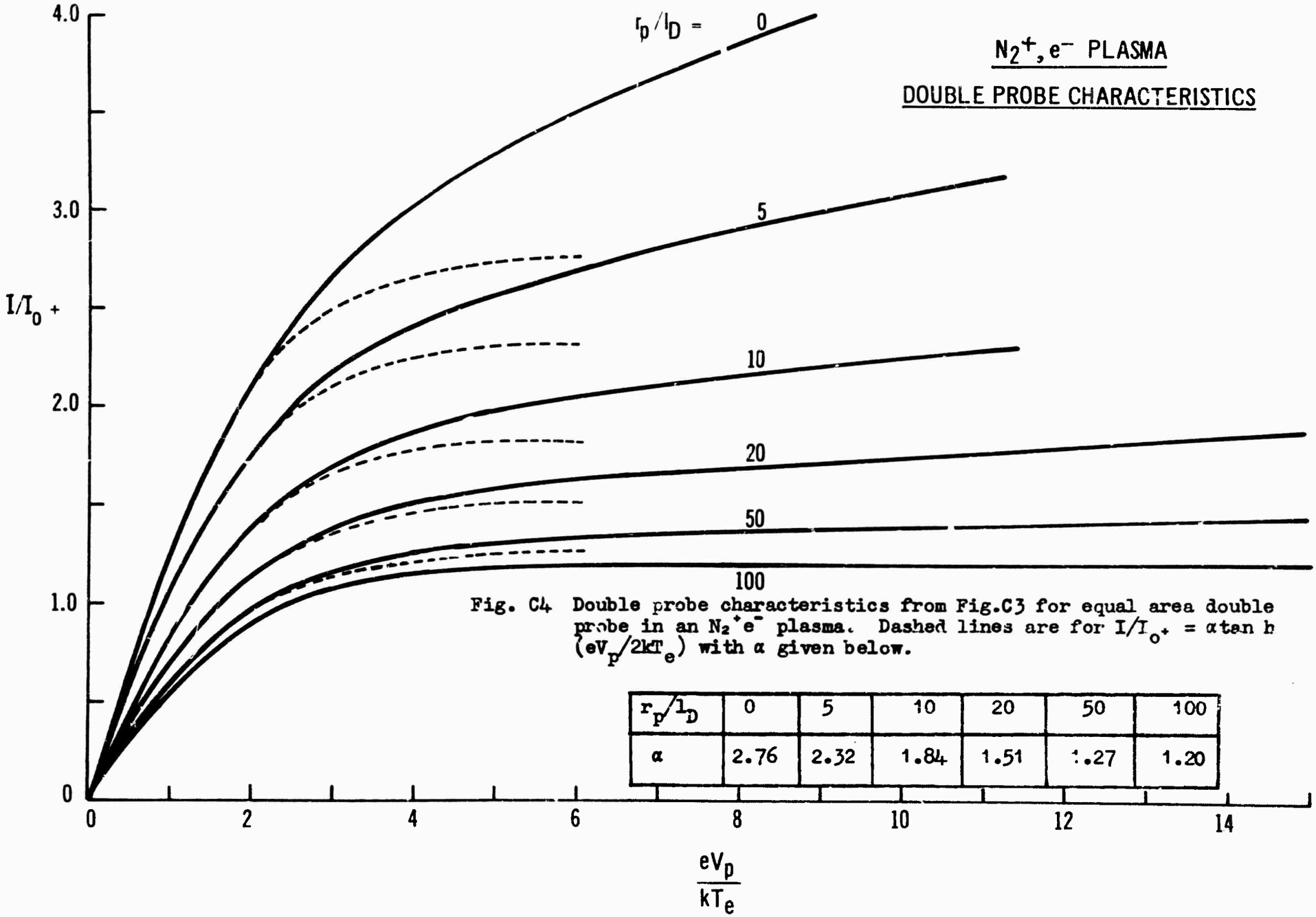

Fig. C4 Double probe characteristics from Fig.C3 for equal area double probe in an $N_2^+e^-$ plasma. Dashed lines are for $I/I_{0^+} = \alpha \tan h (eV_p/2kT_e)$ with α given below.

r_p/l_D	0	5	10	20	50	100
α	2.76	2.32	1.84	1.51	1.27	1.20

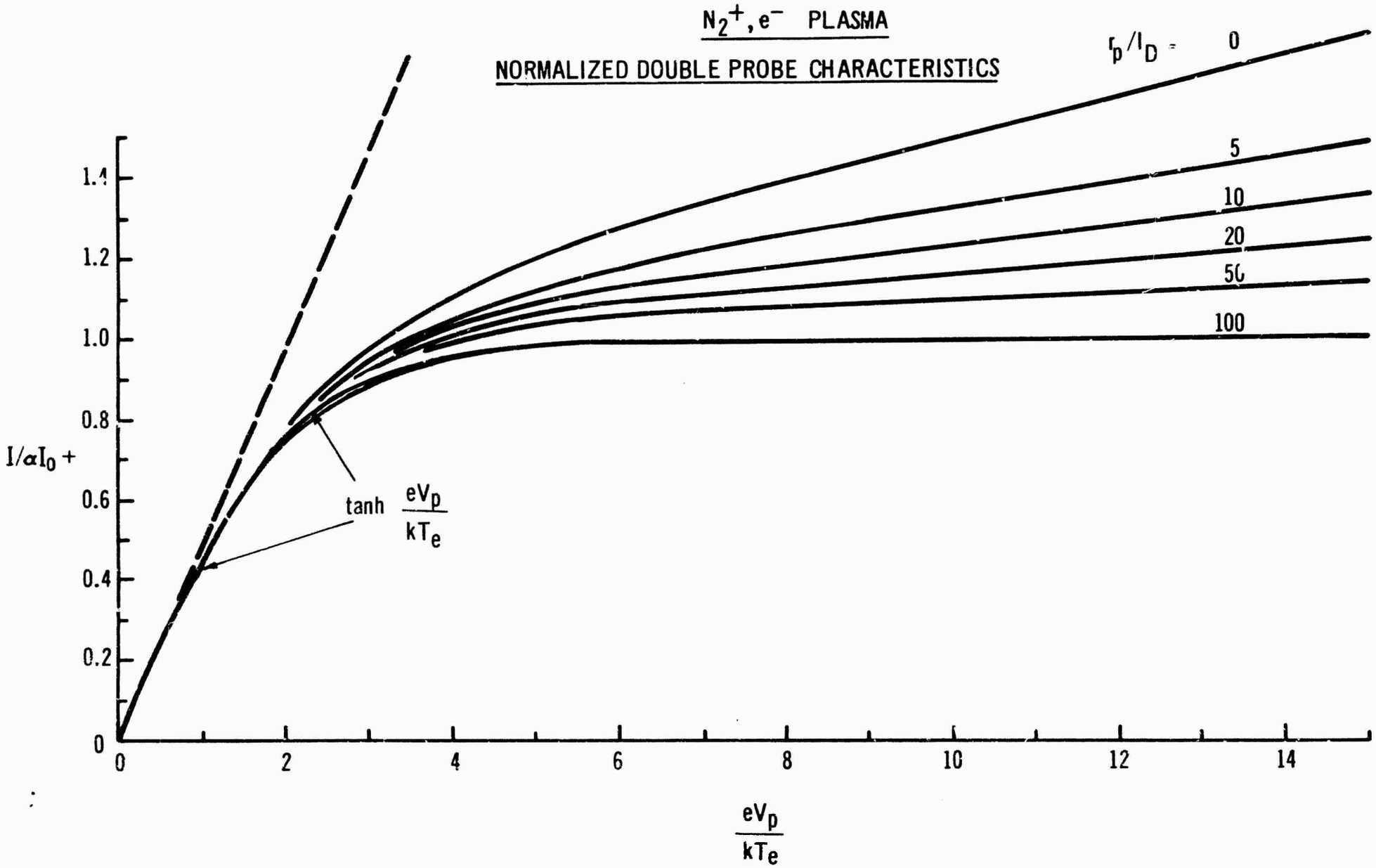

Fig. C5 Normalized double probe characteristics from Fig. C4 for an $N_2^+e^-$ plasma, obtained by division by α. Intercepts of dashed line and asymptote occur for $eV/kT_e \approx 2$, $I/\alpha I_{0^+} \approx 1$.

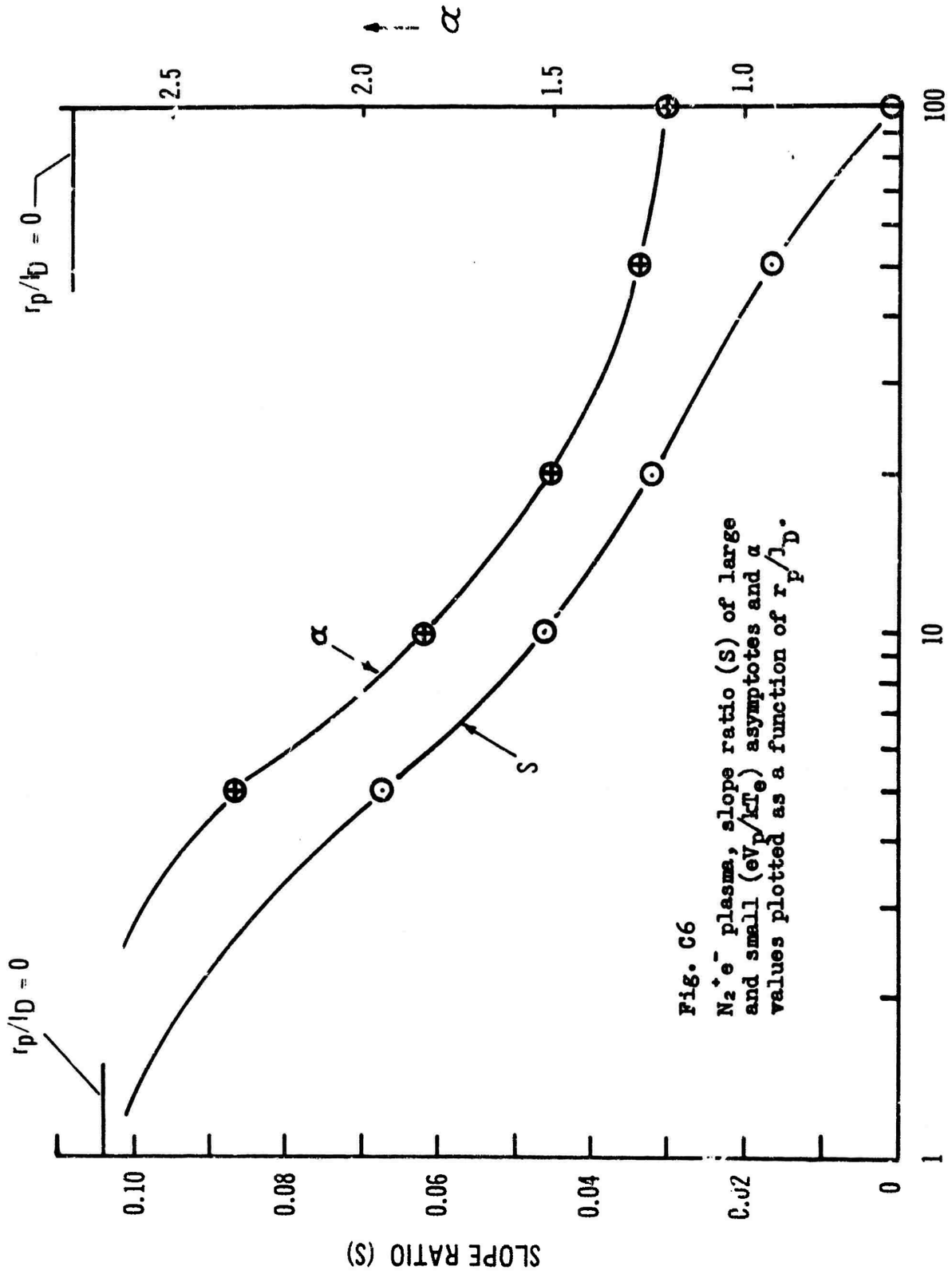

Fig. C6
$N_2^+e^-$ plasma, slope ratio (S) of large and small (eV_p/kT_e) asymptotes and α values plotted as a function of r_p/λ_D.

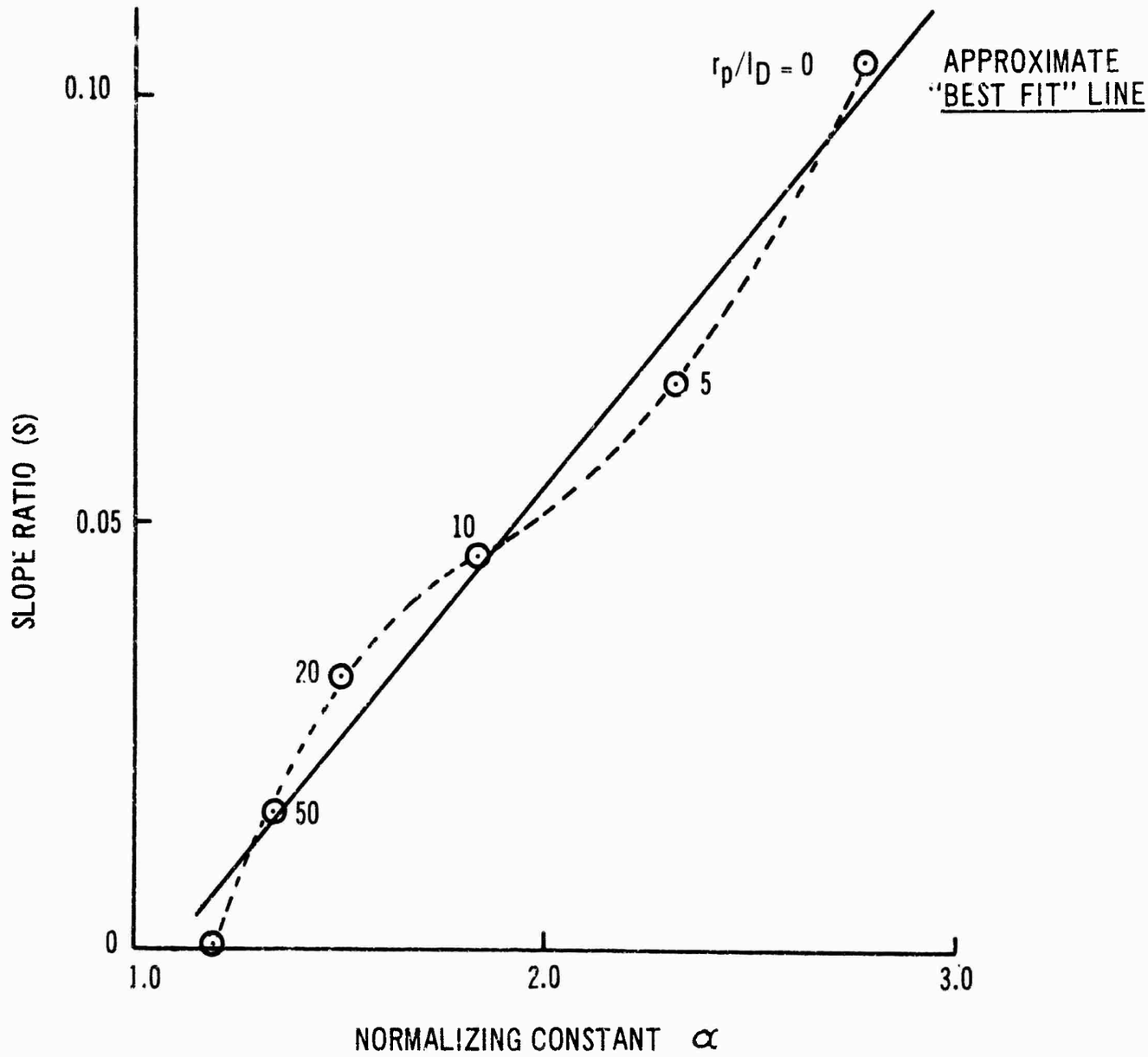

Fig. C7 $N_2^+e^-$ plasma, slope ratio (S) versus normalizing α values with r_p/l_D as a parameter.

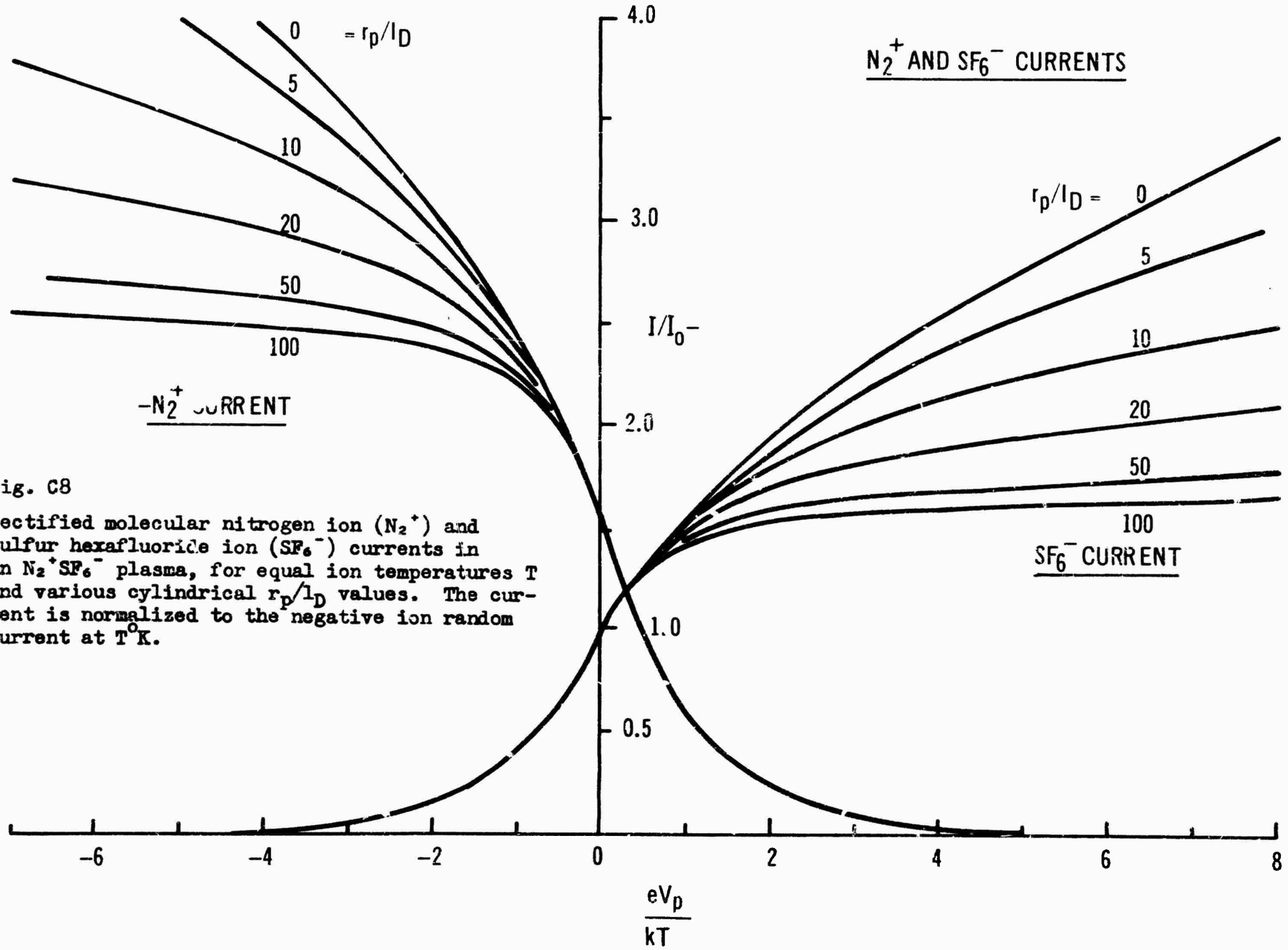

Fig. C8

Rectified molecular nitrogen ion (N_2^+) and sulfur hexafluoride ion (SF_6^-) currents in an $N_2^+SF_6^-$ plasma, for equal ion temperatures T and various cylindrical r_p/l_D values. The current is normalized to the negative ion random current at T°K.

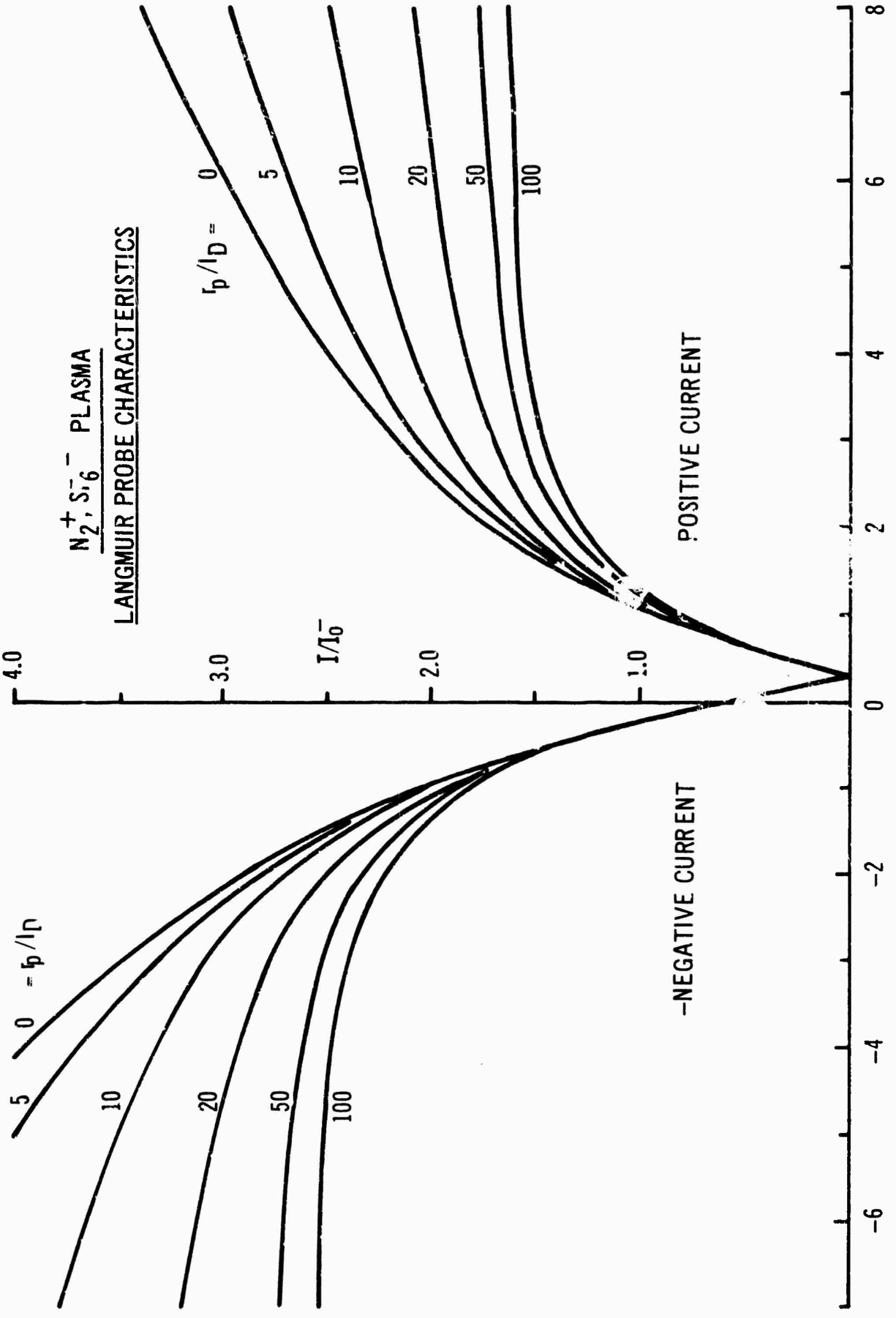

Fig. C9 Rectified cylindrical Langmuir probe characteristics for the $N_2^+SF_6^-$ plasma.

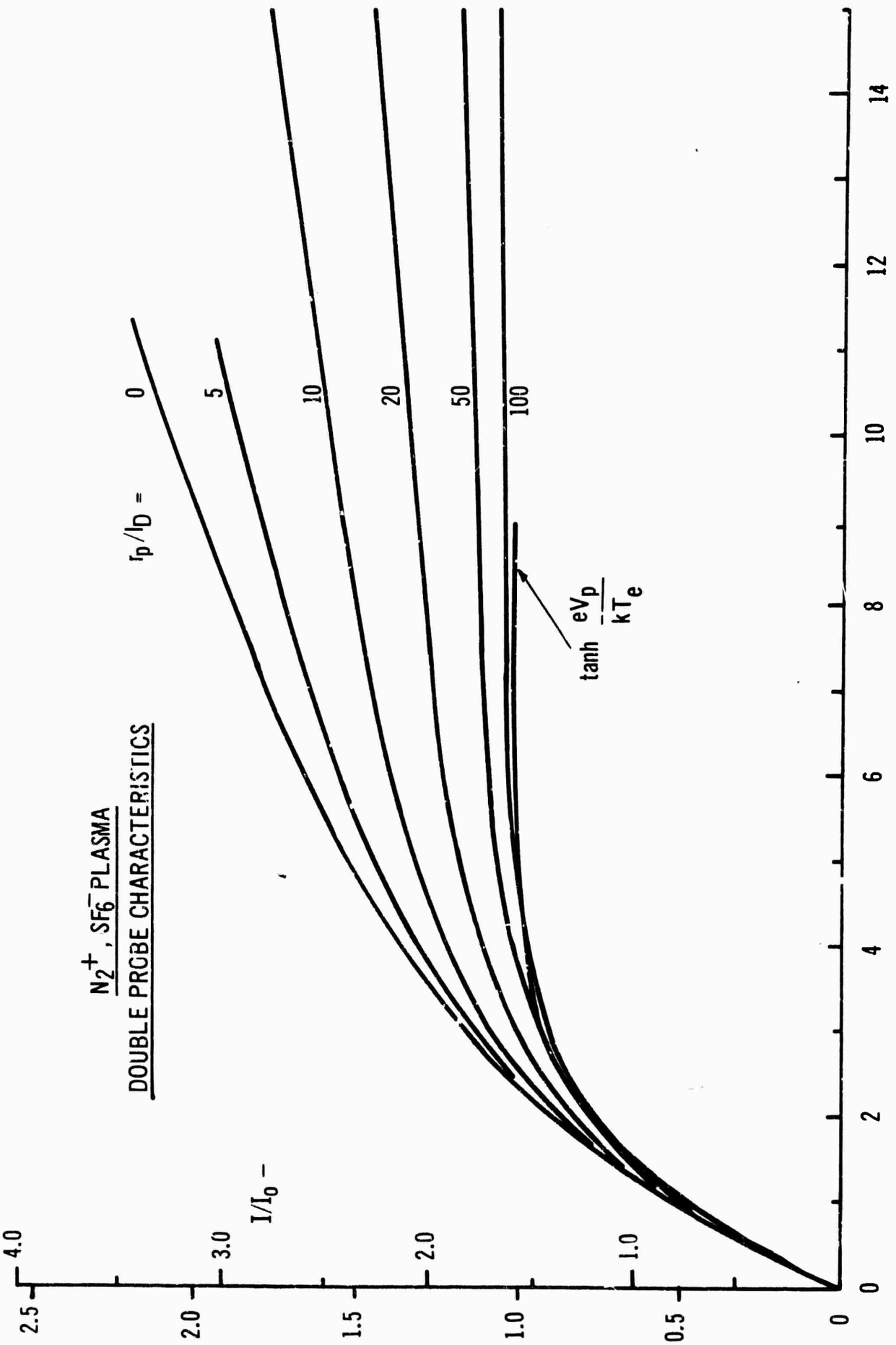

Fig. C10 Equal-area double probe characteristics from Fig. C9 for the $N_2^+SF_6^-$ plasma. The positive ion (N_2^+) random current scale is given as well, for comparison with Fig. C5.

APPENDIX D
Spectroscopic Determination of Plasma Temperatures

Using the electromagnetic spectrum to deduce the temperature in a plasma has certain advantages. By suitable optical means, any part of the plasma may be investigated without disturbing the medium. In addition, the measurement can give direct information about the state of rotation, vibration, and translation of the molecules involved; that is, whether certain reactions may be occurring. The accuracy of the result depends on the resolving power of the instrument employed and the assumption that the molecule is in thermal equilibrium with its surroundings.

For a very low resolution spectrum, the vibrational temperature may be estimated by constructing a synthetic spectrum (Shemansky & Vallance Jones, 1961) for a given temperature and matching the profile with the observed band shape. Several temperatures must be chosen to obtain the best fit, but the accuracy is limited - being a function of the band shape and the signal-to-noise ratio in the observed spectrum - and the process is very tedious. If access to a large high-speed computer is available, it is possible to build up a library of band shapes for various vibration temperatures of molecules of interest for fast reference on a routine basis.

The synthetic spectrum is constructed in the following manner. The wavelength of the various lines in each branch of the band are either tabulated or calculated from the term values for the state of the molecule. The intensity of the lines, $I(K')$ is given by:

$$I(K') \propto S(J) \exp \left[-B_u K'(K'-1) \frac{hc}{KT} \right] \qquad (1)$$

where the line strength factor $S(J)$ varies with the branch investigated,

P, Q or R. The constant of proportionality contains the wavenumber σ, as σ^4 which may affect the calculations if the band is widely spread. A plausible temperature is assumed and the calculation of the I(K') is made. The remaining parameters in the constant of proportionality are fixed for a given band. The branches are plotted to the same scale with a triangular spectral-slit-width function for a spectrometer, a trapezoidal function for a spectrograph, or a $\frac{\sin x}{x}$ function for the spectral slit width of a Michelson interferometer. The branches are summed to give the band change for the temperature assumed which is compared with the observed spectrum, a new temperature is then chosen and the new calculation of I(K') commenced.

For intermediate resolution spectra, of the order of 1 Å, an estimate of the rotational temperature can be made from the intensity distribution of the rotational structure. The intensity of a rotational line may be written as (Petrie 1953)

$$I = c\nu^4 \, s \, e^{-\frac{1.44\,B'}{T}K'(K'+1)} \qquad (2)$$

The frequency factor ν^4 varies very little within a band, s is the "line strength" factor, B' is the rotational constant of the upper state, K' is the rotational quantum number and T the temperature.

At the intensity maximum of the band

$$\frac{dI}{dK'} = 0$$

and we get for T

$$T = 1.44\,B'(2K'+1)K' \qquad (3)$$

Hence by identifying the rotational quantum number for maximum intensity, T can be calculated provided B' is known. Also from equation (2) we find

$$\log_{10}\left(\frac{I}{K'}\right) = \text{const} - \frac{1.44}{T}B'K'(K'+1)$$

This shows that a plot of $\log_{10}\left(\frac{I}{K'}\right)$ against K'(K'+1) will give a

straight line whose slope is related to the temperature by

$$T = \frac{1.44B'}{\text{slope}}$$

Hence, knowing B', one can calculate T. In the present investigation rotational temperatures of the nitrogen discharge and its pink afterglow were measured using the rotational structure of 3914 Å (0,0) and 4278 Å (0,1) bands of the first negative system. A sample rotational spectra of discharge source and plots of $\log_{10}\left(\frac{I}{K'}\right)$ against K'(K'+1) are shown in Section III for the source and the pink afterglow. Following Shepherd & Hunten (1953) an intensity correction was made due to the fact that the height of the unresolved profile at any wavelength depends both on the intensity and the line spacing at that wavelength.

Care must be taken to be certain that none of the rotational lines in the given branch are contaminated by lines from another branch. If estimates of contamination must be made, the accuracy will be no better than that obtained from the vibrational temperature. If rapid measurement of the temperature is desired, an electronic system may be built using either rotational lines or intensities in the band (Hunten, Rawson, Walker, 1963).

For higher resolution, a Fabry Perot interferometer may be used to determine the Doppler shape of a line (Jacquinot, 1960) which will give the actual temperature of the medium. Only an extremely narrow bandwidth is investigated with this instrument.

REFERENCES FOR APPENDIX D

Herzberg, G. - Molecular Spectra and Molecular Structure I. Spectra of Diatomic Molecules. 1959 (D. Van Nostrand, Princeton. N.J.)

Hunten, D., Rawson, E.G. & Walker, I.K. - Can.J.Phys. 41 258 (1963)

Jacquinot, P. - Rept.Progr.Phys. 23 269 (1960)

Petrie, W. - Rotational Temperature of Auroral Nitrogen Bands. J. Atmosp. Terr.Phys. Vol.4 5 (1953)

Shemansky, D. & Vallence Jones, A. - J. Atmosp, Terr.Phys. 22 166 (1961)

Shepherd, G.G. & Hunten, D.M. - On the Measurement of Rotational Temperature from Unresolved Auroral Nitrogen Bands. J. Atmosp, Terr. Phys. Vol.6 328 (1955).